# An Extracellular Matrix-Based High-Throughput Platform for 3D Cell Culture, Drug Screening, and Biological Discovery

A DISSERTATION
SUBMITTED TO THE FACULTY OF
UNIVERSITY OF MINNESOTA
BY

Alexandra L. Crampton

IN PARTIAL FULFILLMENT OF THE REQUIREMENTS
FOR THE DEGREE OF
DOCTOR OF PHILOSOPHY

Dr. David K. Wood, Advisor
August 2019

***Acknowledgements***

This work would not have been possible without the financial support of UMN College of Science and Engineering Graduate Fellowship, the National Science Foundation Graduate Research Fellowship Program, and the Doctoral Dissertation Fellowship.

It is with immense gratitude that I acknowledge the support of my advisor, Dr. David K. Wood. From the beginning of my graduate education, he has supported my scientific interests, and helped refine them through his patience, guidance, and attentive attitude.

I would like to thank my committee members, Dr. Martin Felices, Dr. Brenda M. Ogle, and Dr. Robert T. Tranquillo, for their insightful comments and encouragement, but also for guiding my thesis work in exciting and challenging directions.

I would like to express my special appreciation to our collaborators, particularly Dr. Salman R. Khetani, and the Khetani Lab at University of Illinois at Chicago for working to grow this project into specialized application spaces.

I am grateful to Dr. Steve George, Dr. Matthew O'Connor, and Dr. Luis Alonzo for helping me discover my passion for research, and for your mentorship and encouragement throughout my graduate studies.

Last but not least, I would like to express my deepest gratitude to my family and friends – to my parents who shared their spirit of adventure in engineering pursuits, and to my labmates and colleagues for their optimism, enthusiasm, and unwavering support on this journey.

***Abstract***

There is an urgent need for predictive drug screening and biological discovery tools, as the current standard systems either lack physiological relevance or are logistically incompatible with large-scale screens. Here, we present a solution to this problem – a novel droplet-based workflow to fabricate, culture, and assess cell-matrix interactions on short (<7days) and long (>28 days) timescales. With this technology, we can assess 3D cell-ECM interactions in a high-throughput and high-content manner, opening new avenues for assessing cell performance in response to therapies in a 3D microenvironment. The specific applications of this platform are broad, and we demonstrated the applicability for this technology to improve collagen contraction assays, endothelial barrier function measurements, and human liver model systems for toxicity studies. We also show that microtissue constructs can be cryopreserved, which allows this technology to be disseminated more broadly, as only standard cell culture equipment is needed to culture microtissues after fabrication. Because of the low reagent volumes and small cell numbers required for our system, this platform could become a logistically feasible answer to 3D functional screening of samples (e.g. tumor biopsies) on a patient-by-patient basis. We are eager to continue to refine and expand the capabilities of our technology, as well as amplify the *in vitro* biological systems we can generate with this platform.

***Table of Contents***

***List of Figures***

## ***Chapter 1: Design considerations for in vitro model systems***

### Introduction

Drug discovery relies heavily on model systems to identify, develop, and test drugs before beginning clinical trials in humans. This workflow is predicated on the idea that the behaviors seen in model systems will be good predictors of performance in clinical trials, but this is often not the case**.** Poor representation of human organs and disease states often leads to failure of drugs during late-stage clinical trials, significantly increasing the time and cost required to bring new therapies to market[1].

*Model systems for drug discovery – animal models*

The use of animal models in medical research has resulted in improved understanding of disease progression, treatments, and outcomes in humans. There are many *in vivo* platforms used for drug discovery including, but not limited to, *Drosophila, C. elegans*, mice, rats, rabbits, dogs, cats and non-human primates[1–3]. Each animal model offers advantages and disadvantages in studying human pathologies, making them useful in certain types of studies or phases of drug discovery.

For drug discovery and safety studies, mice have many advantages over other model organisms. Logistically, mice have a short gestation period (approximately 20 days) and reach adulthood quickly[3], reducing the cost of conducting studies in mice models over other mammalian options. Early identification of therapies that will fail testing in higher-level animals or clinical trials lowers the over-all cost of drug development. For these reasons, and others, 95% of all *in vivo* studies use mice[2].

The utility of mice as a relevant platform is limited for understanding and predicting human responses to therapy regarding toxicology and/or disease progression[4,5]. In a large study comparing human and animal drug toxicities, rodent models (including mice) were only found to accurately predict human drug toxicity in 43% of cases[6]. Because of this, the US Food and Drug Administration (FDA) requires testing of drugs in at least two species, one of which must be a non-rodent. Even with this stipulation, animal models were only accurate in 71% of cases[6]. Thus, the safety of drugs cannot be fully assessed and significant risk is transferred to human patients during clinical trials,

which can result in serious consequences including death[6,7]. Although animal models share many characteristics with humans, the species-specific differences and unexpected toxicity results based on these models motivate research into other model systems[8–11].

*In vitro models – 2D culture systems*

While animal models represent the total complexity of living, multicellular organisms, a reductionist approach to creating models has been applied in developing systems for high-throughput drug discovery. The simplest and most well-accepted platforms use two-dimensional (2D) cell cultures, where cells adhere to a flat surface (typically polystyrene or glass) and are maintained with nutrients and growth factors in a liquid bath[12,13]. This is attractive as an efficient and scalable means of culturing cells for high-throughput applications, since many cell types readily adhere to and grow on the stiff 2D substrates and the cellular environment be easily controlled through the cell culture medium[12]. Although these models excel in handling and experimental logistics, they often fail to recapitulate cell behavior accurately. For example, despite the increasing the number of potential anti-cancer agents available for testing, only approximately 10% of compounds successfully progress to market[14]. Often (especially for anti-tumor therapies), these drugs fail late in clinical trials (particularly during phase III[15,16]) after considerable economic investment in the compound has been made.

There are many reasons that these models are not predictive, some of which are due to the substrate on which the cells grow. Tissues in the body have different stiffness and elastic characteristics (e.g. brain vs. bone), so it is unsurprising that cells can detect these differences and respond. Using polyacrylamide gels as a substrate, Engler et al. found that the elastic modulus of the substrate could determine lineage selection for mesenchymal stem cells[17].

The substrate surface also affects cell behavior. Tissues in the body are highly organized, with complex, 3D organization of cells and surrounding matrix proteins. Conventional 2D culture easily supports growth of cells in monolayers, and can be modified with micropatterning (via cell-adhesive islands[18], microwells[19], and micropillars[20]) to control cell shape and organization from the substrate surface.

However, modifications to the substrate surface cannot provide ECM interactions on *all* surfaces of the cell, inducing unnatural apical-basal polarization in cells and ultimately altering how the cells move and respond to their environment[21].

This work highlights the importance of choosing materials that mimic the *in vivo* environment, and thus substrate characteristics and geometries that promote physiologically-relevant behavior should be a design consideration for *in vitro* platform development. This has been recognized by both the Federal Drug Administration (FDA) and its European counterpart to push for *in vitro* organ models that better recapitulate human physiology and pathology[4,5].

*In vitro models – Spheroids*

To remove artifacts from stiff substrate interactions, protocols have been optimized for culturing cells as self-assembled aggregates – termed "spheroids" – without any direct substrate interactions. To generate spheroids, a suspension of cells is distributed (usually as hanging drops[22–25] or onto micropatterned low-adhesion surfaces[22,26]) and cells collect via gravity to create aggregates stabilized by cell-cell interactions. These protocols are highly reproducible, scalable, and are compatible with automated liquid handling systems, making spheroids a more attractive option than the 2D predecessors.

Although cells in spheroids produce some ECM components[27], this method of culturing cells overall lacks 3D ECM interactions. Additionally, the ratio of ECM to cells in spheroids is lower than is found in most tissues, adding bias to cell-cell contacts. For the purposes of mimicking ECM remodeling – a process important in the development of cancer[28–30], fibrosis[28,31,32], and autoimmune disease[31,33,34] – spheroids are not the ideal model system. Thus, there is also a need for platforms that enable incorporation of 3D ECM interactions.

*In vitro models – hydrogel culture systems*

In order to study cells in a more physiologically relevant 3D environment, methods and biocompatible materials for encapsulating cells in these biocompatible

materials have been developed. Three-dimensional culture models with protein-based scaffolds are better suited than synthetic options for studying cell-matrix interactions[35,36] and focal adhesion function[37], and have been shown to be better predictors of drug safety and efficacy than 2D models[38–43]. Moreover, 3D tissue models can capture the complex interplay between drugs, cell mechanics, and matrix interactions.

One of the most common ECM-based material choices for 3D tissue experiments is collagen, which is the most abundant fibrous protein in the body comprising 30% of the total protein mass[44,45], and which represents a non-inflammatory and hydrolysable environment[46–48]. Fabrication of 3D collagen models is typically in the form of relatively large (~mm in diameter) bulk gels, and cells are often grown in or on the gels to study cell function. The readouts from 3D collagen hydrogel experiments vary based on application, but typical metrics include viability[49,50], morphology[50], protein expression via immunofluorescence or immunoprecipitation[51], and cell contraction[52–56].

These 3D models are critical for studying cell-matrix interactions in a 3D environment *in vitro*, but fabrication of large-scale hydrogels is labor and time intensive[57], the gels have significant diffusion limitations for nutrients and signaling molecules[57], and they are difficult and cumbersome to analyze. Because of this, *in vitro* experiments in bulk gels are often limited to small sample sizes. Additionally, quantification within bulk gels could be more extensive, but the large geometry of these tissues can make complete visualization time consuming and often cannot be completed without physically altering the gel, making long-term studies with intermediate time points difficult to conduct[58–60]. **Thus, there is a need for 3D ECM-based *in vitro* models that are amenable to high-throughput studies**.

## ***Chapter 2: Microtissues as an improved in vitro model system***

This chapter contains material from "Rapid generation of collagen-based microtissues to study cell–matrix interactions" by Alexandra L. Crampton*, Marie-Elena Brett*, and David K. Wood. *Technology, The Journal*, volume 4, issue 2, pages 80-97, 2016; permission conveyed through Copyright Clearance Center, Inc. *These authors contributed equally.

### Overview

To answer this unmet need for scalable 3D culture systems, **we aimed to develop an efficient system for high-throughput, 3D, ECM-based cell culture.** Leveraging microfluidic technology, we have alleviated several drawbacks of large hydrogels by miniaturizing the tissues (~14 nL in volume), transforming this tissue-engineering standard into an easy-to-use, high-throughput (>20,000 tissues/hour) platform with novel biological applications and enhanced statistical power. We have demonstrated that this microtissue platform can be used to efficiently perform standard *in vitro* measurements (e.g. collagen compaction, endothelial permeability). We are now exploring applications aiming to improve the drug discovery pipeline (specifically, creating an improved human liver model for toxicology studies). Because the microtissues are small and therefore require fewer cells per assay, we are also excited by the possibility of using these 3D cell culture modules to examine patient samples. In the future, we will aim to use these *in vitro* tissue mimics to accurately test several treatment regimens and assess primary effects (e.g. on a tumor sample) and secondary effects (e.g. liver toxicity).

### Collagen Microtissue Fabrication Protocol

One way to overcome diffusion and throughput limitations in 3D tissue culture is to miniaturize the hydrogel scaffold. The advantages of miniaturized tissue models, or "microtissues," that are only 25-300 μm in diameter include short diffusion times for nutrients and signaling molecules, enabling high cell viability through the tissue and rapid cell-cell communication across the entire gel. The small length-scale additionally facilitates high-throughput imaging and analysis with automated methods. For these

reasons, several groups have developed methods to generate miniaturized gels by dispensing small volumes onto a surface[61–64], polymerizing collagen in small tubing and extracting collagen modules[65], or using agitation to create polydisperse collagen-in-oil emulsions[66].

An alternative option for partitioning the collagen solution is with droplet microfluidics, as liquids can be partitioned quickly, consistently, and with minimal human intervention. Moreover, the resulting emulsions are monodisperse[67,68], making this technology particularly useful for producing consistent replicates for screening applications. To generate droplets, oil and aqueous solutions are introduced to a microfluidic device, and the relative flow rates, viscosities, and device geometry determine the volume of the aqueous compartments[69].

Droplet generators have a historic use in tissue engineering applications. Most of these studies encapsulate live cells in rapidly-gelled, photo-polymerized PEG hydrogels, and is amendable to droplet-based studies[70,71]. PEG is biocompatible, quick to polymerize, and can be functionalized with protein motifs that permit cell interactions[72–75]. However, even with these protein modifications, these gels are ill-suited for studies involving ECM remodeling and cell movement because (1) the pore size of the gels is significantly smaller than natural ECM [76,77] and (2) the cells cannot adhere to the majority of the matrix components (as cells only interact with the protein motifs of the hydrogel). Thus for our application, we directed our efforts on natural ECM as our biomaterial of choice for microtissue fabrication.

Collagen is the most abundant fibrillar protein in the body[44,45] and provides a non-inflammatory and hydrolysable microenvironment[46–48], motivating us to use this material as the base of our microtissues. Collagen I hydrogels are thermally polymerized, meaning the compartmentalization into microtissues needs to be completed while collagen remains aqueous, but the polymerization must occur before the microtissues coalesce into a large hydrogel. Other groups have complicated and/or multilayer devices to complete this polymerization in the microfluidic device[78,79] that greatly increase difficulty of device fabrication, reduce accessibility of the technology, and increase failure modes. Inspired by simpler microfluidic chip designs for droplet fabrication[80], we

planned an easy-to-use protocol to generate and culture collagen microtissues with a single-layer microfluidic device (Figure 2.1). Microfluidic devices are first chilled in a 4ºC cold room and all droplet generation is completed at 4ºC. We will then collect these microtissues and polymerize the constructs outside the microfluidic device at 25ºC -37ºC.

Once this fabrication protocol was optimized, we aimed to validate cell viability and function, and then use our unique material and geometric properties to create novel readouts of cell function in the miniaturized tissues. We anticipated that protein-based microtissues could be the ideal 3D culture platform to study processes that utilize cell-fiber interaction, such as cell adhesion and matrix remodeling, using straightforward methods that are compatible with high-throughput studies. In the following chapters, we will demonstrate the function of our platform as a fabrication method for cell-laden collagen microtissues, and then explore novel readouts and applications of our microtissues platform.

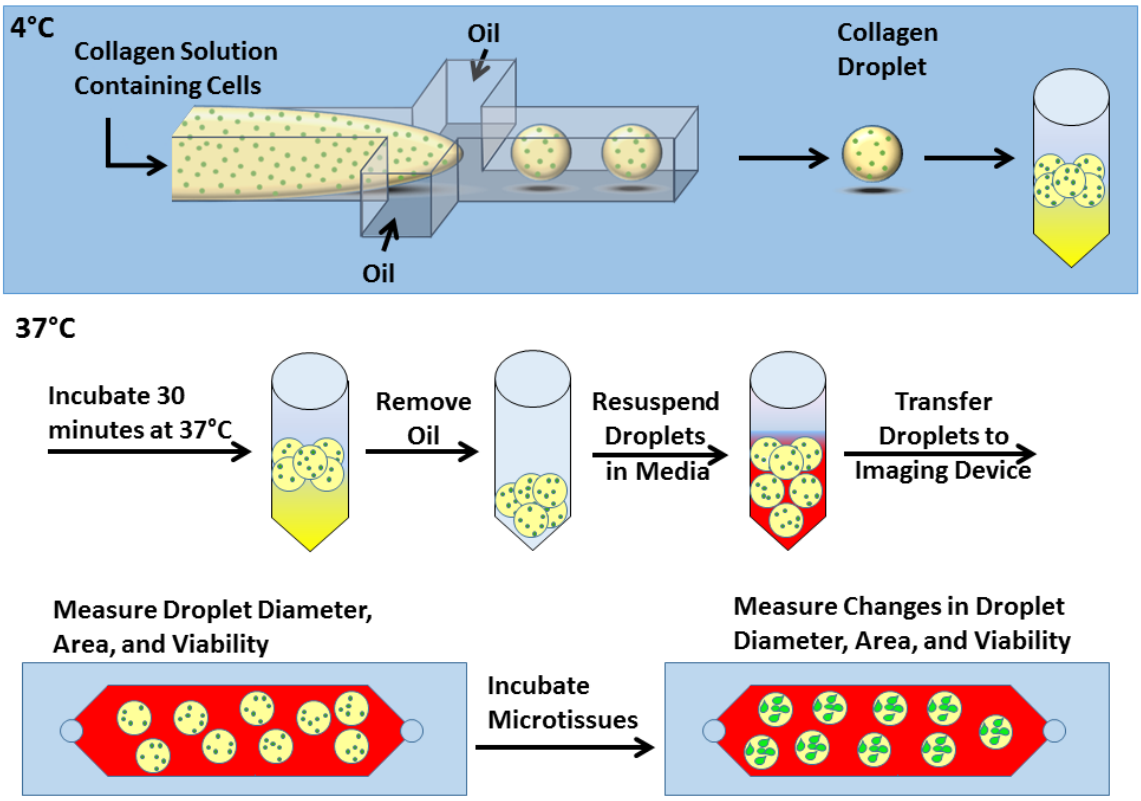


**Figure 2.1:** ***Microtissue fabrication***
Cells were mixed into collagen and the solution was perfused into a microfluidic droplet generator. Fluorocarbon oil was perfused into the device to produce droplets. Droplet formation was performed at 4°C, then droplets were incubated at 37°C for 30 minutes. Oil was aspirated and droplets were resuspended in media and transferred to a microfluidic capture device for imaging and/or further incubation.

## ***Chapter 3: Demonstration of feasibility and biocompatibility of microtissue workflow***

This chapter contains material from "Rapid generation of collagen-based microtissues to study cell–matrix interactions" by Alexandra L. Crampton*, Marie-Elena Brett*, and David K. Wood. *Technology, The Journal*, volume 4, issue 2, pages 80-97, 2016; permission conveyed through Copyright Clearance Center, Inc. *These authors contributed equally.

### Overview

Our goal for this work was to create a method for studying cell-matrix interactions in a more physiologically relevant 3D protein-based hydrogel tissue that could be scaled up to perform large-scale screens, study cell-matrix interactions on a population basis, or be remodeled by cells to build larger tissues. We developed an easy-to-use method that leverages microfluidic droplet technology to miniaturize protein-based hydrogels and thus extend their application to high-throughput studies. With this method, we fabricated cell-laden collagen hydrogels that are uniform in size, without complicated on-chip temperature control[79]. This affords the ability to use a simple protocol to create tens of thousands of identical cell-laden microtissues within a few hours and subject them to a wide variety of experimental conditions. The increased production rate and uniform distribution of the collagen hydrogel droplets created with our device lends itself to quantification of cell-matrix interactions and matrix remodeling of cells on a large-scale microtissue-by-microtissue basis. Here, we describe our method and demonstrate the applicability of these protein-based microtissues for studying cell-matrix interactions. In this study, we demonstrate that (i) cells can interact with the 3D environment both while encapsulated or while interacting only with the surface of the microtissues, (ii) encapsulated cells are highly viable, and (iii) our platform facilitates micropatterned co-culture.

### Innovation

The technology presented in this chapter combines rapid droplet generation with global temperature control to create protein-based microtissues with an easy-to-use

microfluidic device. The microtissues formed with our platform are **composed solely of extracellular matrix protein,** uniform in size, and generated rapidly (>20,000/hour), which facilitates large-scale experiments with large numbers of treatment groups and hundreds of replicates. Our method uses only common laboratory temperatures (4°C and 37°C) and requires no on-chip temperature control or temperature gradients, which means this technology can be easily disseminated and integrated within a high-throughput pipeline. Additionally, we demonstrate novel patterning of cell co-cultures within and around microtissues for controlled studies of cell-cell interactions.

## Methods

*Device fabrication.*

Microfluidic devices were utilized to generate and image microtissues. We fabricated a set of microfluidic devices consisting of a single emulsion droplet generator with a 150 μm nozzle and a microtissue capture device used for imaging, Figure 2.1. To fabricate these devices, we employed soft photolithography of PDMS procedures similar to those described previously[70,71,81–83].

*Cell culture.*

Before encapsulation or adhesion all cells were cultured in tissue treated cell culture flasks and incubated at 37°C with 5% $CO_2$. Endothelial cells were cultured in tissue culture flasks pre-coated with 0.05% collagen. To dissociate cells, flasks were aspirated and washed with HBSS (Gibco), then trypsinized with 0.05% porcine trypsin (Gibco). Media was then added to trypsinized cells and the cell solution was pelleted. Cells were resuspended in serum-free media and were counted using an automated hemocytometer and Trypan Blue (Sigma) to discern viability. Upon counting, cells were added to a solution of unpolymerized collagen and buffered to the desired final concentration. In the case of cells that were used to coat collagen droplets or bulk gels, cells were added to media containing polymerized collagen droplets or bulk gels as described below.

*Microtissue construction.*

Microtissues consisted of collagen I, with or without cells encapsulated within the hydrogel and/or adhered to the hydrogel surface. Microtissue fabrication began with adding either HEPES pH 7 or PBS buffer to high concentration rat tail collagen, type I (Beckton Dixon), to a final concentration of 2, 4, or 6 mg/mL on ice. The pH of the collagen cell solution was then adjusted to 7.4-7.6 pH using 1N NaOH. The solution of 2-6 mg/mL collagen and 8 x $10^5$ cells/mL for cancer cells or 2 x $10^6$ cells/mL for fibroblasts was perfused into the droplet generator inlet at 150 μL/hr, and Fluorocarbon oil (FC-40, Sigma) with 2% EA surfactant was perfused at 1000 μL/hr to produce droplets[71], Figure 2.1. Droplets were formed at 4°C and polymerized for 30 minutes in a 37°C incubator. The final fibroblast concentration in polymerized microtissues (~1.25 x $10^6$ cells/mL) was lower than the initial concentration in the unpolymerized collagen solution due to settling in the syringe coupled to the microfluidic flow-focusing device. Microtissues were collected, washed, and re-suspended in media. Microtissues were then transferred to the droplet capture device, imaged, and incubated for 24-72 hours.

*Dispersity measurement.*

To measure size range of microtissues, oil was aspirated and polymerized microtissues containing 1 μm polystyrene beads were resuspended in appropriate media. Polystyrene beads were used to enhance the image contrast under brightfield microscopy. Microtissues were then transferred to a capture device for imaging, Figure 2.1. An automated image analysis tool was written in ImageJ[84] and used to measure the diameter of each microtissue.

*Viability assessment.*

To determine the viability of encapsulated cells, microtissues were stained with 500 nM propidium iodide and 0.01 mg/mL Hoechst. Microtissues containing cells were resuspended in serum-free media and stained immediately after polymerization to determine viability after microtissue fabrication. Additionally, microtissues coated with fibroblasts (NIH 3T3), breast cancer epithelial cells (SUM 149), or endothelial cells (HUVEC); were stained with 500 nM propidium iodide and 0.01 mg/mL Hoechst to

determine the viability of cells on the outside of microtissues. To assess prolonged viability, microtissues were placed in capture devices with various serum concentrations (0, 1, or 10%) and incubated at 37°C and 5% $CO_2$ for 24-72 hours before staining and imaging several focal planes through the thickness of the microtissues. To quantify viability, maximum projections for each fluorescence channel were calculated using the Extended Depth Of Field plugin in ImageJ[85]. The total cells (from Hoechst) and the number of dead cells (from propidium iodide) were recorded on a microtissue-by-microtissue basis and used to calculate the viability.

*Microtissue co-culture.*

Co-culture was achieved by coating cell-laden microtissues with a second cell type. Triple negative breast cancer cells expressing green fluorescent protein (MDA-MB-231eGFP) were encapsulated in 6 mg/mL collagen microtissues. After polymerization, microtissues were cultured in ultra-low adhesion plates for up to 5 days to allow encapsulated cells time to spread out within microtissues. Approximately 2 x $10^6$ cells of a second cell type were incubated with an average of 500 microtissues overnight in ultra-low-adhesion plates. After incubation, coated droplets were transferred to droplet capture devices and imaged within 24 hours. When coating with human umbilical vein endothelial cells (HUVECs), cells were stained with 5 μM Calcien Deep Red (AAT Bioquest Inc.) to facilitate visualization. MDA-MB-231eGFP microtissues were alternatively coated with SUM 149 (a generous gift from James McCarthy), transfected with mCherry (Clontech) (SUM 149mCherry) for enhanced visualization.

## Results

*Microtissue fabrication.*

A microfluidic flow-focusing device was used to generate collagen pre-polymer droplets suspended in an immiscible, fluoropolymer oil (Figure 2.1). This process was conducted at 4°C to ensure that the collagen solution would not polymerize before being formed into microtissues. The liquid collagen droplets were then collected and incubated at 37°C to facilitate polymerization into microtissue gels, after which polymerized

microtissues were separated from the oil phase. We found that microtissues needed between 15 and 30 minutes of 37°C incubation to polymerize fully (Figures 3.1a and 3.2a). This method generates nanoliter-volume polymerized collagen microtissues very rapidly (>20,000 microtissues/hour), and they can be generated with or without encapsulated cells.

*Microtissue characterization*.

One of the primary advantages of using microfluidic flow focusing is the low polydispersity among the droplets. To quantify the polydispersity in our microtissue populations, we collected polymerized microtissues and quantified their diameters from images similar to those in Figure 3.1a. For a large population of microtissues (n = 591), a histogram of the diameters was created (Figure 3.1b). We observed a narrow distribution of size with a coefficient of variance ranging from 8.4% - 13.9%. This size variance is sufficiently small that it does not interfere with subsequent analyses. Throughout our trial, we found that 1.2% - 1.8% of droplets coalesced into doublets or triplets before polymerization. This population, however, did not influence later analysis as the geometry of the droplet capture devices excluded these larger microtissues based on size.

*Viability of encapsulated cells.*

High cell viability is imperative for conducting biological assays with any *in vitro* platform. As shown in Figure 3.2, we quantified the viability of MDA-MB-231eGFP breast mammary carcinoma cells encapsulated within our microtissues. Cell viability was quantified immediately after microtissue polymerization, and after 72 hours of incubation with various serum concentrations. We observed that the viability of encapsulated MDA-MB-231eGFP cells were consistent throughout the experiment period. The initial viability was high (greater than 90%) (Figure 3.2c), and the extended viability of these cells fluctuated at most by 6% at the end of the 72-hour incubation.

*Matrix interactions.*

To demonstrate our ability to study cell-matrix interactions within our protein-based microtissues, we studied the morphology of breast carcinoma cells, and we quantified the ability of fibroblasts to contract microtissues. As shown in Figure 3.2a, over 72 hours in culture, we observed that encapsulated MDA-MB-231eGFP cells were able to spread out and send projections throughout the collagen matrix. This change in morphology indicates that these cancer cells can to adhere and interact with the 3D environment of the collagen microtissue.

*Coating microtissues with cells*

Another method to incorporate cells with the microtissues is to coat the surface of the constructs. We fabricated acellular microtissues with fluorescent beads to denote the microtissue borders. A single cell suspension of fibroblasts was collected and cells were added to a microfluidic droplet capture device along with collagen microtissues. After 24 hours of culture, we observe that fibroblasts adhere to the surface of the microtissue constructs (Figure 3.3). We observe that cells added to the surface of constructs remained on the surface and did not migrate towards the center of the microtissues within the first 24 hours (Figure 3.3).

*Microtissue co-culture*.

The small size of the microtissues (~100-300 μm) enables a novel method for patterning multiple cell types in 3D. Here, we demonstrate that we can separately encapsulate one cell type within the microtissues while coating the microtissue surface with a separate cell type (Figure 3.4). To illustrate this versatility, we first encapsulated MDA-MB-231eGFP cells within 6 mg/mL collagen droplets. We then seeded calcein-stained HUVECs or SUM 149mCherry (Figure 3.4) cells on the outside of each droplet as described in the methods. After overnight incubation, microtissues were stained with Hoechst and imaged on a confocal microscope. Figure 3.4a depicts where slices for subsequent images were located within the microtissue and Figure 3.4b shows DIC images taken at these locations within the droplet. In Figure 3.4c, Hoechst staining of cell nuclei demonstrates that cells cover the microtissue and Figure 3.4d shows that the

second cell type adhered to the outer surface of microtissues. Figure 3.4e demonstrates that the majority of MDA-MB-231eGFP cells are found within the microtissue and not on the surface. An overlay of each color channel in both the top and middle of the microtissue demonstrates were able to conduct co-cultures with our microtissues. We quantified the viability of cells coating the surface of the microtissues, which was 72% for endothelial cells (HUVECs) and 81% for breast carcinoma cells, similar to numbers obtained for fibroblasts.

Discussion

Here we present an easy-to-use method to rapidly fabricate collagen microtissues using a microfluidic flow-focusing device. With our method, we produce monodisperse collagen microtissues. These microtissues are composed entirely of natural ECM, making them an interesting tool to study cell-matrix interactions and matrix remodeling in a high-throughput manner. Additionally, since we can produce large quantities of microtissues (20,000/hour), the sample sizes in our experiments (n>>25) can be much larger than typical studies with collagen hydrogels (n<=5), supporting robust statistical analysis across experimental conditions.

After optimizing the fabrication process, we examined the cell behavior to ensure high cell viability and expected cell interactions with the collagen matrix. We found the cells had high cell viability in our constructs, and that cells spread out and explored the collagen matrix with long protrusions shortly after encapsulation. This demonstrates that the cells do not only tolerate our fabrication method, but that they thrive in this 3D environment.

Finally, we explored controlling the placement of cells in our constructs. We demonstrated that we could coat just the surface of the microtissues, or use a combination of encapsulating and surface-coating to co-culture cells. This micropatterning of cells in our constructs creates exciting opportunities to examine cell-cell interactions in a 3D environment in future studies.

With this validation of our platform, we began to explore novel readouts and applications that our platform is uniquely suited to address. The following chapters

describe these assays and applications in detail, beginning first with the adaptation of a standard assay to assess fibroblast contractility in 3D.

Acknowledgements

We would like to thank Paolo Provenzano for discussions on collagen–cell interactions and donation of reagents; Daniel Tschumperlin for discussions regarding potential applications of this platform; James McCarthy and Wei Shen for donating cells used in this study; and a special thanks to Geneva R. Doak for her assistance. We would also like to thank the Minnesota Nanofabrication Center for fabrication support. We acknowledge funding from the American Heart Association under Scientist Development Grant 13SDG6450000, and Alexandra L. Crampton was supported by the National Science Foundation Graduate Research Fellowship 00039202. Alexandra L. Crampton and Marie-Elena Brett performed experiments collaboratively.

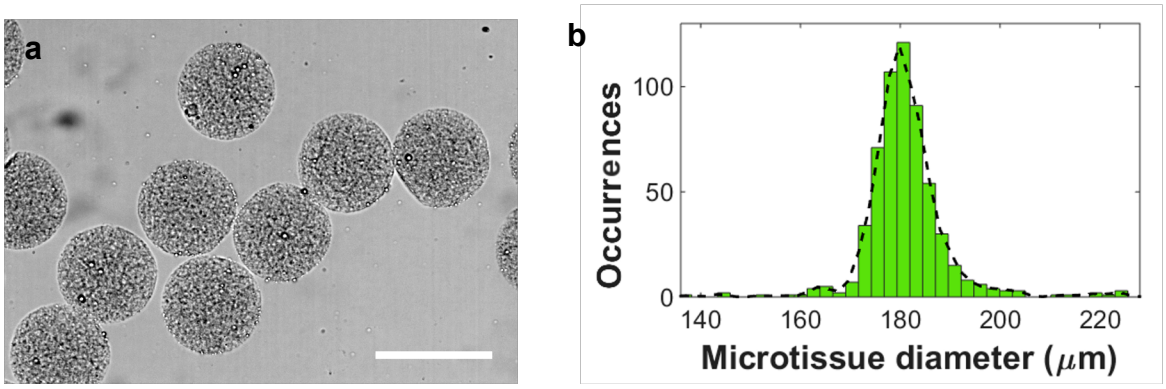


**Figure 3.1** ***Polymerized collagen droplets***

(a) Brightfield image of collagen droplets. Scale bar 300 μm. (b) Histogram of droplet diameters with mean diameter of 182 μm (n=591) and a CV of 8.4% with a smooth histogram (kernel smoothing function) overlaid.

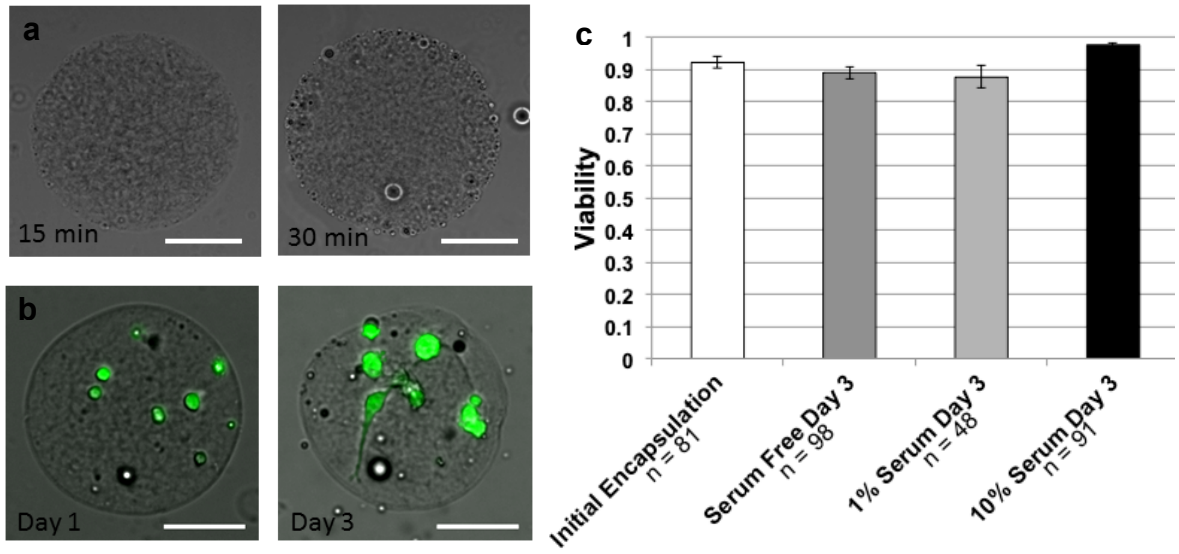


**Figure 3.2.** ***Collagen polymerization and cancer cell viability***

(a) Collagen droplets were generated at 4°C and placed in a 37°C incubator. Aliquots of droplets were removed every 15 minutes and imaged to determine polymerization. (b) Images of MDA-MD-231eGFP immediately following microtissue resuspension in media, and after 3 days in of culture. Scale bar denotes 100 μm. (c) MDA-MB-231eGFP cells were encapsulated in 6 mg/mL collagen microtissues. The cell viability was assessed with propidium iodide/ Hoescht staining and quantified on a microtissue-by-microtissue basis. The average microtissue viability is reported with standard error for various growth conditions. Population sizes are reported for each condition.

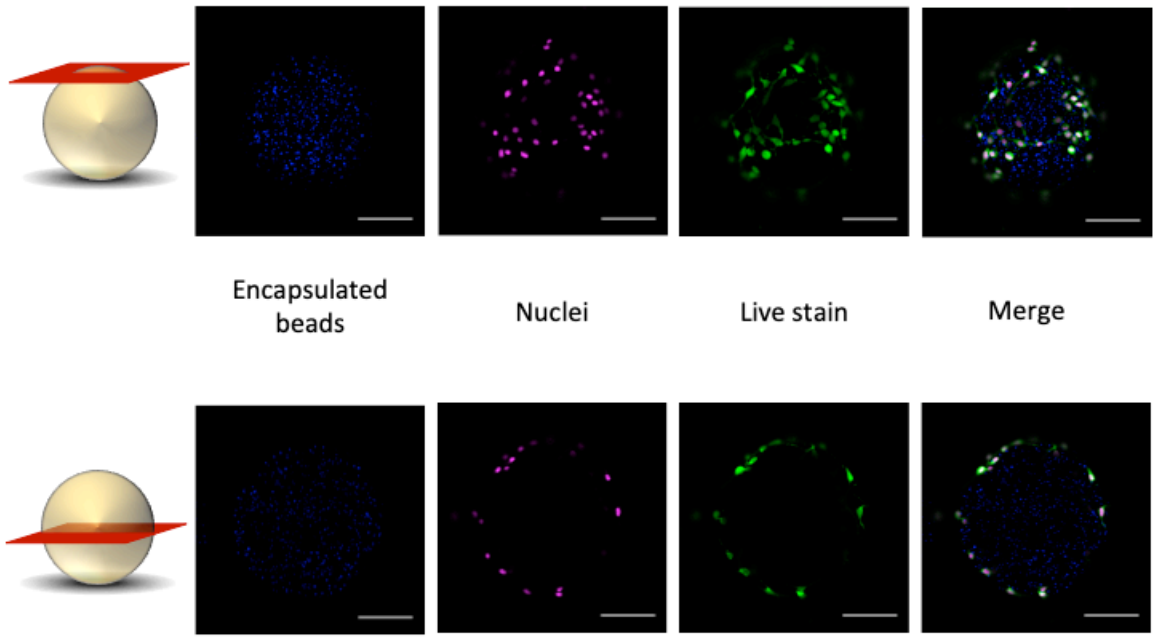


**Figure 3.3:** ***Optical sectioning demonstrates surface coating of microtissues***

Acellular 6 mg/mL collagen constructs with 1 μm fluorescent beads (blue) were fabricated and collected in PBS. NIH 3T3 cells were seeded on the surface of the microtissues in DMEM with 10% FBS. Constructs were cultured for 24 hours before staining with DRAQ5 to label the nuceli (magenta) and calcein AM to label the live cells (green). With confocal imaging we examine optical sections near the top and middle of the constructs, demonstrating that surface-coated cells adhere to the surface of our collagen microtissues. Scale bars are 100 μm.

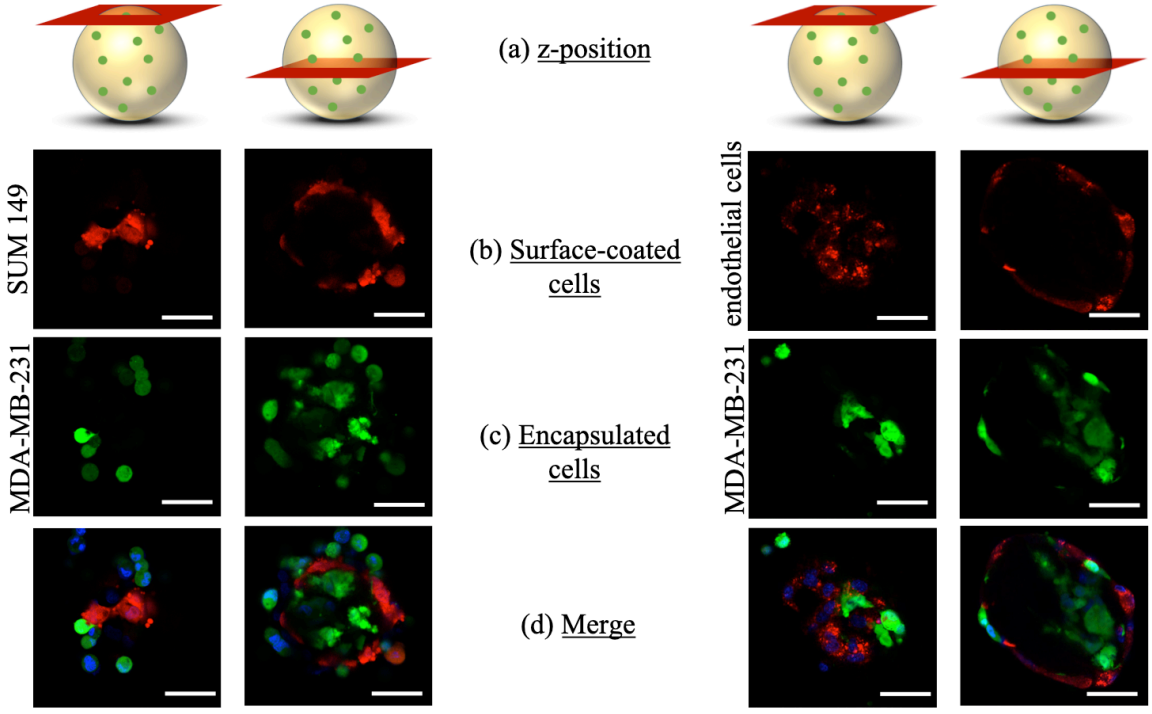


**Figure 3.4:** ***Cell seeding of microtissues***

Cells were encapsulated and / or seeded on the exterior of collagen hydrogels and imaged using a confocal microscope. (a) Schematic of where image slices are located within the droplet. (b) mCherry florescence from SUM 149 mCherry cells or Deep Red Calcein staining of endothelial cells. (c) GFP expression of encapsulated MDA-MB-231eGFP cells. (d) All fluorescent channels over-laid. Scale bar is 50 µm.

## ***Chapter 4: Application – A miniaturized contraction assay***

This chapter contains material from "Rapid generation of collagen-based microtissues to study cell–matrix interactions" by Alexandra L. Crampton*, Marie-Elena Brett*, and David K. Wood. *Technology, The Journal*, volume 4, issue 2, pages 80-97, 2016; permission conveyed through Copyright Clearance Center, Inc. *These authors contributed equally.

### Introduction

There is an unanswered demand for physiologically relevant model systems that improve drug development and depart from traditional cell culture to incorporate cell-ECM interactions and recapitulate ECM remodeling. Three-dimensional cell culture has begun replacing 2D model systems as they are better mimics of the *in vivo* environment. By reducing systemic artifacts due to substrate geometry[12,86,87], stiffness[88–91], and availability of cell-ECM interactions[92–94], these 3D platforms show increased predictive power and improved functional utility when screening for therapeutic efficacy. Furthermore, due to increased interest in studying tissue-level diseases that involve cell-ECM interactions and ECM remodeling (development of cancer[28–30], fibrosis[28,31,32], and autoimmune disease[31,33,34]), there is a need for improved 3D cell culture tools and workflows that support cell-ECM interactions and remodeling.

The current gold-standard *in vitro* model system of 3D wound healing, remodeling, and contraction is the contraction assay, invented by Bell et al. in 1979[95]. In this assay, large cell-laden collagen I gels are polymerized and cells are cultured within the hydrogels. As cells remodel the matrix, the hydrogel contracts and changes in the overall tissue geometry can be quantified. The rate and extent of matrix contraction and remodeling in these contraction assays has been further studied, revealing the influence of co-culture and ECM proteins in these 3D culture systems[96–98]. The mechanical properties of the gel also affect cell contractility, as not only gel density, but also the loading state of the gel (attached to the sides of the container, or free-floating) affects the amount of gel contraction.

These variations of the contraction assay have several advantages – they provide a 3D environment for the cells, the procedures are compatible with cell viability and also cell function, and the systems are highly tunable (as far as gel concentration and exact ECM composition). There are some limitations for these assays, though, because of the large size of the hydrogels. Collagen gels for contraction assays are typically cast in 24-well or 6-well plates, requiring 0.5-2 mL of collagen solution per replicate. These large volumes are expensive in terms of reagent use (especially for high concentration gels), but also limit the number of replicates for experiments as the number of cells required scales linearly with the volume of the gels. For studies interested in large-scale screens or using small patient samples (e.g. tumor biopsies), these large volumes are prohibitive. Additionally, the large volumes mean large geometries, which introduces an issue with diffusion into the gel of oxygen and nutrients, and also challenges with imaging as the tissues are thick (>1 mm). To use a 3D contraction assay for high-throughput screening, this issue of the large volume, large cell requirements, and large geometries needs to be addressed.

Our objective for this study was to create a method for studying cell-matrix interactions in a physiologically relevant 3D protein-based tissue construct that could be scaled up to perform large-scale screens and study cell-matrix interactions on a population basis. We have previously (Chapter 3) developed an easy-to-use method to miniaturize protein-based tissue constructs that maintains the 3D *in vitro* environment, while alleviating several obstacles associated with larger avascular tissue constructs. In this study, we demonstrate – for the first time to our knowledge – that microtissues on this size scale (~200 μm) can be used to quantify cell contractility. This assay highlights the value of miniaturization, as our large population sizes support robust statistical analysis. This versatile platform should facilitate large-scale screens in 3D *in vitro* culture conditions for drug development and high-throughput mechanistic biology.

Methods:

*Cell Culture*

Before encapsulation or adhesion all cells were cultured in tissue treated cell culture flasks and incubated at 37°C with 5% $CO_2$. To dissociate cells, flasks were aspirated and washed with HBSS (Gibco), then trypsinized with 0.05% porcine trypsin (Gibco). Media was then added to trypsinized cells and the cell solution was pelleted. Cells were resuspended in serum-free media and were counted using an automated hemocytometer and Trypan Blue (Sigma) to discern viability. Upon counting, cells were added to a solution of unpolymerized collagen and buffer to the desired final concentration. In the case of cells that were used to coat collagen droplets or bulk gels, cells were added to media containing polymerized collagen droplets or bulk gels as described below

*Microtissues for Contraction Assay*

Microtissues were fabricated following the protocol described in Chapter 3. To measure contraction of microtissues coated with fibroblasts, 0.05% 1 μm diameter FITC beads were encapsulated in collagen to allow visualization of microtissue borders. After polymerization, droplets were resuspended in PBS and stored at 4°C. Droplet capture devices were loaded with droplets and ~250,000 NIH-3T3 fibroblasts in either serum-free or 10% serum growth medium. To isolate the change in shape due only to cell-ECM interactions, droplet capture devices without cells were also loaded and used to measure the initial size of the droplets, as cells began contracting microtissues immediately upon addition to the device and introducing cells after time zero imaging deformed the microtissues. Droplet capture devices were imaged immediately after the addition of cells, as well as after 24 hours of incubation.

*Bulk Gel Fabrication and Analysis*

To fabricate collagen bulk gels for comparison, collagen of varying concentration (2, 4, or 6 mg/mL) was mixed with buffer on ice and 1N NaOH was added until collagen reached a pH within the range of 7.4-7.6. A single cell suspension was added to the collagen before polymerization. Bulk gel fabrication was similar to microtissue fabrication, except the volume required to produce bulk gels was significantly larger (with each experiment requiring ~1.5 mL solution rather than 400 μL to create two orders

of magnitude more microtissues). Cell-laden bulk gels were cast in 96 well plates and allowed to polymerize for 30 minutes. Serum-free media was then added on top of the gels before they were carefully floated and transferred to a 24 well plate. Gels were imaged before adding serum to any of the serum-containing conditions to prevent any serum-induced contraction in initial measurements. Gels were incubated for 24 hours and imaged again. For each experiment, acellular gels were included as negative controls. Each trial was conducted in triplicate and repeated three times. Area measurements were made identically to trials of corresponding microtissues (gels were outlined and area was quantified on a gel-by-gel basis).

To measure contraction of bulk gels coated with fibroblasts, collagen solutions of various collagen concentration with 0.05% 1 μm FITC beads were made similarly to microtissues, but with increased volume. Acellular gels were cast in 96-well plates and polymerized for 30 minutes before gels were floated and transferred to 24 well plates. Gels were imaged before adding ~500,000 fibroblasts/mL media in the plate. After 24 hours incubation, gels were imaged again and the area for both time points was measured. Experiments were repeated three times in triplicate.

*Quantification of Cell Contraction*

Brightfield images were used to identify the area of 2, 4, or 6 mg/mL collagen microtissues containing NIH-3T3 fibroblasts immediately after microtissue polymerization and after 24-hour incubation with or without 10% serum treatment. To quantify contraction, each droplet was outlined by hand in a single-blind analysis, and the area within the outline was measured and recorded. To measure contraction in cell-free microtissues coated with NIH-3T3 fibroblasts, emission from encapsulated fluorescent beads was used to measure the projected area of the droplets, thus excluding any bias in size based on the number or diameter of cells attached to the droplets. An automated image analysis tool was written in ImageJ and used to measure the diameter of each microtissue defined by encapsulated FITC beads. The relative change in area between experimental conditions was compared. The coefficient of variation (CV) was determined from these measurements.

*Statistical Analysis*

The relative difference in microtissue area (contraction) was compared using t-tests or ANOVA with Bonferroni correction. Experimental replicates were analyzed separately, and p-values $<0.05$ were considered statistically significant.

Results

To quantify cell-matrix interactions, we measured contraction of the collagen microtissues by fibroblasts (Figure 4.1a). We constructed hydrogel droplets of varying initial collagen concentrations (2-6 mg/mL) and either encapsulated or coated hydrogels with NIH-3T3 fibroblasts to quantify contraction in two ways with our microtissues. For these experiments, we encapsulated the cells inside the tissues or coated the tissues with cells under serum-free conditions, followed by 24-hour incubation with serum to induce contractility. Figures 4.2a-c show images of individual microtissues coated with fibroblasts before and after treatment with serum at three different initial collagen concentrations and controls not treated with serum. The images clearly show that cells incubated with serum were able to contract the microtissues more than their serum-free counterparts. The images also reveal that the amount of microtissue contraction decreased as initial collagen concentration increased. As shown in Figure 4.2e,f, in which projected microtissue area is quantified, these trends are consistent for the case of cells encapsulated within or coated on the microtissues. The largest contraction was observed for 2 mg/mL initial collagen concentration tissues, in which the average microtissue area decreased by 23% and 40% for encapsulated and coated cells, respectively. The smallest contraction was observed for 6 mg/mL collagen tissues, in which the average area decreased by 10% for coated cells and no significant change was seen with encapsulated cells. We note that the collagen concentrations reported are only the initial concentration, and the concentration is increasing as the cells contract the microtissues, which has been reported previously[99].

To compare these results with traditional assays, we performed identical experiments on large gel constructs (~6 mm diameter), and the results are shown in

Figure 4.2e,f. The observed trends for bulk gels were the same as for microtissues as well as previously published results[53–55,95]. Thus our microtissue platform is able to recapitulate the results from the standard bulk gel assays while simultaneously decreasing labor and time for gel fabrication, simplifying imaging and analysis, and improving the statistical robustness of the results.

We also tested the hypothesis that the trends in cell contractility as a function of initial collagen concentrations were due to differences in cell viability. We quantified fibroblast viability immediately after polymerization and after 24 hours incubation, to mimic the culture conditions of the contraction experiments. As shown in Figure 4.1b, fibroblast viability was initially high in all conditions (79%-95%), and fluctuations in viability were not statistically significant over the 24-hour incubation period. Because cell viability was consistent throughout the experimentation period (Figure 4f), differences in contraction among initial collagen concentrations were not attributed to cell death. Instead, we attribute these trends to inhibition of contraction in the higher concentration collagen matrices. We also attempted to quantify cell viability for cells encapsulated in bulk gels, but the increased diffusion time for the dyes due to the larger size of bulk gels limited our ability to uniformly stain the gels before cell death was induced by the dyes. Overall, the combination of high cell viability in the microtissue culture and the ability of cells to contract the collagen matrices support the goal of this platform to be used to study cell-matrix interactions.

A specific application of this type of assay would be to screen compounds and assess changes in contractility in response to treatments. As a proof-of-concept, we tested our platform with Fasudil (a Rho-kinase inhibitor) and Blebbistatin (a Myosin II inhibitor) to determine if our assay could be used to detect inhibitors of compaction. We fabricated acellular 4 mg/mL collagen microtissues containing 1 μm fluorescent beads, and coated these tissues with highly contractile human lung fibroblasts (HLF 240). Inhibitors and cells were both added at t=0, and constructs were observed at several timepoints for 24 hours (Figure 4.3). We found that for microtissues treated with Fasudil (Figure 4.3a), statistically significant inhibition of compaction ($p<0.05$) was apparent after 2 hours and remained significant after 24 hours ($p<0.0001$), with the final difference

in compaction being 32.0% +/- 5.2%. For the Blebbistatin group (Figure 4.3b), very statistically significant inhibition of compaction was observed after 24 hours ($p<0.0001$), with the final difference in compaction of 23.6% +/- 6.5%. The large dynamic range of this selected screen is promising for the use of this assay for larger-scale screening for discovery of inhibitors of contraction and matrix remodeling.

Discussion

Our goal in the development of this platform was to overcome the limitations of typical bulk gel assays and make 3D tissue culture more amenable to high-throughput screening applications. These protein-based microtissues are well suited to high-throughput screening because they can be rapidly generated, analysis can be automated, and comparisons can be made across uniform populations. Further, the miniaturization of the gels causes no limitations in the potential applications, as the cells can fully interact with and even remodel the matrix. We have demonstrated that with our method, encapsulated cell viability is high (80-98%) and is maintained throughout extended incubation periods, and that behaviors observed in bulk gels (e.g. contraction, spreading) are also observed in our smaller-scale hydrogels. A major advance over bulk gel experiments is that the large numbers of microtissues lead to high statistical power in the results. Moreover, because our growth conditions are compatible with standard cell culture equipment (e.g. multi-well plates), this method could be scaled up even further and be integrated with automated liquid handling systems and automated imaging platforms. We demonstrate that cancer cells, endothelial cells, and fibroblasts can interact with our collagen microtissues – both while encapsulated and while coating the surface of the droplets – which allows for novel co-culture applications where the physical and chemical interactions between cell types can be controlled. Overall, this platform recapitulates the functions of traditional protein-based bulk gels but extends application to high-throughput studies and opens up new possibilities for interrogating cell-cell and cell-matrix interactions.

We demonstrate that we can quantify cell-matrix interactions in our microtissues, including cell spreading and contractility, across large numbers of microtissues, which

lends itself to high-throughput studies and robust statistical analysis. We use serum to induce contraction as this phenomenon has been widely observed[99–102], with lysophosphatidic acid and platelet-derived growth factor thought to be important serum components for inducing cell contraction[100,102]. Encapsulated carcinoma cells and fibroblasts were able to spread within the gels and engage the matrix, and encapsulated fibroblasts were able to significantly contract the microtissues when stimulated with 10% serum. We observed the highest level of gel contraction (25%) at the lowest collagen concentration (2 mg/mL), and the amount of contraction decreased as the collagen concentration increased, with no discernible contraction in the 6 mg/mL microtissues, which agrees with existing trends for bulk gel contraction assays[53–55,95]. These findings are also in line with bulk gel experiments performed in this study, demonstrating reproducibility of the results between our assay and the standard bulk gel assays. We verified that the differences observed in contraction between initial collagen concentrations was not due to cell death, as the viability of these microtissues was high and consistent throughout the observation period. We attribute the decrease in contraction in the higher concentration gels to the increased density of collagen fibers. Although the cells are viable and can interact with fibers in the higher density collagen microtissues, either the force exerted by the cells and/or the strength of the cell-matrix linkage is insufficient to generate matrix reorganization. This finding agrees with previous studies showing that tensional homeostasis in cells works over a limited stiffness range, where extremely soft substrates do not engage cytoskeletal reorganization and contractility, while extremely stiff substrates present mechanical forces that cannot be overcome by the cells[103–106].

Additionally, initial collagen concentration has been shown to affect both the rate and the total amount of contraction[95,107]. Previous studies show that fibroblasts encapsulated within a collagen matrix are able to contract a less dense matrix faster[95]. Although the rate of contraction and the difference in contraction rates between different matrix concentrations decrease over time, gels with a lower initial collagen concentration demonstrate increased overall contraction[95,107]. This suggests the initial matrix concentration itself is able to modulate the total amount of contraction[107]. Further study

of the underlying mechanism of this behavior shows that the viscoelastic properties of a collagen hydrogel are dependent on the initial collagen concentration[108]. This viscoelastic model, initially proposed by Moon and Tranquillo, suggests that cells are able to apply traction forces on the collagen network by pulling collagen fibrils into proximity using pseudopods[108]. The reduction in gel area measured is driven by these cell traction forces which are dependent on the viscoelastic properties of the collagen hydrogel and thus the initial collagen concentration[108]. To the authors' knowledge, this is the first demonstration that individual microtissues with encapsulated fibroblasts can be used to quantify gel contraction, which is a gold standard for assessing fibroblast contractility and matrix reorganization[53,95].

The results from this study implicate the potential for microtissues composed solely of ECM proteins for high-throughput screening applications. One potential application of this platform is in the development of anti-fibrotic agents. It is widely known that fibroblast contraction of the extracellular matrix is highly relevant to increased fibrosis in diseases such as peritoneal fibrosis and that this contraction is mediated by RHO kinases[109]. Peritoneal fibrosis is common in long-term kidney dialysis patients, as peritoneal dialysis stimulates the production of TGF-β and TGF-β plays a fundamental role in fostering fibrosis[110]. One method to abrogate the development of fibrosis in dialysis patients is to inhibit RHO-kinase, and the RHO-kinase inhibitor Fausidil has been shown to diminish fibrosis clinically[110]. The development of such therapies, however, requires high-throughput screening for compounds that can inhibit contractility. Although such a screen would be time and cost prohibitive using bulk gels, it could easily be accomplished using this platform. Our system is capable of generating 2 mg/mL collagen droplets at rates of >20,000 droplets per hour. Given the 0.354 coefficient of variation for contractility in our 2 mg/mL collagen droplets, we would only need 25 microtissues in each treatment group to achieve a statistical power of more than 80%. With 10 devices in parallel for 2 hours, we could test 12,000 unique compounds. Moreover, all of the tissues are batch polymerized and could be automatically dispensed and treated using robotic liquid handlers, thus allowing all treatment types,

concentrations, and controls to be performed in a relatively short period of time with high statistical power.

These microtissues are also ideal for cancer drug discovery and high-throughput cancer biology. Using the same workflow as described above, this platform could be used to test the efficacy of small molecule therapeutics on tumor cell proliferation and viability. Alternatively, new therapeutic targets could be discovered using protein knockdown with RNA interference or gene editing. Additionally, our microtissues have applicability outside the use as individual culture vessels; rather, our rapid generation method could be used to enhance existing methods to 3D print cell-laden collagen tissues[111], serving as the base for quick construction of increasing complex tissue constructs. This could even include larger vascularized tissue constructs, which has applications in the study of cellular behavior *in vitro* as well as translational potential in regenerative medicine. Overall, this is a highly versatile platform for 3D cell culture that is engineered to facilitate quantitative studies of drugs, cellular interactions, and biological mechanisms in high-throughput applications.

Acknowledgements

We would like to thank Paolo Provenzano for discussions on collagen–cell interactions and donation of reagents; Daniel Tschumperlin for discussions regarding potential applications of this platform and for donating cells used in this work; and Wei Shen for donating cells used in this study. We would also like to thank the Minnesota Nanofabrication Center for fabrication support. We acknowledge funding from the American Heart Association under Scientist Development Grant 13SDG6450000, and Alexandra L. Crampton was supported by the National Science Foundation Graduate Research Fellowship under Grant No. 00039202. Alexandra L. Crampton and Marie-Elena Brett performed experiments collaboratively for text and content related to Figures 4.1 and 4.2.

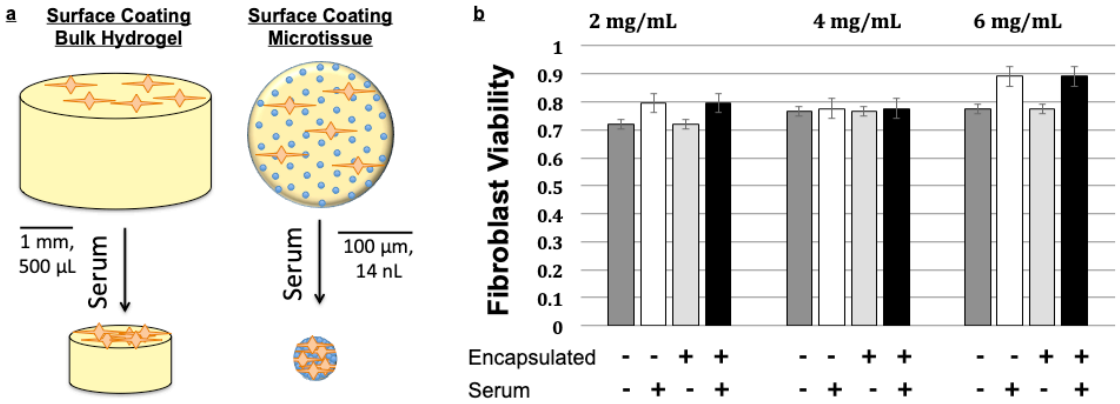


**Figure 4.1:** ***Scaling down the contraction assay for collagen microtissues***

Traditional contraction assays use large volume hydrogels to assess cell contractility. Cells can either be encapsulated in the hydrogel (not shown) or coated on the surface of an acellular hydrogel (a), both resulting in a decrease in gel volume and projected area. Our scaled-down version of this assay (a) follows the same workflow, with the addition of encapsulated fluorescent beads to clearly distinguish the projected area of the microtissues. This system is compatible with a wide range of cell types, and for this study we focus on fibroblasts as they are highly contractile cells. We confirmed that NIH-3T3 cells in both the encapsulated and surface-coated configurations for all collagen concentrations and growth conditions used in this study are highly viable after 24 hours of culture (b).

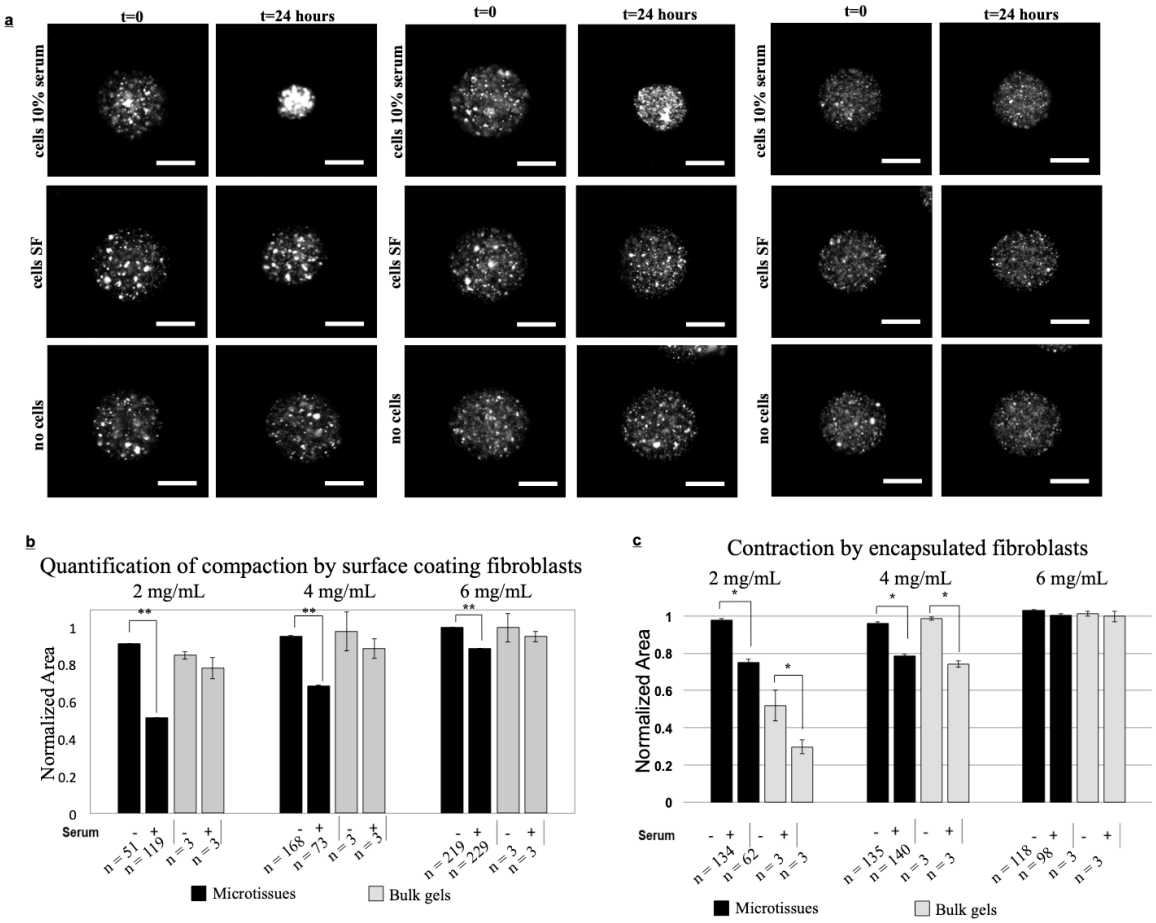


**Figure 4.2:** ***Fibroblast contraction of collagen***

(a-c) Fluorescent images of 2 mg/mL (a), 4 mg/mL (b), or 6 mg/mL (c) collagen microtissues containing 1 µm FITC beads and coated with NIH 3T3 fibroblasts. Microtissues with no cell coating, cell coating in serum-free media, and cell coating with media containing 10% serum were cultured for 24 hours. Scale bars 100 µm. (d) Changes in projected area for large droplet populations were measured and the population change in microtissue area is reported with standard error. Three experimental replicates were examined for each condition. For fibroblasts encapsulated in collagen droplets (d), the difference in contraction was statistically significant ($p \leq 0.01$) in 2 mg/mL trials, and for two of the three replicates the difference was very statistically significant ($p<0.0001$). For all of the 4 mg/mL trials, the difference in contraction was statistically significant ($p<0.05$). For the 6 mg/mL trials of encapsulated fibroblast microtissues, none of the differences in contraction were statistically significant. For all concentrations of

collagen of microtissues coated with fibroblasts (e), the difference in contraction was very statistically significant ($p<0.0001$) with n values of n = 51, 168, and 219 and n = 119, 73, and 229 for trails of 2, 4, or 6 mg/mL microtissues in serum-free or 10% serum media respectively. For Bulk gel examination (d,e) n =3 for each trail of coated and encapsulated fibroblasts, three individual trials were performed for each condition. + signifies that the data above was collected from trials containing microtissues, encapsulated fibroblasts, or 10% serum in media. Population sizes for all microtissue trials were $n \geq 62$.

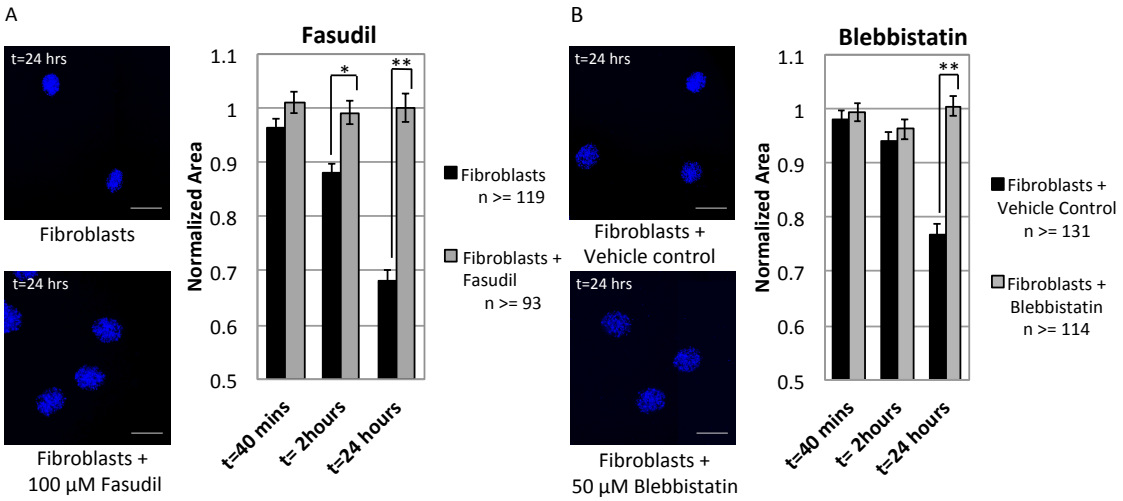


**Figure 4.3:** ***Fasudil and Blebbistatin inhibit compaction of microtissues***.

Fluorescent images of 4 mg/mL collagen microtissues containing 1 µm fluorescent blue beads and coated with HLF 240 fibroblasts in DMEM with 10% serum. Microtissues were then treated with (a) 100 µM Fasudil or (b) 50 µM Blebbistatin with a DMSO vehicle control. Representative images for each condition after 24 hours of treatment are displayed (scale bars = 200 µm). Changes in projected area for large droplet populations were quantified and the population change in microtissue area is reported with standard error. For microtissues treated with Fasudil, statistically significant inhibition of compaction was apparent after 2 hours ($p<0.05$, denoted by *), as well as after 24 hours ($p<0.0001$, denoted by **). For microtissues treated with Blebbistatin, very statistically significant inhibition of compaction was observed after 24 hours ($p<0.0001$).

## ***Chapter 5: Adaptation of the microtissues platform for long-term studies of ECM remodeling***

This chapter contains material from "A High-Throughput Workflow to Study Remodeling of ECM-Based Microtissues" by Alexandra L. Crampton*, Katherine A. Cummins*, and David K. Wood. *Tissue Engineering Part C: Methods*, volume 25, issue 1, pages 25-36, 2019; permission conveyed through Mary Ann Liebert, Inc., New Rochelle, NY. *These authors contributed equally.

### Overview

Changes to the cellular microenvironment are an integral characteristic of numerous pathologies including cancer, fibrosis, and autoimmune disease. Current *in vitro* methodologies available to study 3D tissue remodeling are ill-suited for high-throughput studies as they are not scalable for large-scale experiments. Combining droplet microfluidics and patterned low-adhesion culture surfaces, we have engineered a workflow to incorporate cell-ECM interactions in a versatile and high-throughput platform that is compatible with existing high-throughput liquid handling systems, enables long-term experiments (>1 month), and is well-suited for traditional and novel biological measurements. With our platform, we demonstrate the feasibility of high-throughput ECM remodeling studies with collagen microtissues as one application of a tissue-level function. In this study, we use our workflow to examine ECM remodeling at the tissue, cell, and subcellular levels, leveraging assays ranging from immunohistochemistry and live-cell imaging, to proliferation and contraction assays. With our unique culture system, we can track individual constructs over time and evaluate remodeling on several scales for large populations. Using these methods, our ECM-based system becomes a viable platform for modeling diseases characterized by tissue reorganization as well as a scalable method to conduct *in vitro* cell-based assays for drug screening and high-throughput biological discovery.

Impact Statement

The described microtissue-microwell workflow is uniquely suited for high-throughput study of ECM remodeling at the molecular, cellular, and tissue-levels and demonstrates possibilities of studying progressive, heterogeneous diseases in a way that is meaningful for drug discovery and development. We outline several assays that can be utilized in studying tissue-level diseases and functions that involve cell-ECM interactions and ECM remodeling (e.g. cancer, fibrosis, wound healing) in the pursuit of an improved 3D cell culturing system.

Introduction

Alteration to extracellular matrix (ECM) composition and organization is a key hallmark of several diseases including cancer[28–30], fibrosis[28,31,32], and autoimmune disease[31,33,34]. The ECM not only provides structural support and enables cell-ECM signaling but acts as a reservoir for endogenous growth factors[112–115], behaves as a barrier to therapy[116–118], and participates in generation of bioactive protein fragments involved in diseased state cell signaling[119,120]. Furthermore, these pathologies progress and evolve over time, and tissue disorganization requires prolonged periods to fully develop. Mechanisms that involve cell-ECM interactions and remodeling over time are prominent in cancer, fibrosis, and autoimmune research and are favored targets for drug development however there remains an unmet need for model systems that could be used in the initial stages of drug development at a tissue level[121,122]. Further, ECM remodeling is difficult to visualize and quantify especially in the case of degenerative disease as these timescales can be difficult to recapitulate *in vitro*, revealing a need for platform that is compatible with high-throughput screening and retains complex cell-cell, cell-ECM, and architectural cues while enabling quantification of cell behavior over time.

Current *in vitro* methodologies available to perform high-throughput and long-term culture studies include both standard two-dimensional culture and spheroids[12,123–125] but they are ill-suited for probing the mechanisms of matrix remodeling as they lack an ECM component[126,127]. Platforms that are more appropriate for addressing these questions exist, however fabrication is rate limiting and handling is time consuming,

ultimately reducing sample size and preventing use for high-throughput applications. The most relevant examples are large hydrogels and microfluidic model systems. Hydrogels allow for incorporation of ECM proteins and are compatible with automated liquid handling systems, but they require substantial volumes of matrix and cells, elevating cost and reducing throughput with finite cell sources. Furthermore, these gels are often so large they are: 1) limited by diffusion, reducing nutrient transport and constraining staining choices[57,128], and 2) restricted in compatible imaging modalities[58–60]. Microfluidic devices meanwhile provide opportunities to incorporate spatial organization, can integrate multiple matrix proteins, and require smaller reagent volumes than other methods[129–131]. However, these platforms depend on consistent tissue geometry to maintain complex flow patterns, development of chemical gradients, and the ability to track movement of cells over time, making compaction to physiologically relevant ECM densities difficult to study. In addition, chip scalability is limited even with advanced device design, indicating a persistent need for high-throughput ECM remodeling platforms.

Leveraging droplet microfluidics, we have previously demonstrated use of protein-based microtissues for high-throughput, short-term studies of cellular phenotypes and interactions with ECM[132,133]. To expand the capabilities of our microtissue platform, we engineered a workflow that couples microtissue fabrication with culture in patterned agarose microwells in a manner that is compatible with existing liquid handling techniques, enables long-term experiments (>1 month), and is well-suited for several traditional and novel biological measurements. Here we demonstrate compatibility of our long-term ECM-based culture platform with several molecular, cellular, and tissue level measurements to assess cell phenotype and function (Figure 5.1). In this study, we focus on ECM remodeling as a tissue level function that is quantifiable in our platform and is highly relevant to developing therapeutics for cancer, fibrosis, and autoimmune disease. We demonstrate that we can quantify local and global compaction, reversible and irreversible remodeling, and heterogeneity in compaction rates of individual microtissues. Using these methods, our ECM-based system becomes a viable platform for modeling

diseases characterized by tissue reorganization as well as a scalable method to conduct *in vitro* assays for drug screening and high-throughput biological discovery.

## Materials and Methods

### *Cell culture*

Normal human lung fibroblasts (NHLF) were cultured in FGM-2 (Lonza) supplemented with 1x antibiotic-antimycotic and used between passage 3 and 7. National Institute of Health 3T3 (NIH 3T3) cells were cultured in Dulbecco's Modified Eagle Medium (DMEM) with 10% fetal bovine serum (FBS) and 1x antibiotic-antimycotic and were used between passage 15 and 20. MDA-MB-231 cells were cultured in the same DMEM-based media and used at passage 9. Lastly, human umbilical vein endothelial cells (HUVEC) were cultured on gelatin coated flasks in EGM-2 (Lonza) and used at passage 2. Cells were released from flasks with 0.05% trypsin-EDTA and trypsin was neutralized with respective growth media before counting cells.

### *Microtissue fabrication*

Collagen microtissues approximately 300 μm in diameter were fabricated using previously established protocols[132,133]. Briefly, high concentration rat tail collagen I (Corning) was buffered with 10x Dulbecco's phosphate-buffered saline (DPBS), neutralized to pH 7.4, and diluted to a concentration of 6 mg/mL. For cell-laden microtissues, cells were resuspended in the collagen solution to a final concentration of 2 million cells/mL. At 4°C, the collagen solution was partitioned into droplets using a flow-focusing polydimethylsiloxane (PDMS) (Dow Corning) microfluidic device. The continuous phase from the droplet generation (FC-40 with 2% 008-FluoroSurfactant, Ran Biotechnologies), was collected with the collagen microtissues in a low retention Eppendorf tube and polymerized for 20 minutes at room temperature. The oil phase was removed and the collagen microtissues were resuspended in 1x DPBS with a manual micropipette.

### *Microwell fabrication*

Polystyrene multi-well plates were coated with a thin layer of 2% agarose and dehydrated in a sterile laminar flow hood overnight. PDMS stamps featuring a radial pattern of 300 μm diameter posts were plasma treated for 2 minutes to produce a hydrophilic surface and sterilized with boiling water. For a 24-well plate, 175 μL of molten 2% agarose solution was pipetted into each well and the hydrophilic PDMS stamp placed immediately onto the agarose. After cooling for 5 minutes, stamps were removed gently from the polymerized agarose and hydrated with DPBS. Wells were washed with appropriate culturing media prior to adding microtissues with a manual micropipette. The stamped plates are referred to as "microwell plates."

*Microtissue coating protocol*

50,000 cells were added to each well of a microwell plate and allowed to settle into the microwells for 5 minutes. Acellular microtissues were then added and allowed to settle into microwells. Finally, an additional 50,000 cells were added, sandwiching the tissues between two layers of cells.

*Viability assays*

Microtissues containing encapsulated cells were fabricated and cultured for up to 1 month. At various timepoints, tissues were gently pipetted and removed from microwells and collected in an Eppendorf tube. For viability staining, constructs were washed thoroughly with DPBS and then incubated with a staining solution of 5 μM DRAQ5 (Invitrogen) and 5 μM Calcein AM at 37°C for 20 minutes. A Zeiss Axio Observer was used to image z-positions throughout each microtissue with a step size of 10 μm, which is sufficiently small to account for each cell. Collected z-stacks were analyzed and the total number of cells (from the nuclear stain) and the number of live cells (from the Calcein) were counted for each microtissue. The percentage of live cells for each construct was calculated and reported values are for populations of microtissues greater than 38.

*Contraction assay*

Following the protocol outlined in Chapter 4.2 Methods, projected areas and shape descriptors were measured by thresholding images of encapsulated fluorescent, 1 μm diameter Fluoro-Max Microspheres (Thermo Scientific). Outliers, determined as areas three standard deviations above or below the average, were removed from the data sets.

*SHG imaging and analysis*

NHLF-coated microtissues were incubated in 0.1%, 2%, and 10% FBS and collected and fixed with 3.7% formalin after 1 and 3 days of culture. Nuclei were stained with 80 nM Hoechst before the constructs were immobilized in 1% agarose for imaging. Second harmonic generation (SHG) signal from the collagen fibers was collected with a custom multiphoton laser-scanning microscope (Prairie Technologies/Bruker) with a Mai Tai Ti:Sapphire laser (Spectra Physics). Fibers were excited at 880 nm. SHG signal intensity and construct circularity were measured using ImageJ[84] (n=4-6 microtissues per condition).

*EDTA release*

Microtissues were cultured for up to 5 days, with collections at 2 hours and 1, 2, and 5 days. At each timepoint, half of the tissues were fixed with 3.7% formalin and the remaining microtissues were washed with DPBS and incubated in 5 mM EDTA solution at 37°C overnight before fixation with formalin.

*Immunofluorescence staining*

Microtissues were collected in low-retention Eppendorf tubes and fixed with 3.7% formalin overnight at 4°C. Formalin was quenched with 0.1 M glycine and constructs were blocked and permeabilized with 10% FBS and 0.1% Triton X-100 for 1 hour at room temperature. The tissues were then incubated with primary antibody (rabbit anti-fibronectin (1:200, Abcam), mouse anti-collagen IV (1:200, Abcam)) at 4°C overnight. The microtissues were washed thoroughly, and incubated with secondary antibodies (1:200, Jackson) and/or phalloidin (1:100, Santa Cruz Biotech) at 4°C

overnight. Nuclei were visualized with 20 μM Hoechst. A Zeiss Axio Observer with Apotome was used to obtain optical sections.

*Tracking and multiplexing*

Collagen microtissues containing 1 μm Fluoro-Max Microspheres and encapsulated NHLFs were cultured in 0.1%, 2%, and 10% FBS for a period of 6 days and imaged at several timepoints. Cultures were maintained with half-volume media changes every other day. On the final day of the experiment, tissues were fixed in microwells with 3.7% formalin and then stained with phalloidin (1:100, Santa Cruz Biotech). Microtissues were then imaged on widefield in microwells using a Zeiss Axio Observer. A semi-automated custom macro was used to calculate the projected tissue area for all timepoints and, for the final timepoint, actin fluorescence was also quantified.

*Statistical analysis*

All experiments reported in this manuscript were completed at least 3 times with similar results. Statistical significance of EDTA release experiments was performed with paired t-tests and significance was determined using Bonferonni's correction. Significance of tracking experiments was calculated with a student's t-test. Lastly, ANOVA with Scheffé's method where p-values less than 0.05 were considered significant was used to determine significance in SHG experiments.

Results

*The combination of droplet technology and agarose microwells enables a high-throughput workflow and long-term culture of protein-based microtissues*

A major hurdle that must be overcome in any high-throughput tissue engineering application is scalability of construct fabrication as well as the cost and availability of required reagents. To address these concerns, our protocol leverages a microfluidic flow-focusing device to produce tens of thousands of nanoliter-volume microtissues per hour (Figure 5.1). We fabricate more than 20,000 microtissues using the same reagent volume as is used to cast 6 traditional hydrogels in a 96-well plate. Additionally, all described experiments utilized a maximum of 20 cells per construct, meaning these assays could be scaled for large compound-screens with a limited number of cells.

Although we have previously demonstrated that these protein-based microtissues are useful for observing short term tissue remodeling, it has been widely documented that most 3D tissue culture systems, including our microtissues, typically aggregate in static culture (Figure 5.2a), limiting their use for long term culture and high content readouts[65,134,135]. To address this challenge, we fabricated patterned agarose microwells using PDMS molds (Figure 5.2c,d). We chose agarose as it is affordable, but also biocompatible, amenable to patterning, does not bind to proteins or cells, and has precedence in the field for this purpose[136–139]. It also does not interact with compounds of diameters <60nm[140,141], making this an ideal material for small molecule compound screening. These microwells physically separated microtissues and prevented aggregation (Figure 5.2e). When microtissues were cultured in *c*ommercially available low-adhesion plates, we observed a reduction in individual microtissues over a period of 1 week as they coalesced at the center of the well and formed aggregates (Figure 5.2a), resulting in a 600-fold reduction in individual microtissues (Figure 5.2b). By contrast, microtissues cultured in microwells demonstrate no loss in the population over 1 week (Figure 5.2b). With the microwell culturing method, we cultured microtissues as independent entities for up to 1 month (greater than 90% viability of encapsulated NHLFs after 30 days).

Below, we demonstrate the utility of this platform and workflow for quantifying tissue remodeling.

*Long-term compaction of microtissues reveals reversible and irreversible ECM remodeling by fibroblasts and endothelial cells*

Wound healing is an ECM remodeling process involving fibroblast-driven wound contraction followed by ECM deposition and crosslinking to return mechanical integrity to a tissue. *In vivo*, this process occurs over the span of days to weeks, making it difficult to study with short-term *in vitro* model systems lacking an ECM component. Using our microtissue-microwell platform and leveraging its long-term culturing abilities, we modeled this dynamic wound-healing process with NHLFs in collagen constructs. For the purposes of this study, we used short-term culture to refer to timepoints that occur before 48 hours of culture, a conservative estimate for protein synthesis to occur, and use the phrase long-term to denote culture greater than 2 days. To identify reversible and irreversible changes to ECM over short and long timescales, we collected tissues at various stages of remodeling and examined ECM compaction and deposition before and after cell release. There are several enzymatic methods to remove cells from ECM, but many of these treatments are detrimental to the structural integrity of the ECM itself. Thus, we elected to use EDTA as it destabilizes calcium- and magnesium-dependent integrin linkages, and is a gentle and minimally disruptive agent for both the cells and the matrix. From widefield imaging we found that the fibroblasts compacted the collagen microtissues (Figure 5.3a), but permanence of this remodeling was not immediately evident. Cell-ECM interactions likely stabilize microtissue compaction, and thus releasing cells would result in an increase in projected area for the tissue constructs. For both encapsulated and surface-coated NHLF conditions, we treated constructs with EDTA after 24 hours of culture and we found significant expansion of 33.3% and 24.5% respectively ($p<0.00025$). The reversibility of ECM compaction decreased over time, with the cell release resulting in no significant expansion for encapsulated and surface-coated conditions (Figure 5.3b).

After observing irreversible matrix expansion after 5 days, we hypothesized that ECM deposition may contribute to remodeling as microtissue compaction did not increase greatly from days 1 and 2 to day 5. Using immunofluorescence, we found that after 5 days of culture cells deposit collagen IV and fibronectin when encapsulated in or coated on collagen I microtissues. Furthermore, in addition to removing the cells, EDTA disrupted collagen IV, a finding observed previously[142,143]. Incubating in EDTA solution, however, did not affect synthesized fibronectin and deposition of this and other matrix proteins not vulnerable to chelating agents may have prevented microtissue expansion (Figure 5.3c).

In addition to fibroblasts, endothelial cells also participate in ECM remodeling, and to probe this endothelial function, we measured microtissue compaction of HUVEC coated microtissues. The endothelialized constructs were only minimally compacted after 24 hours (Figure 5.3b) and thus did not show significant expansion after cell release, a distinct difference to the nearly total amount of compaction performed by NHLFs in the first 24 hours. After 2 days, however, we observed a significant expansion of 12.2% ($p<0.012$) with EDTA treatment (Figure 5.3b) as the HUVECs were able to contract and compact the matrix beneath them but again calculated no significant difference (2.6%) after 5 days of culture. This inability to detect reversible changes in construct size at late timepoints mimicked the behavior of both coated and encapsulated NHLFs. Although our results show that HUVECs compact microtissues more slowly than NHLFs, endothelial cells are also able to make irreversible changes to the ECM (Figure 5.3b). Staining of extracellular matrix proteins confirmed that matrix was deposited at later time points in endothelial cell conditions as well (Figure 5.3c). These results show that ECM remodeling by different cell types follow unique time courses, but it may also be possible that there is heterogeneity within the remodeling time course even within the same cell type. As microwells enable long-term culture and retention of individual microtissues in a consistent spatial arrangement, we can gather additional time scale related data through tracking compaction time courses of discrete microtissues over the entire duration of an experiment.

*Long-term tracking of individual microtissues reveals heterogeneity in cell-ECM interactions*

We have previously shown that ECM-based microtissues can be used for high-throughput, short-term compaction assays[132], and we here demonstrated how microwells can extend the experiment duration (Figure 5.2a). In addition, our ability to retain microtissues as discrete samples in the same spatial arrangement allows for identifying and tracking constructs as unique entities to enable characterization of subpopulations. Over 1 week, we tracked compaction for over 125 fibroblast-laden microtissues per condition (Figure 5.4a) and observed a distribution of compaction rates, with most major changes in size occurring on days 1, 2, and 4 (Figure 5.4b, c). Despite different compaction rates we observed that nearly all microtissues compacted to similar sizes (final area of 13,000 $\mu m^2$), with the greatest difference in projected area observed on days 1 and 2 (Figure 5.4d). Plotting the probability density function for each serum condition revealed a bimodal population on days 1 and 2 that returned to a unimodal distribution by day 4 (Figure 5.4e, f) indicating that a heterogeneous population of microtissues existed in each condition and that our system enables us to quantify these divergences within an experimental condition. Characterizing construct-level heterogeneity in our microtissue populations is beneficial as histology of pathologies like cancer and fibrosis are variable throughout the diseased tissue.

To better understand the molecular origin of this heterogeneity, we visualized the cytoskeleton of cells within microtissues and found that tissues cultured in high serum expressed more actin than those cultured in low serum conditions ($p<0.0001$) (Figure 5.4g). As expected, we found that microtissues in 10% serum were not only on average brighter but compacted faster, decreasing to 30% of their original projected area more quickly than microtissues in the 0.1% condition ($p=0.002$). Additionally, we also found variation in the actin intensity within each condition. As the staining protocol did not disturb microtissue positions, we compared the compaction profile and the actin signal on an individual microtissue basis. For each microtissue, we calculated the timepoint at which the projected area had decreased by 30% and compared this value to the final phalloidin intensity. We found microtissues that compacted faster demonstrated increased

actin intensity: we calculated a Pearson's correlation coefficient of -0.68 and -0.65 for 0.1% and 10% FBS conditions respectively between these variables, indicating a strong negative linear relationship for both conditions (Figure 5.4g). By combining the contraction assay with immunofluorescence, we observed that actin intensity was related to but not directly correlated with final microtissue size.

*Cells remodel microtissues on a local and global scale*

Increased density of collagen and other ECM components is proportional to the stiffness of a tissue, an important factor in cancer and fibrosis[144–146]. Multiphoton microscopy is a well-established tool used to investigate changes to global and local collagen densities through visualization of second harmonic generation (SHG) signal. Increased signal correlates to a higher density of fibers and it is known that cells will organize and bundle fibers both *in vivo* and *in vitro*[45,147,148]. Using SHG, we visualized changes in local collagen density and observed changes in both global and local ECM remodeling. First, we confirmed the fibrillar nature of acellular microtissues. We observed collagen fibers throughout the constructs and found they projected out of the microtissue free boundary surface, demonstrating their entangled nature and complex topography (Figure 5.5a). Then, to assess ECM remodeling via collagen fiber organization and bundling, we examined collagen microtissues coated with fibroblasts. As found in analogous large gel studies, we observed high serum conditions resulted in significant ECM remodeling[149,150], with a statistically significant increase in SHG signal with 10% serum (Figure 5.5b). At early timepoints for all conditions, we observed increased collagen fiber intensity adjacent to nuclei, indicating that local remodeling and compaction of fibers is predictably occurring nearest to cells. After 3 days in culture, the global ECM remodeling was more evident as this localized intensity change was less apparent and the entire construct exhibited elevated SHG signal (Figure 5.5a). We also observed that higher serum concentrations resulted in more significant changes to overall construct shape, changing the circularity from 0.88 to 0.47 after 3 days of culture in 10% FBS (Figure 5.5c).These differences in collagen density may help explain the discrepancy in actin intensity staining observed in NHLFs cultured in low (0.1%) and

high (10%) serum culturing conditions (Figure 5.4g) despite similar construct size as was quantified from widefield imaging.

Discussion

In the context of high-throughput screening, maintaining large populations of discrete microtissues is critical for feasibly completing large-scale experiments, and our agarose microwells enable such a workflow. When used in conjunction with agarose microwells, we cultured upwards of 500 microtissues per well in a standard 24-well plate, which equates to large numbers of conditions and hundreds of replicates per condition in any given experiment. Additionally, the familiar well-plate format of our microtissue-microwell platform is compatible with automated liquid handling techniques and automated imaging systems, making this culture method a practical system for large-scale screening. We conducted our studies in 24-well plates as a proof-of-concept to show the potential of this platform for use in larger-scale studies. However, this microwell system could be adapted to 96- or 384-well plates as the agarose patterning method is independent of well size.

In this study, the application of this platform, allowed us to track individual constructs over time, measuring dynamic changes in overall construct geometry as well as performing endpoint readouts with a consistent spatial arrangement. Coupling compaction with other non-destructive live cell measurements (e.g. reporter lines or cell migration), we envision that tracking microtissues over time could provide time-lapse information on the development and progression of disease states *in vitro*. This would allow for testing the efficacy of therapeutics at several stages of disease as well as the long-term effects of drugs on specific populations. This could be particularly important for identifying drug-resistant populations in diseases such as cancer. If used in conjunction with primary cells from patient biopsies, these methods offer additional metrics to investigate drug efficacy on diseased cells' ability to remodel and interact with their microenvironment.

By tracking individual microtissues over time, we were able to observe that ECM remodeling by different cell types follow unique time courses and that there is

heterogeneity within the remodeling time course even within the same cell type. One likely driver of heterogeneity in the microtissue compaction rates is the variance in the initial cell seeding density. In large collagen hydrogels, the rate of collagen compaction is dependent on initial cell density, and in droplet systems, it is well characterized that cell encapsulation methods follow a Poisson distribution[151]. Notably, the microtissues eventually converge to a narrower distribution, which is consistent with previous literature suggesting that as gels approach a common smaller size, cell density reaches a critical threshold and becomes a less significant factor[95]. The workflow described here facilitates the simultaneous study of large numbers of replicate microtissues and thus enables the possibility to study heterogeneity that may derive from factors like cell number, variability in underlying ECM, and heterogeneity in the underlying cell population.

We also found that compaction in our system was reversible at early timepoints, and over time the remodeling became more permanent. We examined the effects of encapsulating versus coating cells on the surface and found the surface-coated version to produce irreversible remodeling more quickly. Differences in cell numbers between these two conditions may also explain this observed effect. Because we encapsulated relatively low numbers of cells (<20 per microtissue), we may have had more cells adhered to the surface of the microtissues than were encapsulated. An alternative hypothesis is that the surface-coated NHLFs create a more stable ECM modification because the deposited ECM is supporting the remodeled geometry consistently from the outer edge of the microtissue. In comparison, the encapsulated fibroblasts deposit matrix throughout the microtissues, which provides less organized modification near the surface of the microtissues on average, as alluded to by the ECM staining results in Figure 5.3. Thus the surface deposition would provide more resistance to tissue expansion and thus would result in a diminished increase in size after releasing cells with EDTA.

In combination with measuring tissue compaction as a functional assay, we have demonstrated the ability to measure molecular readouts that provide insight into the mechanistic drivers of the function. Notably, our microtissue platform permits simultaneous measurement and correlation of cell function (compaction) and molecular

mechanism (actin) in the same cells and in the same microenvironment. Previously, correlation of actin polymerization and its effect on gel contraction have been reported by separately measuring actin in a 2D culture system while separately measuring compaction in a 3D bulk gel[152,153]. This separation of experimental readouts was required because the large size of the hydrogels hindered imaging[58–60]. Thus the scale of our system enables a more direct connection between mechanism and function.

As our assays and protocols are modular and can be combined and used to assess tissue-level behaviors for a variety of applications, this platform becomes flexible and amenable to study wide classes of diseases.

## Conclusion

We have developed an *in vitro* platform that enables long-term tissue remodeling on a cellular scale for large populations. Using agarose microwells to culture collagen microtissues, we have cultured microtissues as independent entities for up to 1 month and have tracked and measured them as discrete tissues for 1 week. Additionally, we have quantified both local and global as well as short and long-term remodeling that occurs in our culturing system. Establishing high-throughput metrics of remodeling is crucial for development of drug screening models for fibrotic and cancerous disease, though the merit of the platform extends beyond these pathologies to include any disease in which ECM interactions are considered important.

## Acknowledgements

Portions of this work were conducted in the Minnesota Nano Center, which is supported by the National Science Foundation through the National Nano Coordinated Infrastructure Network (NNCI) under Award Number ECCS-1542202. We thank the American Heart Association (13SDG6450000), the National Heart, Lung, and Blood Institute (R21 HL132256), the National Institute of Environmental Health Sciences (R21 ES027622), and the National Science Foundation (CBET 1704332). Alexandra L. Crampton acknowledges the National Science Foundation GRFP (00039202) for support. We also thank Dr. Paolo Provenzano for the use of his multiphoton microscope and

donating MDA-MB-231 cells, Dr. Daniel Tschumperlin for donating NHLFs, Dr. Wei Shen for donating NIH-3T3 cells, and Julia Nguyen and Dr. Gregory Vercellotti for isolating and donating HUVECs. Experiments for this chapter were performed collaboratively with Katherine A. Cummins.

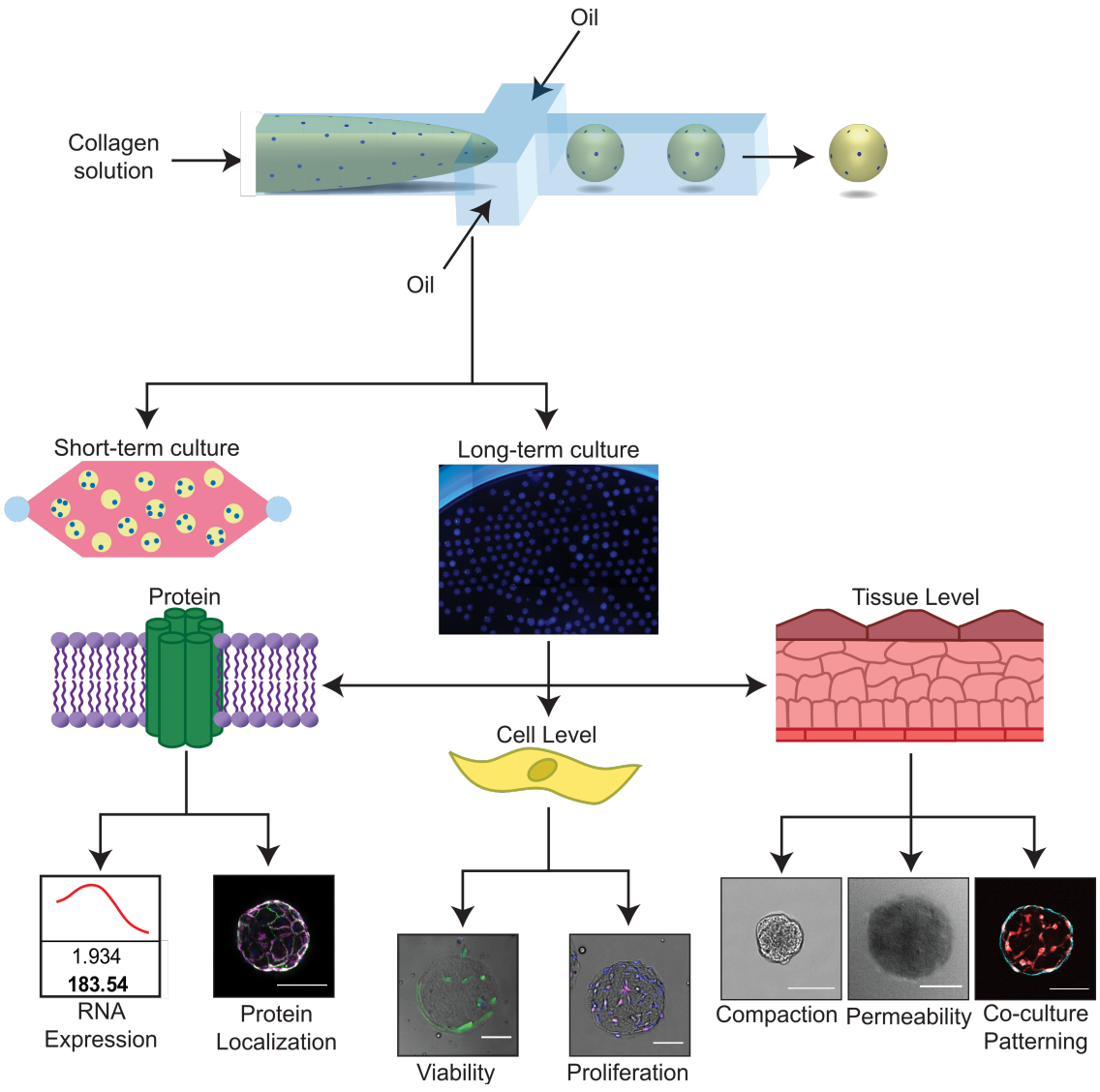


**Figure 5.1:** ***The microtissue-microwell workflow facilitates functional and mechanistic analysis at multiple scales***

Our workflow facilitates studies of tissue remodeling and disease progression on tissue, cellular, and subcellular scales in short- and long-term studies, while visualizing global and local behaviors. This system is compatible with a wide range of cell types, ECM proteins, and biological assays, making this a practical solution for high-throughput fabrication and handling of 3D tissue engineering construct. Scale bars are 100 μm.

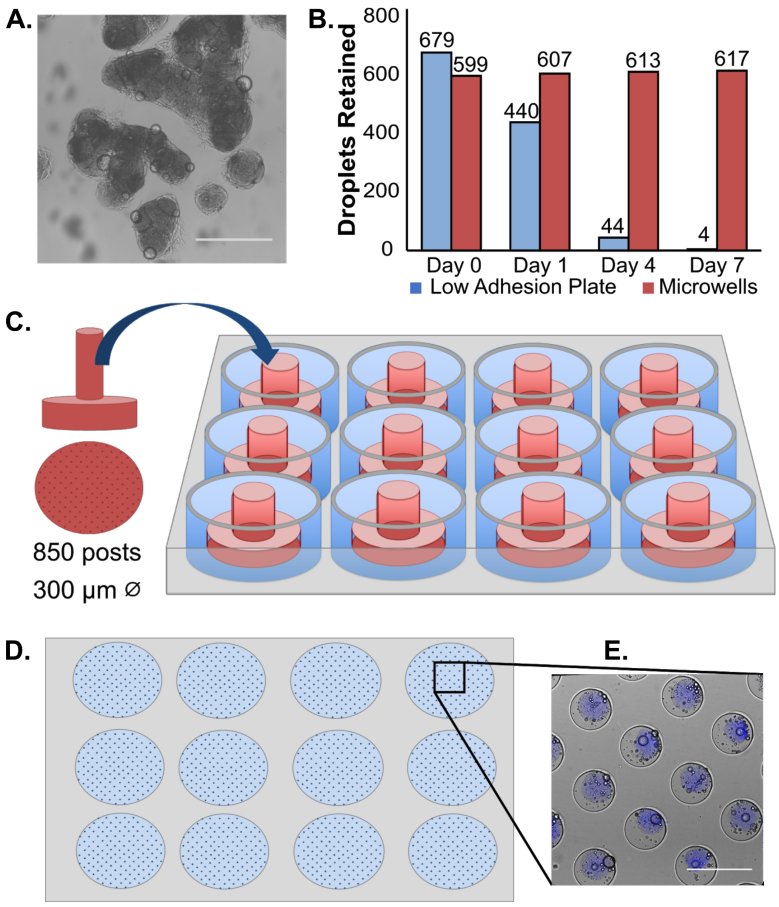


**Figure 5.2:** ***Microwells enabled long-term culture of large microtissue populations***

(**A**) Brightfield imaging reveals that microtissues aggregate when cultured for 4 days in standard low adhesion plates. (**B**) Quantification of individual microtissues after 1 week of culture in standard low adhesion plates (blue bars) reveals that the population is reduced by over 100-fold. By contrast, microtissues cultured in patterned agarose microwells (red bars), remained separated over the same 1-week period. (**C**) To fabricate microwells, plasma-treated PDMS stamps with 300-µm diameter posts were placed into 2% agarose solution and (**D**) removed once polymerized. (**E**) Brightfield combined with blue fluorescence imaging shows microtissues contained in agarose microwells in a 12-well plate. Microtissues are labeled blue by encapsulating blue fluorescent beads within the polymerized collagen matrix. Scale bars 500 µm.

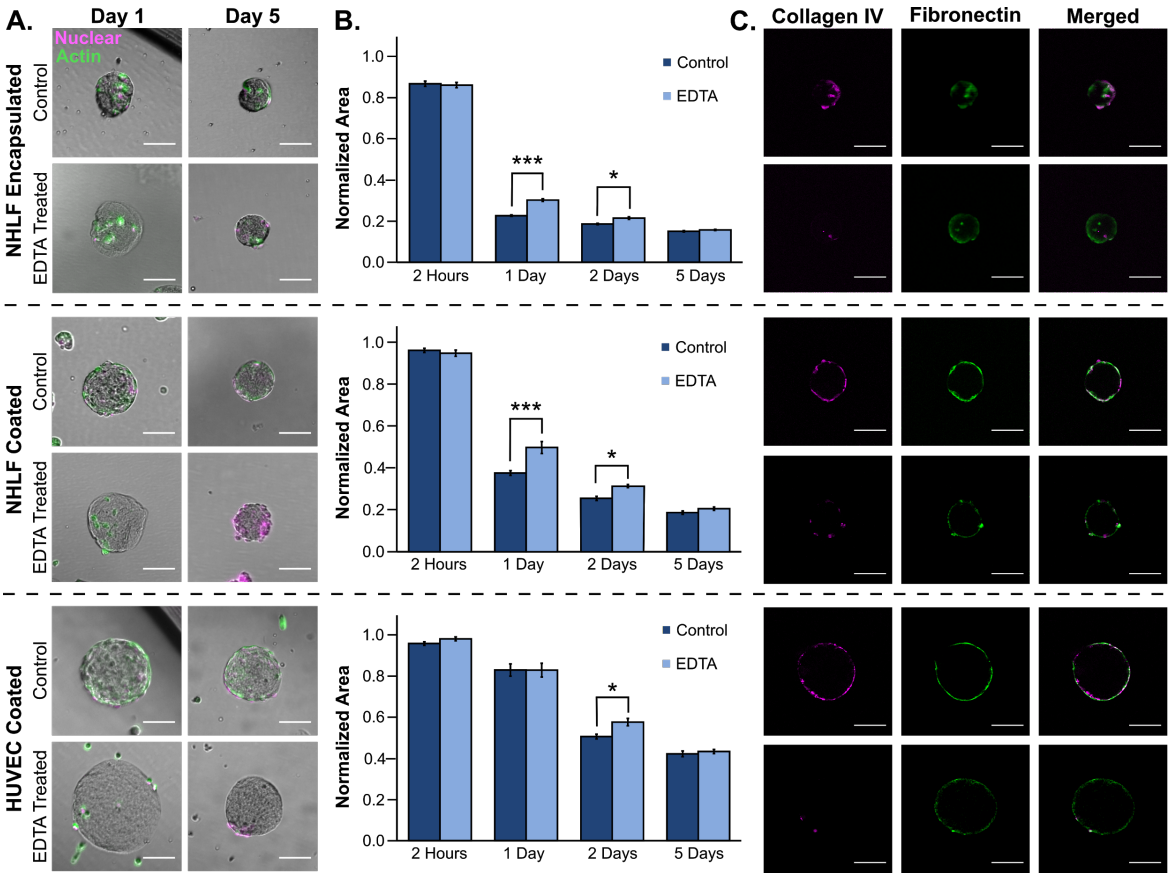


**Figure 5.3:** ***EDTA release allows for studying microtissue remodeling on short and long timescales***

(**A**) Brightfield imaging of microtissues after 1 and 5 days of culture with encapsulated NHLFs or coated with NHLFs or HUVECs. The actin cytoskeleton was visualized with phalloidin (green) and nuclei with Draq5 (magenta). After 1 day, we observed a reduction in construct size, which was partially reversed after releasing cells with EDTA. After 5 days, this reversal was not observed. To quantify these effects with construct size, we measured (**B**) microtissue projected area and confirmed that on a population-scale at early timepoints, compaction was partially reversible, while after 5 days of culture remodeling was not reversible. We calculated significance with a paired t-test with a Bonferroni correction for multiple comparisons ($p<0.00025$ = ***, $p<0.013$ = *, standard error shown). Projected area is normalized to the average area of each microtissue batch after fabrication. (**C**) Fluorescence imaging with optical sectioning shows that fibronectin (green) and collagen IV (magenta) were deposited on the surface of the microtissues, however the collagen IV was disrupted by EDTA treatment. All scale bars 100 μm and sample sizes were an average of 38 microtissues per condition.

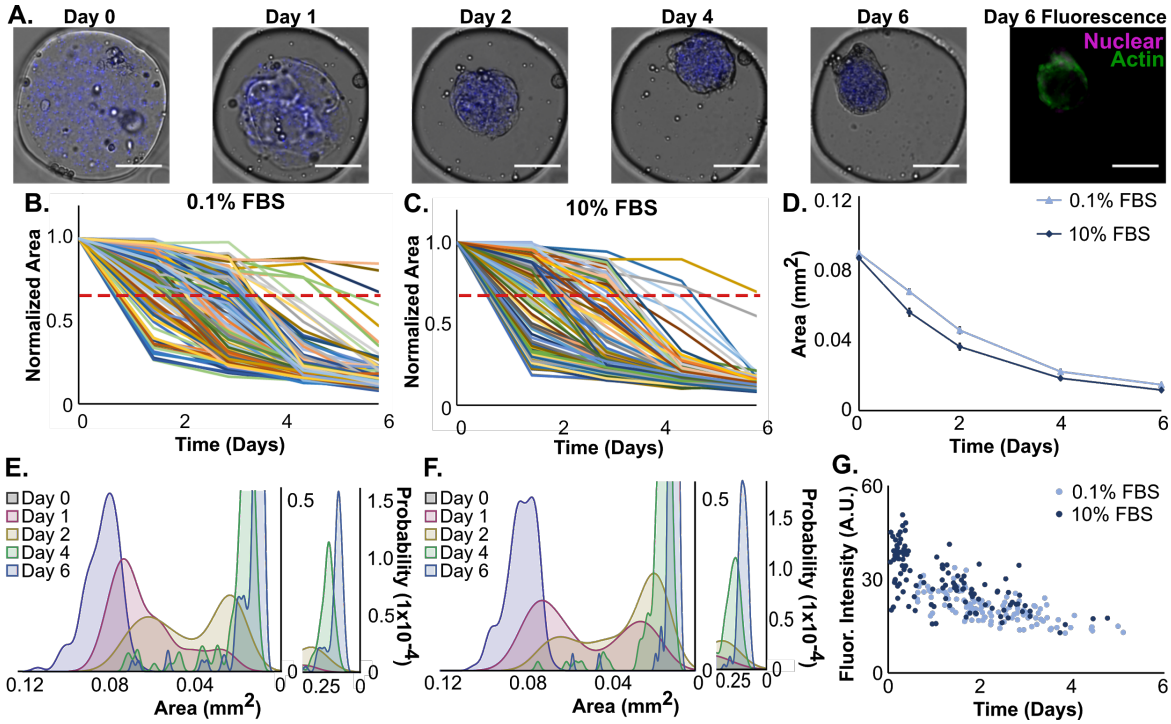


**Figure 5.4:** ***Microwells facilitate tracking of discrete microtissues and coupling live imaging data with endpoint staining***

(**A**) Brightfield and fluorescence imaging of collagen microtissues containing NHLFs and encapsulated fluorescent beads (blue) to mark construct borders were cultured in 0.1% (or 10%) serum for 1 week. All scale bars 100 µm. (**B**, **C**) Areas of 121 individual microtissues cultured in 0.1% FBS (**B**) and 137 constructs cultured in 10% FBS (**C**) were measured and plotted. A red dashed line indicates a threshold compaction level of 30% compaction. Projected area is normalized to day 0 for each microtissue compaction trajectory. (**D**) Population averages show similar compaction trajectories between 0.1% and 10% serum conditions. Shown with standard error. (**E**, **F**) Probability density functions of microtissue area at each timepoint reveal heterogeneity in the populations, indicated by bimodal distributions on day 1 (red) and day 2 (yellow) populations. (**G**) We observed a strong negative correlation between actin intensity and the time at which a 30% reduction in projected area occurred, as indicated by correlation coefficients of -0.68 (orange linear trendline) and -0.65 (red linear trendline) for 0.1% and 10% FBS conditions respectively. This suggests that a faster compaction rate is correlated to increased

actin expression. We also found that higher serum conditions corresponded to elevated actin intensity and increased compaction rates.

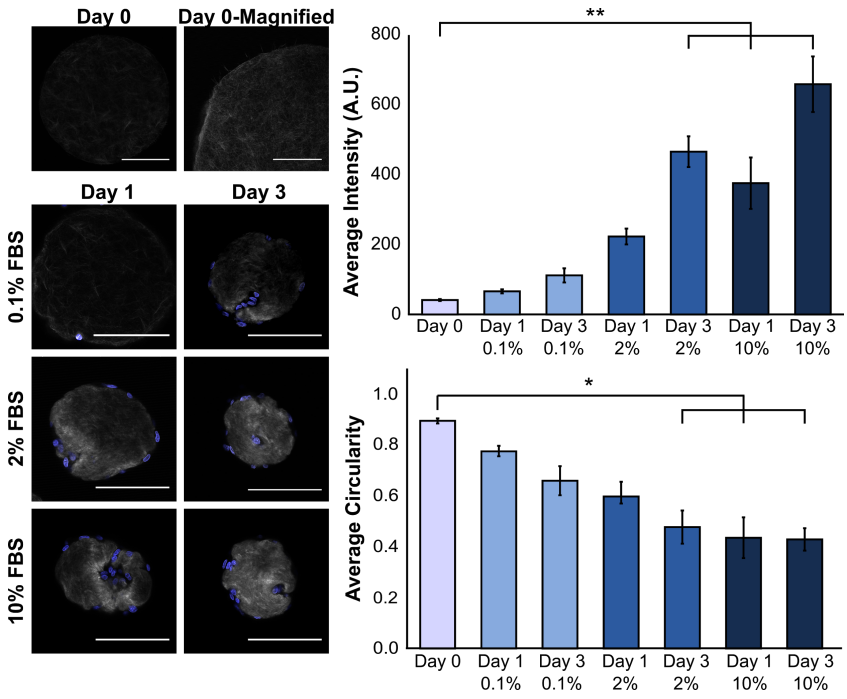


**Figure 5.5:** ***SHG microscopy revealed local ECM remodeling of collagen constructs***

(**A**) Acellular collagen microtissues were coated with NHLFs and cultured for 3 days in varying serum concentrations. Collagen compaction and ECM remodeling were observed using SHG to visualize collagen fibers (grey) and Hoechst to stain the nuclei (blue). A section of an acellular slice is magnified (scale bar 50 μm) and the brightness adjusted to demonstrate the complex topography and fibrilar nature of the constructs. (**B**) Increased SHG signal intensity correlates to increased collagen fiber density and we qualitatively observed that with increasing serum and incubation time, cells interact with and increasingly modify their microenvironment. All other scales bars are 100 μm. (**C**) Average signal intensity from the collagen fibers was determined for each optical slice for each condition (n=4-6 microtissues per condition). We observed that as serum concentrations increase, collagen fiber density increases due to compaction of fibroblasts. (**D**) Circularity of each construct is reported and with increasing serum concentrations and time, we found that microtissues became less circular ($p<0.05$ = *, $p<0.01$ = **, shown with standard error).

## ***Chapter 6: Application – Endothelial micromimics for high-throughput drug screening***

This chapter contains material from "A High-Throughput Microtissue Platform to Probe Endothelial Function *In Vitro*" by Alexandra L. Crampton, Katherine A. Cummins, and David K. Wood. *Integrative Biology*, volume 10, issue 9, pages 555-565; permission conveyed through Copyright Clearance Center, Inc.

### Overview

A critical role of vascular endothelium is as a semi-permeable barrier, dynamically regulating the flux of solutes between blood and the surrounding tissue. Existing platforms that quantify endothelial function *in vitro* are either significantly throughput limited or overlook physiologically relevant extracellular matrix (ECM) interactions and thus do not recapitulate *in vivo* function. Leveraging droplet microfluidics, we developed a scalable platform to measure endothelial function in nanoliter-volume, ECM-based microtissues. In this study, we describe our high-throughput method for fabricating endothelial-coated collagen microtissues that incorporate physiologically relevant cell-ECM interactions. We showed that the endothelial cells had characteristic morphology, expressed tight junction proteins, and remodeled the ECM via compaction and deposition of basement membrane. We also measured macromolecular permeability using two optical modalities, and found the cell layers: (1) had permeability values comparable to *in vivo* measurements and (2) were responsive to physiologically-relevant modulators of endothelial permeability (TNF-α and TGF-β). This is the first demonstration, to the authors' knowledge, of high-throughput assessment (n>150) of endothelial permeability on natural ECM. Additionally, this technology is compatible with standard cell culture equipment (e.g. multi-well plates) and could be scaled up further to be integrated with automated liquid handling systems and automated imaging platforms. Overall, this platform recapitulates the functions of traditional transwell inserts, but extends application to high-throughput studies and introduces new possibilities for interrogating cell-cell and cell-matrix interactions.

Introduction

The vascular system serves crucial roles in supplying nutrients to and removing wastes from peripheral tissues, facilitating immune cell trafficking, and maintaining osmotic homeostasis. These functions depend on the endothelium to act as a semi-permeable barrier between the blood and tissue, which requires the body to regulate and modulate endothelial permeability and thus the flux of cells and/or solutes across the barrier. For example, in inflammatory processes, the endothelial barrier becomes more permeable, facilitating transport of immune cells into the tissue space and inflammatory signals out in order to support the immune response.[154,155] Endothelial barrier function may also be disrupted in disease processes (e.g. atherosclerosis[156–158], rheumatoid arthritis[159–161]), leading to local changes in transport of proteins, fluid volume, and cell populations (including immune cells) into the surrounding tissue. There is also a growing recognition that endothelial barrier function is a critical consideration for delivery of many classes of therapeutics, which can be hindered (e.g. blood-brain barrier[162–166]) or enhanced (e.g. enhanced permeability and retention in solid tumors[167–172]) due to endothelial regulation. Our ability to understand how endothelial barrier function is (dys)regulated in health and disease and how it affects delivery of therapeutics requires robust models of the endothelium and accurate measurement of the barrier function.

One of the standard measurements of endothelial function *in vitro* is macromolecular permeability of monolayers grown on porous transwell inserts.[162,166,173,174] Monolayers are cultured on the insert, and movement of various solutes across the cell layer are typically measured with colorimetric or fluorescently labeled solutes. Although cells attach and consistently form monolayers on these inserts, the endothelial layers are often more leaky than *in vivo* vessels.[173,175–178]. One explanation for the discrpency between *in vitro* and *in vivo* measurements is that the interaction of the endothelium with the tissue compartment is also important for endothelial function. Others probed this hypothesis by coating transwell inserts with ECM molecules[179,180], and found that the exclusion of maromolecular molecules was closer, but still not equivalent to *in vivo* measurements. These findings support the need to create *in vitro* platforms that recapitulate the endothelium in the context of an ECM-

rich tissue space. Thus, there has been significant effort towards developing more physiologically relevant tissue-level models of vasculature *in vitro* using microfluidic devices.[181–184] These models create complex vasculature that directly interacts with ECM and demonstrates characteristic morphology and barrier function. However, the low throughput of these platforms ultimately limits utility for high-throughput screening, revealing a need for an *in vitro* model of the endothelium that is robust, recapitulates the endothelium-ECM interactions in a physiologically meaningful way, and is also amenable to high-throughput studies. Our group[132] and others[80,185,186] have shown that microcarrier systems can be used to culture endothelial cells, however dynamic measurements of endothelial behavior (e.g. ECM deoposition, changes in endothelial permeability) have yet to be characterized in a high-throughput manner.

Combining the rich cell-ECM interactions of microfluidic platforms and the high-throughput capabilities of droplet technology, we used ECM-based droplets as a substrate for endothelial cells to grow and remodel (via compaction and ECM deposition) – capturing the endothelium-ECM interactions in a format that is compatible with rapid fabricaiton. We demonstrate that microscale (~300 μm diameter) collagen microtissues can be used as ECM-rich carriers on which to culture endothelial cells and can be used to assess factors that regulate endothelial barrier function. These microtissues are fabricated using flow-focusing microfluidic devices, generating ~20,000 droplets/hour, making this ECM-based platform amenable to large-scale studies of endothelial permeability. We show that characteristic behaviors of *in vitro* endothelial layers (confluence of the monolayer, deposition of ECM, and behavior of the semi-permeable barrier) are observed in our microtissue constructs. Additionally, we show for the first time to the authors' knowledge, high-throughput assessment of endothelial function on natural ECM, supporting robust statistical analysis and feasability for large-scale applications. Miniaturization of tissues also minimizes cell number requirements, making this platform amenable to precious cell and ECM sources. We also demonstrate that we can detect biologically relevant modulators of endothelial permeability, using inflammatory cytokines as a sample case.

Methods

*Microtissue fabrication*

Acellular collagen microtissues were fabricated with a modified protocol outlined previously (Figure 6.1).[132] Briefly, High Concentration Rat Tail Collagen I (Corning) is buffered with 10x PBS, pH adjusted to 7.4, and diluted to a final concentration of 6 mg/mL. At 4°C, the collagen solution was partitioned into microtissues using a flow-focusing microfluidic device. The continuous phase from the droplet generation (FC-40 with 2% EA Surfactant, Ran Biotechnologies), was collected with the collagen microtissues in an eppendorf tube. Microtissues were polymerized in bulk at room temperature for 20 minutes. The oil phase was drained and microtissues were resuspended in 1X sterile PBS.

*Microtissue endothelial coating*

Human Umbilical Vein Endothelial Cells (HUVECs) were cultured in EGM-2 (Lonza) on gelatin-coated flasks. Cells were used between passage 2 and 4 for all experiments. Cells were washed with HBSS and released from the culture flask using 0.05% trypsin (Gibco). Trypsin was neutralized with media, washed with fresh media, and counted. In 12-well low adhesion plates (coated with agarose), 350-500k cells were added to ~750 collagen microtissues. Constructs were cultured in these low-adhesion plates for 5 days, with media changes every 2-3 days. Coated microtissues were recovered from plates with gentle pipetting for experiments.

*Crosslinking collagen microtissues*

Stiffness of collagen microtissues was increased by crosslinking with formalin. Microtissues were incubated with 3.7% formalin for 1 hour at room temperature. Tissues were washed thoroughly with 1X PBS to dilute formalin to <0.001%.

*Immunofluorescence staining*

Coated constructs were collected and fixed with 3.7% formalin for at least 1 hour at room temperature. Microtissues were washed with 1X PBS, then quenched with 25

mM glycine. Microtissues were washed, then blocked and permeabilized with 1% BSA and 0.1% Triton X-100. Primary antibodies (VE-Cadherin (Cell Signaling), CD31 (Cell Signaling), Laminin (Abcam), Collagen IV (Abcam)) were diluted in 1% BSA to ratios of 1:100-1:500. Secondary antibodies (Jackson) were diluted in 1% BSA to a ratio of 1:500. Each sample was incubated with 100 uL of antibody solution for either 2 hours at 37°C or overnight at 4°C. Nuclei were labeled with Hoechst (Invitrogen) or Draq5 (Invitrogen).

*Permeability measurement*

After culturing microtissues for 5 days, microtissues were collected and placed in a large volume of 12.5 μg/mL 150 kDa TRITC-dextran (Sigma) in a 96-well plate coated with pHEMA (Sigma). Dye diffused into the droplets for 20 minutes before imaging at 10X with the Zeiss Axio Observer. To obtain optical sections, an Apotome was added to the light path and 5 images per slice were collected. Images from both methods were analyzed for local intensity using custom macros written in Fiji.[187] Modulators of permeability were 5 mM EDTA, 10 ng/mL TNF-α (Sigma), 2 ng/mL TGF-β (Sigma).

To calculate permeability from optical sectioning, we assumed the microtissues initially had no fluorescent solute inside the tissue and that all of the solute must pass through the endothelial barrier to reach the center of the tissue. We established an unsteady mass balance where the number of moles of solute on the inside of the tissue was equivalent to the moles of solute that had crossed the endothelial barrier. This was described as:

$$\frac{dC_{drop}}{dt} V_{drop} = A_m P\left(C_{bath} - C_{drop}\right) \quad (1)$$

where $C_{drop}$ was the molar concentration of solute inside the microtissue, $V_{drop}$ was the volume of the microtissue, $A_m$ was the surface area of the microtissue, P was permeability, and $C_{bath}$ was the concentration of the dye bath. As $V_{bath}$ was much greater than $V_{drop}$, we treated $C_{bath}$ as a constant and simplify Eq. 1:

$$\frac{dC_{drop}}{dt} = \left(\frac{A_m}{V_{drop}}\right) P\left(C_0 - C_{drop}\right) \quad (2).$$

We solved for $C_{drop}$ and applied the initial condition that $C_{drop} = 0$ when t=0. This resulted in the final expression for permeability as:

$$P = -\ln\left(\frac{C_0 - C_{drop}}{C_0}\right)\left(\frac{V_{drop}}{A_m}\right)\left(\frac{1}{t}\right) \quad (3).$$

Additionally, by removing the cell layer using EDTA and calculating permeability of the remodeled ECM, we can identify the contribution of the cell layer and the construct itself separately with:

$$\frac{1}{P_{total}} = \frac{1}{P_{collagen}} + \frac{1}{P_{membrane}} \quad (4).$$

*Second harmonic imaging to visualize collagen fibers*

Second harmonic imaging microscopy was used to visualize collagen fibers in microtissues. Constructs were collected and mounted onto coverslips with 1% agarose. Agarose was chilled to polymerize the gel and the samples were kept hydrated with 1X PBS. Constructs were imaged using a custom multiphoton laser-scanning microscope (Prairie Technologies/Bruker) with a Mai Tai Ti:Sapphire laser (Spectra Physics) exciting fibers at 880 nm. Image intensity within the region of the microtissues were quantified using Fiji.[187]

*Statistical analysis*

Large sample sizes allowed for parametric statistical analysis. Comparisons for multiple groups were completed with one-way ANOVA with post-hoc Tukey HSD comparison.[188] Results were reported as statistically significant with p-values less than 0.05.

## Results and Discussion

*Endothelial cells form confluent monolayers and compact ECM microtissues*

It has been previously shown that endothelial cells compact ECM hydrogels *in vitro*[106,189], and we expected that endothelial cells would also compact our collagen microtissues (Figure 6.1a,b). We further hypothesized that this tissue compaction would result in improved endothelial barrier function. Thus, to compare compacted and

uncompacted tissues, we created two types of collagen microtissues. “Soft” microtissues were generated with no post-polymerization modification as described in the Methods. “Stiff” microtissues were generated by crosslinking the polymerized collagen with formalin for 1 hour at room temperature, followed by extensive washing to remove residual fixative. Soft and stiff microtissues were then coated with endothelial cells as described in the Methods.

As shown in Figure 6.2, endothelial cells formed confluent monolayers on the surface of soft and stiff collagen microtissues. Microtissues were coated with endothelial cells and cultured for up to 5 days, and immunofluorescence was used to assess location and expression of VE-cadherin and CD-31. We used optical sectioning to confirm that cells were on the surface of the microtissues and had characteristic cobblestone morphology (Figure 6.2a). CD31 and VE-cadherin were detected at the intercellular interfaces of the cells as early as 24 hours after coating (data not shown) as well as 5 days after seeding (Figure 6.2a). We also measured compaction by the endothelial cells using the projected area of collagen microtissues before and after coating with endothelial cells. We found that the average radius of soft microtissues decreased from 214.68 ± 15.21 μm to 118.66 ±10.32 μm ($p<0.001$) (Figure 6.2c). As predicted, the average radius of stiff microtisues did not change significantly after coating with cells, with the average radius shifting from 225.28 ± 57.45 μm to 216.45 ± 25.39 μm after 5 days of culture with endothelial cells (Figure 6.2d). Thus, we confirmed that our platform generates confluent monolayers of endothelial cells that interact with the collagen substrates via adhesion and tissue compaction – both of which are physiolgoically relevant endothelial functions.

*Endothelial cells anisotropically remodel collagen microtissues*

To examine remodeling via compaction in more detail, we used second harmonic generation (SHG) to visualize the collagen architecture throughout the culture process (Figure 6.3a). We confirmed our finding that soft microtissues were compacted significantly more than stiff microtissues, and that the majority of this compaction was completed within the first 24 hours of culture. We qualitatively observed that the image intensity is brighter for the compacted soft tissues than for the other conditions and

quantified this by measuring the average intensity for the entire construct (Figure 6.3b). The average intensity of the microtissues before and after crosslinking (on day 0) were not statistically different, indicating that the crosslinking process did not affect local collagen distribution or signal from this measurement. We also found that the addition of cells to the stiff microtissues did not change their intensity across any of the days measured (one-way ANOVA, with post-hoc Tukey HSD test). Contrastingly, soft microtissues showed a statistically significant increase in intensity in the first 24 hours after coating ($p<0.01$), and this difference was maintained in all subsequent timepoints (Figure 6.3b).

Although we observed a dense ring of bright collagen fibers immediately beneath the cell surface (Figure 6.3a), we wondered if our measured increase in SHG signal intensity was due solely to this dense ring under the cells or if the interior of the microtissue was also affected. To quantify this, we took several linescans from the center to the edge of the microtissue. We defined a significant increase in intensity to be at least 5 times brighter than the initial measured intensity of acellular constructs (d0). With this, we found that there was little to no remodeling of stiff microtissues in any region of the microtissue. Conversely, the soft microtissues showed significant remodeling deep in the interior of the microtissues, with significant changes in intensity occurring up to 97 μm into the microtissue (Figure 6.3c).

We found that endothelial cells not only change the diameter of soft microtissues, but also make fundamental changes to the structure of the ECM in the interior of the construct. This predictable pattern of collagen remodeling makes this a simple method for creating dense collagen layers beneath the endothelial layer, which has previously required explicit patterning of ECM[190]. For the stiff constructs, we confirmed that endothelial cells adhere to and interact with the matrix, but were unable to compact the matrix on the local or global scale.

*Endothelial cells deposit basement membrane on collagen microtissues*

Endothelial cells are known to not only compact ECM hydrogels, but also to deposit basement membrane proteins including collagen IV[191–193], laminin[193], and

fibronectin[194] on *in vitro* substrates. To assess this functionality in our platform, we cultured endothelial cells on both soft and stiff microtissues for 5 days. We probed for basement membrane proteins using immunofluorescence and found that endothelial cells deposit collagen IV and laminin on the surface of both soft and stiff microtissues (Figure 6.2b). This deposition of basement membrane to the surface of the microtissues transforms the plain, isotropic collagen I microtissues into a more physiologically-relevant model of endothelium *in vitro*.

The regulation of basement membrane layers is important in the dynamics of the endothelium. For example, angiogenic processes require degradation of basement membrane before cells can migrate towards an angiogenic signal.[195,196] Thus, the presence of basement membrane in our model system not only supports the existing endothelial layers, but also provides potential for a high-throughput model to study basement membrane dynamics *in vitro*.

*Endothelialized microtissues demonstrate permeability similar to that observed in vivo*

One of the most important functions of the endothelium is to act as a semi-permeable barrier, dynamically regulating the flux of solutes between blood and the surrounding tissue. The endothelium is selectively permeable, with transport of molecules larger thatn 40-70 kDa excldued very well by healthy endothleium[183,197–199]. We opted to use a tracer comfortably larger than this range (150 kDa) to ensure exclusion by heathy endothelium and to afford more temporal flexibility for our imaging readouts. To assess macromolecular permeability, we examined the flux of 150 kDa TRITC-dextran through soft and stiff microtissues (Figure 6.4a). To quantify the permeability, we first measured the fluorescence intensity inside and outside of the microtissues. We observed some variability in the absolute intensity of the bath (likely due to photobleaching[200,201]), but we found the difference in intensity between the interior of the microtissue and the surrounding dye bath to be more robust (we report this value as $\Delta I$) (Figure 6.4b). Using $\Delta I$, we determined that the soft and stiff acellular constructs exhibit similar low impedance to the movement of dye, indicating that the initial stiffness of the construct alone does not affect dye transport for this assay. Both endothelial coated conditions

showed a statistically significant increase in $\Delta I$, with the soft-coated condition showing the largest increase in $\Delta I$ (Figure 6.4c). Whether this difference was due to the cell layer, to ECM remodeling, or to both required us to examine the endothelium and the ECM separately. To accomplish this, we removed the cell layer using EDTA, releasing the cells off of the surface of the microtissues and leaving the modified construct behind. We found that the EDTA-treated samples had an intermediate phenotype between the acellular and cellular controls, indicating that the change in $\Delta I$ in these microtissues was due to both the impedance from the cell layer and from the remodeling of the constructs. To determine the contribution of each of these factors, as well as to compare our platform to other macromolecular flux assays, we used the calculated $\Delta I$ measurements to determine permeability.

Using an unsteady mass balance, we found the average permeability of the acellular constructs to be $1.09 \times 10^{-07} \pm 5.19 \times 10^{-08}$ cm/s and $1.26 \times 10^{-07} \pm 9.26 \times 10^{-08}$ cm/s for the soft and stiff microtissues respectively. When a layer of cells is added to these constructs, there is a statistically significant decrease in average permeability to $5.29 \times 10^{-09} \pm 1.6 \times 10^{-09}$ cm/s and $2.9710^{-08} \pm 5.59 \times 10^{-09}$ cm/s for the soft and stiff constructs respectively. Once the cell layer is removed using EDTA, we found that the average permeability was $6.56 \times 10^{-09} \pm 7.62 \times 10^{-10}$ cm/s and $4.98 \times 10^{-08} \pm 2.84 \times 10^{-08}$ cm/s for the soft and stiff constructs respectively (Figure 6.4d). For the stiff constructs, this EDTA treatment resulted in a statistically significant increase in permeability, but this effect was not observed for the soft constructs. Using these permeability values to calculate the cellular component with Eq. 4, we found the average permeability of just the cell layer to be $2.75 \times 10^{-08} \pm 1.30 \times 10^{-08}$ cm/s and $7.34 \times 10^{-08} \pm 4.19 \times 10^{-08}$ cm/s for the soft and stiff constructs respectively. Although the total construct permeabilities were very different between the soft and stiff conditions, the contribution of the cell layer alone was on the same order of magnitude.

The measured permeability of our endothelial layers is lower than other reported values for endothelial cells with comparable tracers cultured *in vitro*[173,198] and is comparable to permeabilities reported for vasculature *in vivo*[202,203]. It is well known that ECM interactions improve barrier function *in vitro*[189,191,193,194], and thus we believe the

presence of these cell-ECM interactions explain the low permeabilities observed in our constructs. Our endothelial layers (for both the soft and stiff conditions) demonstrated lower permeability values than reported for traditional systems, suggesting that even without the additional resistance to dye movement from compacted tissue, the cell-ECM interactions supported a more *in vivo*-like phenotype. Our soft and stiff constructs demonstrate different transport profiles, which is expected as increasing collagen concentration is known to increase resistance to macromolecular movement within the gels. And thus, our platform is capable of represnting tissue-scale model to study endothelium (soft constructs) as well as an ECM-rich method to examine the endothelium on its own (stiff constructs). This gives us the ability to mimic the *in vivo* environment of endothelium interacting with tissue, but also to observe changes to the endothelium in isolation. Finally, our endothelial constructs demonstrate this lower permeability value in a short culture period of just five days whereas other groups require up to 15 days of culture to obtain comparable results[175]. Our expedient and versatile platform for measuring permeability makes our culture method more amenable to applications in biological discovery and drug screening.

*A high-throughput assessment of endothelial permeability with widefield imaging*

Quantification of endothelial permeability using optical sectioning affords direct comparison with *in vivo* measurements, but collecting optical sections is significanlty more time-consuming than other modalities, which limits the throughput of the analysis. We hypothesized that by using the $\Delta I$ value from widefield images, we could semi-quantitatively assess the permeability of endothelial-coated constructs, which would be appropriate for high-throughput studies in which comparison between conditions is more relevant than absolute quantification.

These experiments were conducted similarly to those described for the results in Figure 6.4. We first implemented a detection scheme that would accommodate a larger population of microtissues (Figure 6.5a). With the brightfield channel, we used Fiji[187] to threshold the images and bring microtissue constructs to the foreground. We then converted these images to black and white, and used built-in object analysis tools to

detect the area, centroid, and edges of each construct. Using the red fluorescence channels, we recorded the intensity across a line from the centroid of the microtissue to 100 pixels outside the edge of the microtissue. We repeated this intensity measurement for a total of 5 linescans per microtissue and averaged the results. This process was automated to expedite the image processing, with a runtime of 1.66 – 7.22 seconds per droplet analyzed. An example of an intensity profile for an endothelial-coated construct is shown (Figure 6.5a). With widefield imaging, we hypothesized that the majority of the out-of-plane signal would come from the dye bath above the microtissues. To minimize noise from out-of-plane signal, we also introduced a larger size construct to our experiments, testing the original size (~200 μm radius) and a larger construct (~300 μm radius). We qualitatively observed that the acellular microtissues appeared to be saturated with dye, whereas there was some exclusion of dye with the cell layers for both the endothelial-coated and EDTA-treated conditions (Figure 6.5b). We calculated the radius of the microtissues (Figure 6.5c), the average intensity inside and outside of the droplet, and used these values to calculate ΔI for widefield (Figure 6.5d). The images for each treatment group were collected in 55 seconds, and the average population size examined in this representative dataset is 152 microtissues.

As with our previous experiments, we observed significant changes in the diameters of soft constructs (acellular vs. coated for all conditions $p<0.01$), and observed little to no effect when coating stiff microtissues with endothelial cells (Figure 6.5c). Next, we examined the transport of 150 kDa TRITC-dextran across the endothelial layer (Figure 6.5d), which was expected to largely be excluded by a healthy endothelial barrier. For all size and stiffness combinations, we were able to detect a statistically significant change in $\Delta I$ between the acellular and coated conditions. This again demonstrates that for all stiffness and size conditions, the addition of the endothelial cell layer created a barrier to solute transport -- either via the cell layer, changes to the ECM, or a combination of the two. Finally, we determined changes in $\Delta I$ could be detected with widefield imaging after perturbation of the cell layer by releasing cells with EDTA. We found that with the small, soft condition, we were unable to detect a statistically significant change in $\Delta I$; however, for the large and small stiff constructs as well as the

large, soft microtissues, the difference between the coated and EDTA treated conditions were statistically significant ($p<0.01$).

Additionally, endothelial permeability is known to be modulated by cytokines[180,204,205], hormones[206,207], and endotoxins[180,208]. We tested the effect of two inflammatory cytokines – TNF-α and TGF-β – which were expected to increase the flux of dye through the endothelial barrier by disrupting adherens junctions. We found that for both sizes of stiff constructs, there was a statistically significant decrease in $\Delta I$ (comparing coated to either TNF-α treated or TGF-β treated, $p<0.01$), meaning that our assay detected the response to the inflammatory cytokines. This change was not observed for either size of the soft constructs, likely due to the additional resistance to diffusion by the compacted ECM. We have shown that using just widefield imaging, we can detect changes in permeability in response to inflammatory signals, using TNF-α and TGF-β for this sample case.

There are several modes of endothelial disruption that are valuable to study *in vitro*. We have shown that the effects of high-concentration chelating agents (e.g. EDTA) can be observed both with optical sectioning and with widefield measurements. This resulted in total physical disruption of the endothelial layer, which could represent a physical injury to the endothelium or could be used to study endothelial healing and remodeling in response to injury in a high-throughput *in vitro* platform. Additionally, lower concentrations or different incubation methods could be used to study physiologically relevant effects of chelating agents, which has applications from studying nitric oxide pathways to optimizing dosing and drug combinations for treating atherosclerosis. We also demonstrated that stimulation with inflammatory cytokines had detectable changes in endothelial permeability. The large sample sizes and ease of fabrication makes this platform well-suited for studying dosing of inflammatory stimuli, as well as screening for vascular toxicity in compound libraries. Finally, as transport across the endothelial barrier is required for all drugs administered intravenously or absorbed through the gastrointestinal tract, this model system could be used to determine the ability of therapeutics to cross the endothelium as a drug screening assay.

Conclusions

Our method for coating ECM-based microtissues with endothelial cells results in endothelium that interacts directly with a collagen tissue compartment – remodeling ECM via compaction as well as deposition of basement membrane proteins. Although others have used microcarries to culture endothelial cells[80,185,186], we have demonstrated, for the first time to the authors' knoledge, high-throughput assessment of endothelial permeability on natural ECM, supporting robust statistical analysis. Streamlining our measuremnt furhter, we showed that widefield imaging is a viable method for semi-quantitatively assessing endothelial macromolecular permeability for tissue-level measurments (compacted soft constructs) as well as for just the endothelium (stiff constructs). Changes in dye exclusion were seen in our control conditions (acellular, coated, and EDTA treated); but more importantly, we can use our microtissue platform to detect changes in permeability with physiologically relevant stimuli. With these permeability measurements, we found that our platform recapitulates barrier function that is comparable to *in vivo*, which we hypothesize is due to the direct coupling of remodeled 3D ECM with the endothelial cell layer.

Our platform enables rapid fabrication (over 20,000 carriers produced per hour), quickly acquires images, and permits automated data analysis of our constructs. The miniaturization of the tissues also minimizes the cell number requirements, making this platform amenable to precious cell and ECM sources. Moreover, because our growth conditions are compatible with standard cell culture equipment (e.g. multi-well plates), this method could be scaled up further and be integrated with automated liquid handling systems and automated imaging platforms. Overall, this platform recapitulates the functions of traditional transwell inserts, but affords novel application to high-throughput studies and opens up new possibilities for interrogating cell-cell and cell-matrix interactions. Permebility assays are not currently used for drug screens as no scalable platforms exist to make this measurement, making our platform an invaluable tool in studying how molecules enter the interstitial space and how they may affect sick or leaky vasculature. Potential applications also include detection of ECM deposition and remodeling in a high-throughput culturing platform, as well as studying specialized

endothelial and/or epithelial function *in vitro* -- including the blood-brain barrier. And due to the increased physiological relevance and the high-throughput nature of microtissues, our platform could facilitate screens for edematous agents or other modulators of endothelial permeability.Additionally, the use of widefield microscopy (as opposed to optical sectioning/confocal) and simple fabrication makes this platform more widely applicable and easier to disseminate to other labs for practical application of this measurement. With the ease of fabrication, flexibility in cell type, and large sample sizes, this platform has a myriad of potential applications.

Acknowledgements:

We thank the American Heart Association (Scientist Development Grant 13SDG6450000), the National Heart, Lung, and Blood Institute (NHLBI R21 HL132256), the National Institute of Environmental Health Sciences (NIEHS R21 ES027622), the National Science Foundation GRFP (Grant 00039202) for support. Portions of this work were conducted in the Minnesota Nano Center, which is supported by the National Science Foundation through the National Nano Coordinated Infrastructure Network (NNCI) under Award Number ECCS-1542202. We also thank Dr. Paolo Provenzano for the use of his multiphoton microscope, and Julia Nguyen and Dr. Gregory Vercellotti for isolating and generously donating HUVECs.

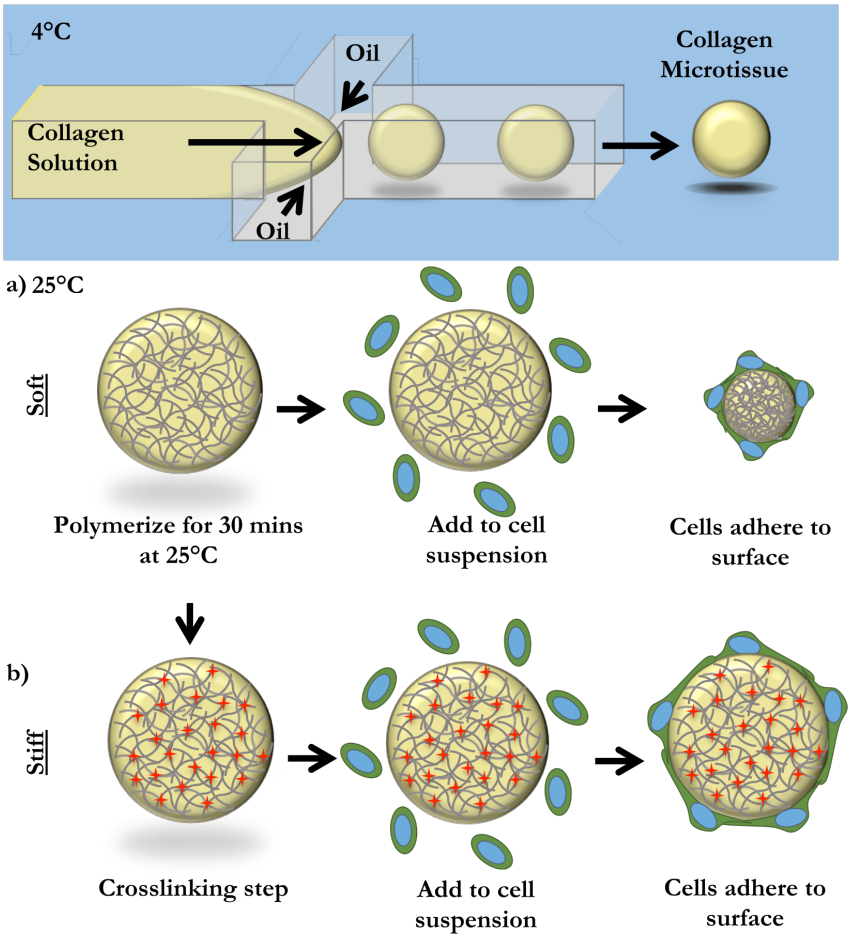


**Figure 6.1:** ***Fabrication of endothelial-coated collagen microtissues***

Liquid 6 mg/mL collagen I microtissues were generated using a chilled flow-focusing microfluidic device. Microtissues were collected and polymerized off-chip at 25°C for 30 minutes. (a) In the case of "soft" microtissues, we did not need to further manipulate the collagen microtissues. To coat with cells, microtissues were mixed with a single-cell suspension of endothelial cells. In this "soft" mode, cells compacted the collagen microtissues. (b) To prevent compaction, we created "stiff" microtissues. After polymerization, microtissues were crosslinked with formalin. "Stiff" microtissues were then washed thoroughly and coated by incubating with a single cell suspension of endothelial cells. Cells created a monolayer on the surface of the microtissues, but did not change the overall size of these "stiff" microtissues.

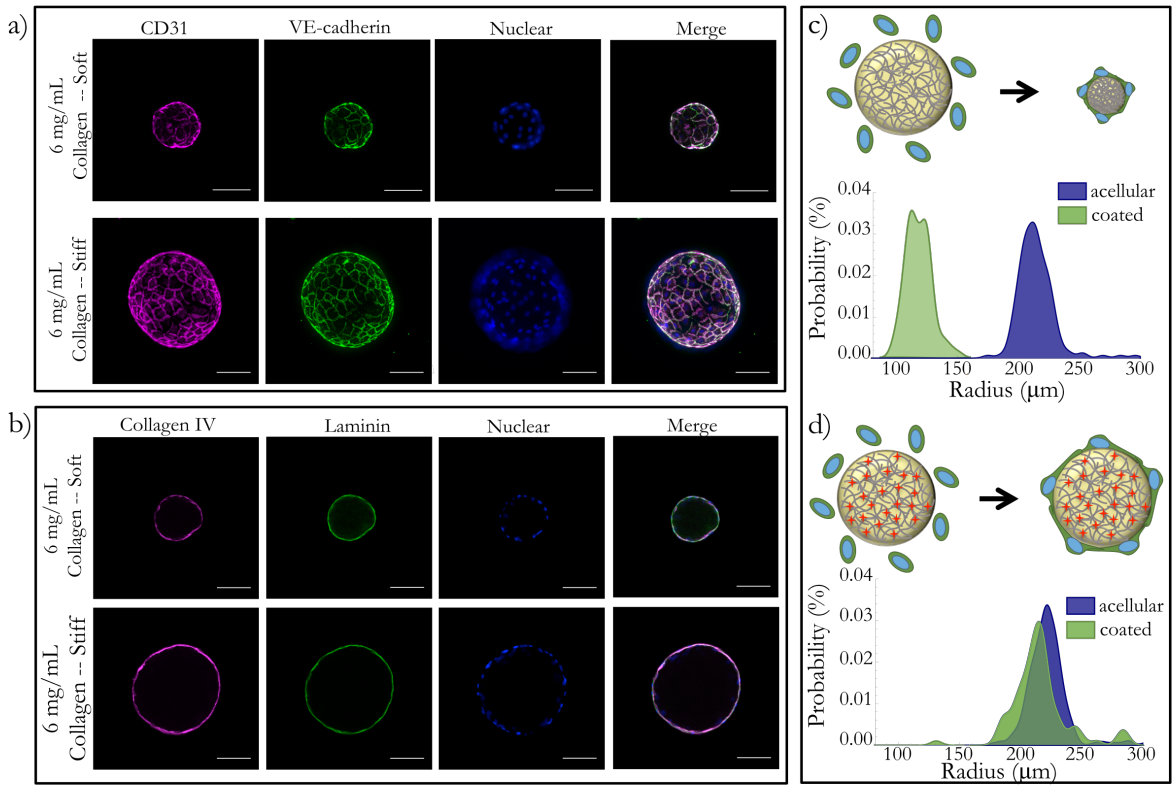


**Figure 6.2:** ***Endothelial cells formed confluent monolayers and remodel ECM-based microtissues***

Both soft and stiff microtissues were coated with endothelial cells and cultured for 5 days. (a) On both soft and stiff microtissues, cells create confluent monolayers. Cells in all conditions have characteristic morphology and tight-junction expression, visualized with CD31 and VE-cadherin. (b) Using immunofluorescence, we observed that the endothelial cells deposited Collagen IV and Laminin on the surface of the collagen constructs for both the soft and stiff conditions. We qualitatively observed that (c) coating soft matrices with endothelial cells resulted in compaction, but (d) stiff matrices did not have a significant size change. We quantified the projected area of the droplets before and after coating to quantify this result and found the population shift for the compaction to be extremely statistically significant, but observed no statistically significant change for the stiff matrices. Scale bars 100 μm.

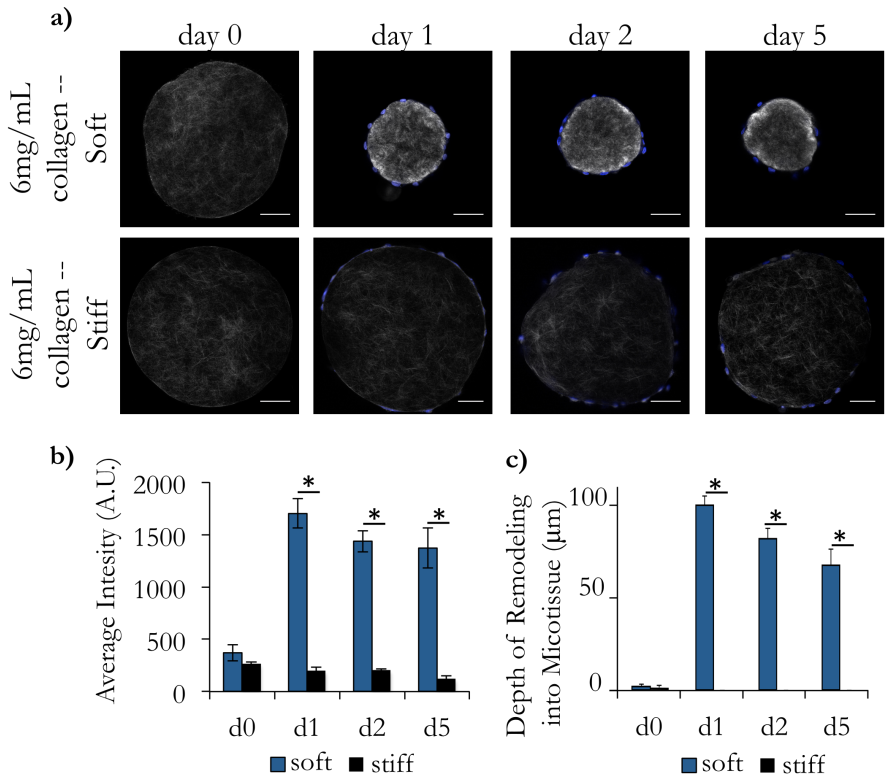


**Figure 6.3:** ***Second harmonic generation imaging reveals local remodeling of collagen architecture***

Acellular collagen droplets were coated with endothelial cells and cultured for 5 days. (a) At intermediate timepoints, droplets were collected and imaged using Second Harmonic Generation (SHG) to visualize the collagen fibers. (b) We observed that the average intensity of the soft microtissues on d1, d2, and d5 after coating with endothelial cells was significantly higher than acellular as well as the corresponding timepoints for the stiff tissues. In (a), we observed a dense ring of collagen at the surface of the microtissues. (c) To quantify this, we took linescans from the center of the microtissues to the surface and recorded the image intensity along the line. We repeated this 5 times for each droplet and reported a moving average with standard error of these linescans for each condition. (d) Using these intensity profiles, we measured the distance into the droplet that displayed large differences in intensity (defined as 5-fold brighter than the baseline average on the d0 measurements). We found that the stiff droplets showed very little remodeling of the interior of the droplet, but the soft constructs had large changes in intensity up to 97 μm from the surface of the droplet. Scale bars 100 μm.

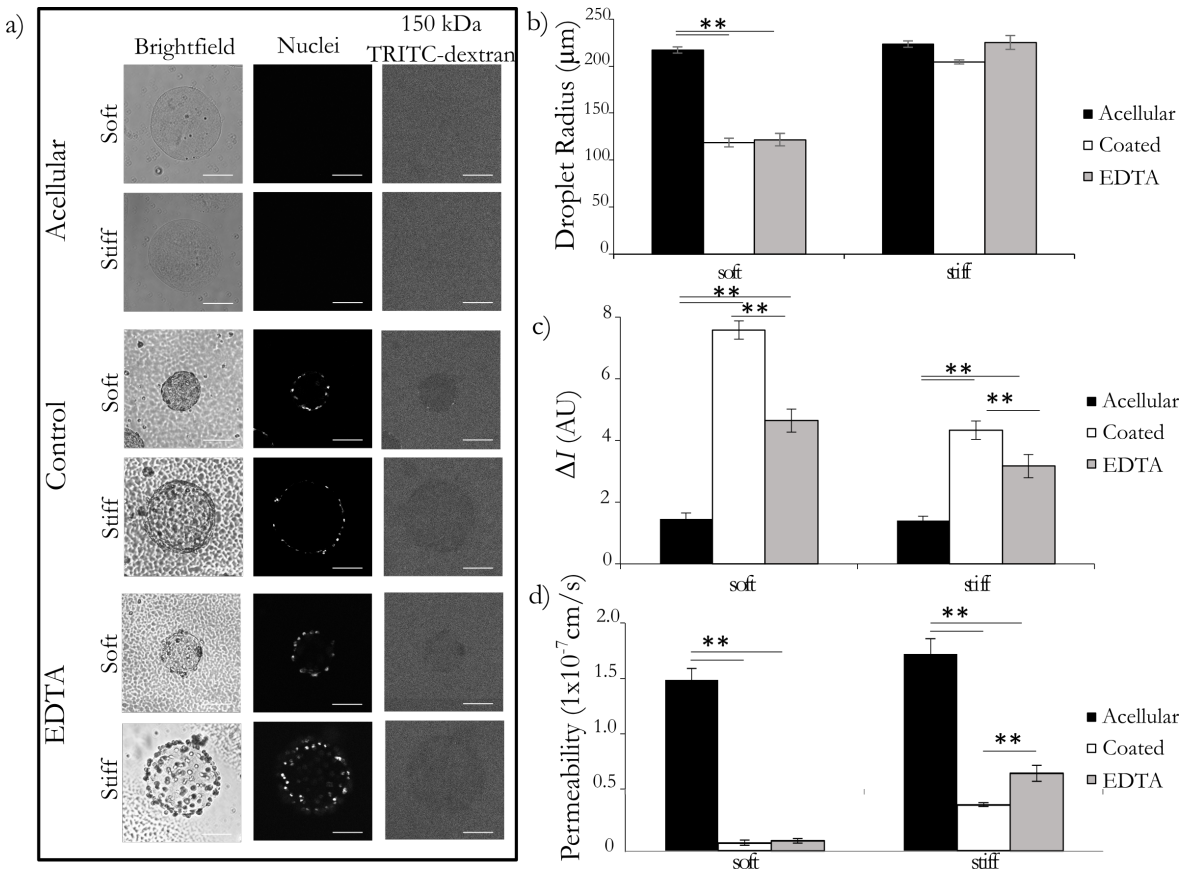


**Figure 6.4:** ***Microtissue endothelial barrier function is comparable to in vivo permeability***

Endothelial cells were cultured on the surface of soft and stiff collagen microtissues for 5 days. Tissues were collected and some were treated with 5 mM EDTA for 30 minutes. Constructs were placed in a 12.5 μg/mL dye bath and incubated for 20 minutes. (a) Constructs were imaged with brightfield and optical sectioning. Brightfield imaging shows the location and geometry of the microtissues, nuclear stain confirms the presence of cells, and the movement 150 kDa TRITC-Dextran was visualized with fluorescence microscopy. We qualitatively observe that acellular constructs do not impede dye movement, whereas the control condition showed exclusion of the dye from the interior of the microtissue for both the soft and stiff conditions. The EDTA treated condition appeared to have an intermediated phenotype. Background noise was reduced in representative images for clarity. (b) We report the average droplet radius with standard error, showing that the soft constructs were compacted significantly, and the stiff constructs were largely unchanged in diameter. (c) Comparing the intensity inside and outside the droplet (ΔI), we found that ΔI was small for acellular constructs, and largest for coated constructs for both soft and stiff microtissues. We found that the removal of the cell layer resulted in an intermediate ΔI for

both stiffnesses. (d) Converting the $\Delta I$ to the permeability using Eq. (3), we found the acellular constructs to have the largest permeability, and the coated controls to have a permeability that was statistically significantly smaller for both cases. For the EDTA treated group, we found that this increased the average permeability for the stiff constructs in a statistically significant manner. There was a slight increase in the average also for the soft constructs, but this difference was not statistically significant. We used these permeability values to calculate the contribution of the ECM and the cell layers individually and found the permeability of the cell layer to be on the order of $1x10^{-8}$ cm/s. All comparisons completed with one-way ANOVA with post-hoc Tukey HSD test; $p<0.01$ = **. Scale bars 100 μm.

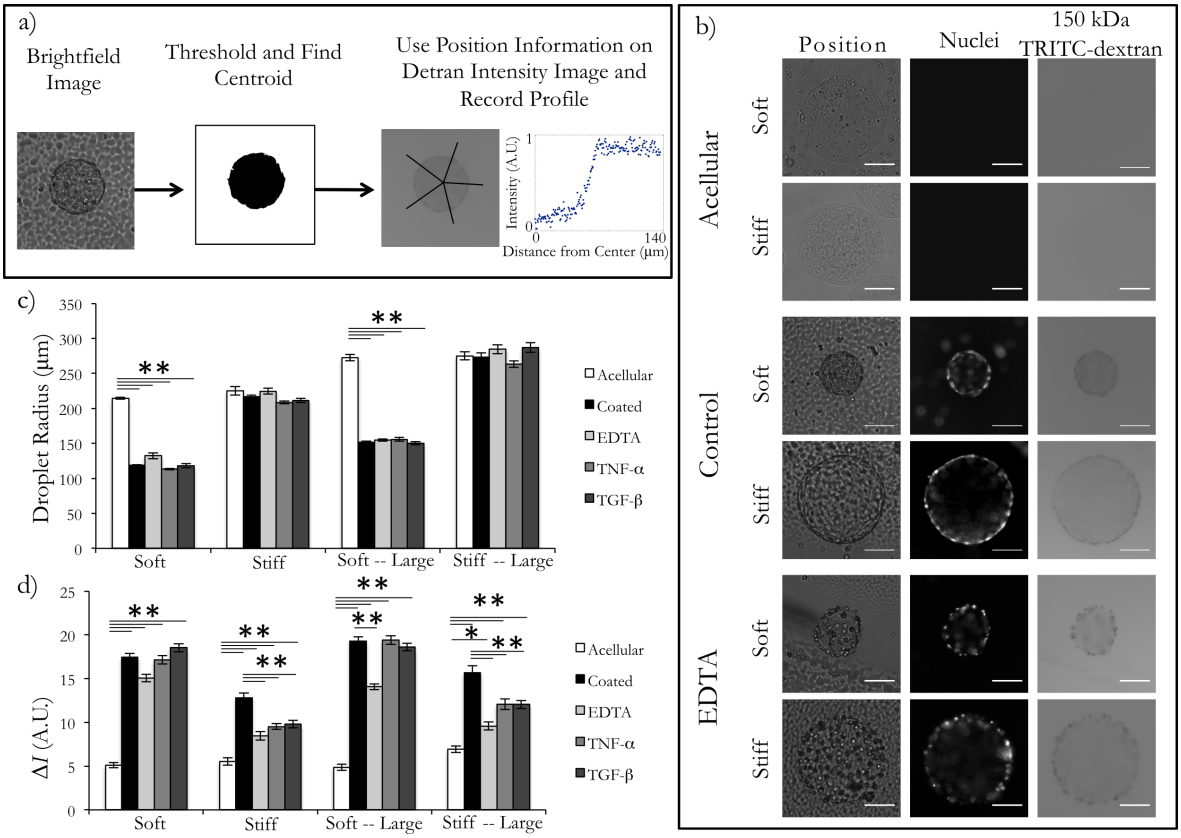


**Figure 6.5:** ***Endothelial barrier function can be assessed with widefield imaging for high-throughput studies***

Endothelial cells were cultured on the surface of collagen microtissues for 5 days before assessing permeability. Constructs were soaked in 12.5 μg/mL bath of 150 kDa fluorescent dextran. Constructs were then imaged with widefield microscopy for the brightfield and fluorescent channels. (a) To assess permeability, we used brightfield images to detect the centroid and edges of each microtissues and collected linescans from the center of the droplet to 100 pixels outside the edge of the construct. (b) Representative images from acellular, control HUEC-coated, and 5 mM EDTA treated microtissues are shown. (c) When comparing the average microtissue radius (shown with standard error) for each condition, we observed consistent compaction of soft microtissues, and little change in size of stiff microtissues. (d) To assess permeability, we calculated the difference in intensity between the outside and inside of the droplet ($\Delta I$). We observed that the acellular constructs were more saturated with dye in all construct conditions for both sizes of dye. However, the cell monolayer demonstrated semi-permeable qualities, which was especially visible on the stiff constructs. We found the addition of the cell layer increased $\Delta I$ for all conditions ($p<0.01$). In the large-soft and both stiff conditions,

the modulation of the cell layer with EDTA resulted in a statistically significant decrease in $\Delta I$. When we tested inflammatory cytokines on our platform, TNF-α and TGF-β resulted in statistically signficant decreases in $\Delta I$ (relative to the coated control) for both sizes of stiff microtissues. From this, we concluded that the stiff microtissues were better suited for the macromolecular permeability assay (one-way ANOVA with post-hoc Tukey HSD test; $p<0.01$ = **, $p<0.05$ = *). Scale bars 100 μm.

## *Chapter 7 :* Application – *Liver Micromimics*

### Introduction

One of the leading causes of preclinical and clinical drug attrition, post-market drug withdrawals, and acute liver failures is drug-induced liver injury (DILI)[209]. These failures are costly, both in terms of cost and time to successfully bring a new drug to market. In an effort to streamline drug discovery and prioritizing lead compounds, there is increasing interest in predicting liver toxicity earlier in the drug development process. Because of species-specific differences in the liver's metabolic pathways (e.g. drug metabolism)[6,210], there is a need for predictive *in vitro* human liver models during the preclinical stages of drug development.

A major challenge in creating *in vitro* systems is that the microenvironment in which cells are grown affects their function significantly. The "gold standard" cell source are primary human hepatocytes (PHHs), isolated from human livers[211]. Typically these cells are cultured on collagen-coated 2D multi-well plates for and the response to different drug concentrations is assessed using cell viability, morphology, and metabolism of substrates in the culture medium[212,213]. Even with the addition of adsorbed ECM proteins, these platforms are unable to faithfully reproduce the 3D cell-ECM and cell-cell interactions found in physiology. Additionally, long-term culture in these platforms can be challenging, as hepatocytes are prone to de-differentiate and apoptosis in traditional 2D culture[212,213]. Thus, there is interest in new model systems that incorporate a 3D microenvironment for the hepatocytes.

A popular method for creating a 3D environment with a high density of cell-cell interactions for the hepatocytes is spheroid culture. While self-assembled 3D spheroids mitigate some limitations of 2D cultures, this method is ineffective and fails for greater than 50% of PHH donor sourced cells. Usually this is due to issues with structural stability, as the only ECM components in spheroids are produced by the hepatocytes and the rates of ECM secretion are variable across donors[213,214]. To improve the structural stability of the constructs, encapsulating spheroids into bioinert agarose[215] or poly(ethylene glycol)[57,216] hydrogels has been tested, but neither provide 3D ECM interactions as occur *in vivo*.

To mimic the cell organization seen *in vivo*, others have used 3D bioprinting methods to create liver models. Although these have several advantages as far as material choice and patterning of the cells, the final constructs are large (~mm in diameter) thus requiring large volumes of cells and reagents. Ultimately, the large volumes of cells required for these large constructs constrains these platforms to low-throughput applications[61]. Microfluidic liver-on-a-chip devices have also attempted to mitigate the previously discussed issues with liver model systems. However, these systems remain low throughput, require complex fluid handling, use large amounts of often limited novel drugs via the tubing's dead volume, and often layer 2D cell layers on membranes in lieu of a truly 3D cell culture[63,67]. Outside of the biological relevance, these chip setups are undesirable logistically for industry-scale drug screening and drug development as they are incompatible with high-throughput liquid handling systems typically used for large-scale screens[70,211].

The ideal *in vitro* human liver model is scalable, reproducible, modular, and displays long-term phenotypic stability at physiologically-relevant levels for elucidating the effects of chronic compound exposure as in humans; furthermore, the model needs to accessible within a culture format that is compatible with the established screening infrastructure in the pharmaceutical industry. To address this need, we adapted our microtissue platform to develop breakthrough 3D human liver microtissues and supportive fibroblasts that display the critical features necessary for drug development, including scalability, reproducibility, modularity, long-term phenotypic stability, and clinically-relevant utility for DILI assessment[217]. In addition to drug screening, our platform is uniquely-suited to answer questions regarding 3D ECM interactions and their role on liver cell function in our constructs. We explore the modular nature of our liver microtissues workflow, performing a targeted-screen of combinations of ECM proteins in our liver microtissues. We also use our platform for biological discovery, investigating the effect of combinations of liver-specific ECM proteins, as well as testing various cell sources for liver mimics including stem cell derived iHeps.

## Materials and Methods

*Microfluidic and device fabrication*

Microfluidic devices were fabricated following the protocol in Chapters 3 and 5. Before use, tubing was sterilized with 70% ethanol and microfluidic devices were autoclaved to avoid contamination.

*Agarose Microwells*

Agarose microwells were fabricated following the protocol described in Chapter 5. After fabrication, agarose microwells were sterilized with 70% ethanol for 1 hour and washed extensively before use.

*Monoculture Microtissues*

Cell-laden microtissues were fabricated by modifying the protocol described in Chapter 3. Briefly, a solution of rat tail collagen, type I (Corning Life Sciences, Tewksbury, MA) in acetic acid was first diluted in 1X phosphate buffered saline (PBS, Corning) to 6 mg/mL on ice, and then the pH was neutralized to 7.4-7.6 using 1N NaOH. Cryopreserved PHH (Lonza) or Induced Pluripotent Stem Cell–Derived Human Hepatocytes (iHeps; Cellular Dynamics International) were thawed, counted, and viability (>85%) was assessed as previously described[218] and resuspended in the neutral collagen solution. Chilled ferromagnetic beads (Spherotech) were mixed into the collagen solution at a final concentration of 5% v/v. The collagen solution containing cells was perfused into a flow-focusing microfluidic droplet generator inlet at 150 μL/hour in a cold room (4ºC) while fluorocarbon oil (FC-40, Sigma-Aldrich) with 2% 008-fluoroSurfactant (RAN Biotechnologies, Beverly, MA) was perfused to produce collagen droplets. Microtissues were collected in a 1.5 mL low-retention tube that was heated at 37°C to promote collagen polymerization. Polymerized microtissues were washed with PBS, resuspended in culture medium, counted, and seeded into the agarose microwells within a 24-well plate (~600 microtissues/well). Culture medium, the composition of which was described previously[219,220] was collected and replaced on microtissues every 4 days (400 μL/well).

*Co-cultures of PHHs and 3T3-J2 murine embryonic fibroblasts*

3T3-J2 fibroblasts were growth arrested by incubating with 1 μg/mL mitomycin-C (Sigma-Aldrich, St. Louis, MO) in culture medium for 4 hours prior to detachment from the culture substrates using trypsin as previously described[221]. PHH monoculture microtissues were fabricated, counted, and placed into agarose microwells within a 24-well plate. 3T3-J2 fibroblasts were then seeded onto the polymerized PHH microtissues at ~1:1 PHH to fibroblast ratio. The fibroblasts preferentially attached to the collagen microtissues as opposed to the non-adhesive agarose to coat co-culture microtissues. Culture medium was collected and replaced as described above for monocultures.

*Hepatocyte functional assessments*

Culture supernatants were assayed for albumin using a sandwich enzyme-linked immunosorbent assay (ELISA, Bethyl Laboratories) with horseradish peroxidase detection and 3,3',5,5'-tetramethylbenzidine (TMB, Rockland Immunochemicals, Boyertown) as the substrate[221]. Absorbance values were quantified on the Synergy H1 multi-mode plate reader (BioTek).

Cytochrome P450 (CYP450) 3A4 and 2C9 enzyme activities were measured by incubating the cultures with luciferin-IPA or luciferin-H substrates (Promega Life Sciences, Madison, WI), respectively. The metabolite, luciferin, was quantified via luminescence detection on the Synergy H1 multi-mode plate reader according to manufacturer's protocols. CYP1A2 and CYP2A6 activities were measured by incubating the cultures with 5 μM 7-ethoxyresorufin or 50 μM coumarin (Sigma-Aldrich), respectively. The metabolites, resorufin and 7-hydroxycoumarin (7-HC), generated from 7-ethoxyresorufin and coumarin, respectively, were quantified via fluorescence detection (excitation/emission: 550/585 nm for resorufin, and 355/460 nm for 7-HC) on a Synergy H1 multi-mode plate reader[220]. Substrates were incubated in cultures for 3 hours for PHH cultures, and 2 days for trials using iHeps.

*Encapsulating rhodamine-labeled laminin in microtissues*

Rhodamine-labeled laminin (Cytoskeleton, Inc) was mixed into 6 mg/mL collagen solution at 4C to a final concentration of 10 μg/mL. Microtissues were fabricated, polymerized, and samples were moved to 96-well plates before breaking the emulsion. Time-lapse widefield imaging was used to track the movement of rhodamine-labeled laminin before and after breaking the emulsion with PBS.

*Supplementing culture media with proteins of interest*

Complete culture media for PHHs and iHeps was prepared as described previously[219,220]. Proteins of interest were stored at manufacturer recommended temperatures, and were added to cold media before warming to 37°C and adding to microtissues. Human laminin (Sigma), fibronectin (VWR), collagen III (Sigma), and collagen IV (Sigma) were added to final concentrations of 10 μg/mL and media on cultures was replaced every 4 days.

*Data analysis*

Data processing was performed using Microsoft Excel and image analysis was performed using ImageJ[84]. GraphPad Prism (La Jolla, CA) was used to display results. Mean and standard deviation are displayed for all data sets. Statistical significance was determined using Mann-Whitney U test, one-way ANOVA followed by a Tukey-Kramer HSD post-hoc test ($p < 0.05$).

## Results

*Droplet microfluidics for generating reproducible and functional PHH microtissues*

In this adaptation for liver-specific applications, we modified the workflow described in Chapter 5. PHH microtissues were fabricated using flow-focusing droplet microfluidics and seeded into agarose microwells within industry-standard 24-well plates as illustrated in Figure 7.1. Highly reproducible microtissues were fabricated and cultured for 21 days.

*3T3-J2 murine embryonic fibroblasts enhance PHH functions in microtissues*

3T3-J2 fibroblasts are known to enhance PHH functions in both 2D co-cultures[221] and 3D self-assembled spheroids[222]. PHHs and growth-arrested 3T3-J2 fibroblasts (1:1) were coated onto the surface of the collagen-based PHH microtissues and compared to PHH-only (control) microtissues (Figure 7.2a). Supporting previous results with PHH cultures in our microtissue system[217], coated microtissues functionally outperformed monoculture microtissues, as indicated by at least a 1.6-fold increase in albumin secretion and CYP450 activity. Specifically for albumin, coated microtissues outperformed PHH-only microtissues by 1.6- and 7.6-fold at 5 and 21 days (Figure 7.2b). For CYP3A4, coated microtissues outperformed monoculture constructs by 1.6-, 11.7- and 25.1 fold after 5, 13, and 21 days, respectively (Figure 7.2c). For CYP2A6, coated microtissues outperformed PHH-only microtissues by 6.4- and 7.4-fold after 13 and 21 days, respectively (Figure 7.2d). For CYP2C9, coated microtissues outperformed PHH-only microtissues by 19- and 14-fold after 9 and 17 days (Figure 7.2e). Lastly, for CYP1A2, coated microtissues outperformed PHH-only microtissues by 1.6-fold after 9 days (Figure 7.2f).

*Validating methods for doping ECM proteins in collagen microtissues*

While a variety of natural ECM materials are compatible with hepatocyte culture[215,223], rat tail collagen I was selected for our initial model system since it is abundantly and cheaply available at high concentrations needed for gelation (>2 mg/mL) and has been utilized extensively for PHH culture without adverse effects[215,219]. The ECM of the liver, though, is much more complex, including a wide range of collagen proteins (including collagen types I, III, IV, and V[224–226]) as well as glycoproteins (such as laminin, fibronectin, tenascin, and nidogen[226]) and proteoglycans (including heparin, dermatan, chondroitin sulphate, perlecan, hyaluronic acid, biglycan and decorin[227]).

To study the effects of other ECM proteins, we first optimized a method for incorporating supplemental ECM proteins into our microtissue constructs. We initially used rhodamine-labeled laminin as a tracer molecue to visualize the movement and final location of supplemented protein in our setup. Constructs were doped with 10 μg/mL rhodamine-labeled laminin before polymerization (Figure 7.3a), rhodamine-labeled

laminin was easily detected in polymerized microtissues still in the FC-40 oil emulsion. However, after breaking the emulsion with an aqueous phase, the protein escaped the microtissue and the concentration within the microtissue was reduced significantly after only 10 minutes (Figure 7.3a). Alternatively, we soaked acellular microtissues in media with 10 μg/mL laminin or 10 μg/mL fibronectin and using immunofluorescence staining, found that these constructs had detectable levels of the proteins of interest after 24 hours (data not shown). The fluoresence intensity stabilized after 5 days (Figure 7.3b), and was verified for long-term culture (21 days, data not shown) .

*Targeted ECM screen on PHH-laden microtissues*

We have observed that PHHs survive and are functionally stable for at least 3 weeks in our system using only collagen I as the construct ECM. We hypothesized that including more of the complexity of the *in vivo* liver ECM in our model system may improve the performance of hepatocytes in our platform. We supplemented our collagen I constructs with laminin, fibronectin, collagen III, and collagen IV in various combinations (+ALL with all 5 proteins, and +ALL condition minus one protein only) and cultured the constructs for 21 days. Using immunofluoresence, we visualized the albumin in our constructs for all conditions tested for PHH monoculture (Figure 7.4a) and PHH co-culture with 3T3-J2 (Figure 7.4b). As observed previously with ELISA, the staining revealed increased albumin staining intensity with co-culture with 3T3-J2 cells for the control collagen I constructs. Within the monoculture and co-culture groups, however, no tested supplemental ECMs resulted in statistically significant increases in fluoresence intensity outside the range of the assay defined by the controls.

We continued our assessment of PHH function via quantification of secreted proteins and CYP450 enzyme activity with ELISA (controls run in duplicate). In the PHH monoculture microtissues, we observed similar responses (no statistically significant differences) between the control (collagen I) and supplemented ECM protein conditions, with a steady decline in albumin secretion (Figure 7.4b) and activity of CYP3A4 (Figure 7.4c), CYP1A2 (Figure 7.5c), CYP2A6 (data not shown), and CYP2C9 (data not shown) for all conditions tested. For the co-culture conditions of PHH and 3T3-

J2s (Figure 7.5b-d), we again observed similar performance (no statistically significant differences) between the collagen I controls and any conditions with supplemented protein. From both the immunofluorescense and ELISA readouts (Figure 7.5), no tested combinations of ECM produced a significant increase or decrease in PHH function in our platform outsdie the range of the assay defined by the controls. This trend was true for both coated and uncoated conditions.

*Targeted ECM screen on iHep-laden microtissues*

Although PHH perform well in specific *in vitro* models, PHHs are a severely limited resource and there can be significant variability in the quality of cells between donors. Thus, there is interest in pursuing other cell sources, and induced Pluripotent Stem Cell–Derived Human Hepatocytes (iHeps) have the potential to be: (i) adequately scalable for large-scale compound screens, and (ii) serve as a patient-specific cell source, facilitating toxicity screens for individual patients[228–232]. We examined the performance of iHeps in our microtissues, and assessed the impact of supplemental ECM proteins on these cultures.

Based on previous work[220], we cultured all conditions in the presence of 3T3-J2 cells. We performed a similar targeted ECM screen, soaking iHep-laden collagen I constructs with laminin, fibronectin, collagen III, and collagen IV individually, as well as all 5 of these proteins simultaneously (+ALL). We used immunofluorescence to visualize albumin in the constructs after 32 days of culture (Figure 7.6a). We observed more heterogeneity in the cell morphology with the iHeps than with the PHHs. With the exception of the +Laminin and +ALL conditions, two distinct morphologies were single cell distributions of cells that were weakly positive for albumin, and clusters of cells that were strongly positive for albumin. For the + Laminin and +ALL conditions, only the single-cell distribution that stained weakly for albumin was observed.

These qualitative differences in morphology and immunofluorescence staining were reflected in the quantitative functional readouts. Quantifying albumin production with ELISA over the timecourse of the experiment (Figure 7.6b), we observe an extremely significant decrease in albumin production for the +Laminin condition ($p<0.0001$) and a

significant decrease for the +ALL condition ($p<0.001$) relative to the control condition (collagen I only). This trend continued for the CYP functionality tested, reflected in CYP3A4 (Figure 7.6c), CYP1A2 (Figure 7.6d), and CYP2C9 (Figure 7.6e). We also examined alpha-fetoprotein (AFP) levels as an indicator of iHep maturity, and found no clear increase or decrease in AFP concentration (Figure 7.6f).

Discussion

An ongoing challenge for assessing the effects on the liver of chronic compound exposure *in vitro* is the lack of a model system that is scalable, reproducible, modular, and supports long-lasting organotypic liver function. In this study, we adapted our collagen microtissues platform to create human liver microtissues in a 3D ECM-based microenvironment. Further, culture of the microtissues within agarose microwells in industry-standard multiwall plates makes this technology more relevant for real-life application of toxicity screening.

It has been shown previously that the cell-cell interactions between hepatocytes and NPC types can affect hepatocyte function in developing and adult livers[215,223]. For our *in vitro* model, we replicated this effect by co-culture with 3T3-J2 murine embryonic fibroblasts[233], as this line (over other potential choices such as human liver sinusoidal endothelial cells[219], hepatic stellate cells[234], and Kupffer cells[235]) has been shown to induce higher PHH functions in 2D co-c ultures[221]. In our 3D culture system, we observed that the fibroblasts enhanced PHH functions over PHH mono-cultures. Examining albumin and urea secretion as well as activity of multiple CYP450 isoenzymes, we found the coated microtissues displayed long-term phenotypic function[217]. Such enhanced longevity could enable the elucidation of the chronic effects of drugs, industrial chemicals, and disease stimuli on PHH functions.

We further hypothesized that our modular microtissues would be uniquely suited for 3D ECM screens. We first optimized a method to incorporate supplemental ECM proteins into collagen I microtissues. We investigated first the most reagent-conservative approach of doping the proteins in with the liquid collagen solution before microtissue fabrication. We found that the supplemental protein was compatible with our fabrication

process, as signal from our tracer protein (rhodamine-labeled laminin) was distributed evenly in collagen microtissues while still in the oil phase. However, shortly after breaking the emulsion (~10 minutes) the supplemented protein was evenly distributed in all of the aqueous phase and was not confined or concentrated in the droplet space. This is likely due to the highly porous nature of collagen I hydrogels, which have a mesh size of ~ 1 μm[77], which is too large to contain our supplemental proteins of interest (~400-900kDa) by confinement.

A second approach to incorporate other ECM proteins into our collagen I constructs was to supplement the culture media with the proteins of interest and allow them to diffuse into the constructs. We found that soaking constructs in protein-supplemented media resulted in detectable levels of protein in the constructs after 24 hours, with saturation of the constructs being reached after 5 days. From a logistics standpoint, this method of incorporating supplemental protein has several advantages. Because all of the replicates for all conditions are fabricated from the same run of microtissues, potential variation in cell handling, collagen solutions, and polymerization conditions are controlled between conditions. And for cases where cells are a precious resource, this method requires only one droplet setup to fabricate tens of thousands of microtissues, reducing waste from dead volume in the system.

Using our optimized method, we augmented collagen I constructs with additional liver-inspired ECM molecules such as other collagens (e.g. collagen III, collagen IV), fibronectin, and laminin. We confirmed that our scaled-up version of the experiment was still successful, as our collagen I control constructs had a strong response to co-culture with 3T3-J2 cells, with albumin production and CYP activity improving over the course of the 21-day experiment. The stability of these constructs is imperative for studies of chronic drug toxicity and biological discovery of phenomenon that take time to develop. Examining the effects of supplemented ECM proteins on PHH monocultures, we hypothesized that the addition of these ECM proteins may improve hepatocyte function *in vitro* even in the absence of the supporting cell layer. We found, though, that none of the combinations of proteins tested resulted in a statistically significant change in function when quantified with the described assays. Running the same ECM screen in the

presence of the supporting 3T3-J2 cell layer, we also did not find any combinations of ECM that improved or diminished PHH function in a meaningful way. These results indicate that the effect of the supporting cell type is not replicated solely by the introduction of more ECM proteins and while incorporating more of the complexity of the *in vivo* liver in our model, we may be more interested in investigating cell-cell interactions for future studies.

We completed a targeted ECM screen also with an alternative cell source – human stem-cell derived cells (iHeps). We observed albumin secretion and CYPP450 enzyme activity for iHeps encapsulated in collagen I with surface-coating of 3T3-J2 cells. Examining the supplemental ECM protein conditions, we conclude from our results that the presence of supplemented laminin (even with other supplemented ECM proteins) interferes with several key functions of iHeps in our model system. We observed morphologically that culture conditions with supplemented laminin failed to form clusters of cells and instead remained as single cells in the constructs. It is known that homotypic interactions are important for iHep viability and function *in vitro*[220], so this difference in cell patterning within the microtissues may be the cause of the poor cell performance and warrants further investigation. Finding the ideal culture conditions for iHeps in our system could be extremely valuable, as this cell source is both scalable and patient-specific[228–232], potentially facilitating personalized screening for off-target effects (e.g. liver toxicity) in the future.

We demonstrate that our platform supports 3D culture of human liver cells (PHH) and stem cell derived liver-like cells (iHeps). Cells display phenotypic stability, including CYP450 enzyme activities, for 3 weeks, and can be used within industry-standard multiwell plates to assess clinically-relevant compound metabolism and toxicity. We also demonstrate the potential for this platform for ECM screens, and similar experiments could be scaled up and conducted for compound screens. Ultimately, this platform can serve to reduce drug attrition, enable the screening of molecules to optimize cell functions in cell-based therapies, and aid in the studies of liver physiology and disease.

Acknowledgements

Portions of this work were conducted in the Minnesota Nano Center, which is supported by the National Science Foundation through the National Nano Coordinated Infrastructure Network (NNCI) under Award Number ECCS-1542202. We thank the National Science Foundation Division of Chemical, Bioengineering, Environmental, and Transport Systems (NSF CBET 1704332) and the National Institute of Environmental Health Sciences (NIH R21ES027622) for supporting this work. Experiments for this chapter were performed collaboratively with the Microfabricated Tissue Models Lab, directed by Dr. Salman R. Khetani. Alexandra L. Crampton completed translation of the microtissue technology and initial optimization. David Kukla performed continued optimization of PHH-specific workflow and readouts, and Reagent Panday optimized iHeps-specific workflow and readouts. Experimental design was a collaborative effort between David K. Wood, Salman R. Khetani, Alexandra L. Crampton, David Kukla, and Regeant Panday. Data for the experiments described in this chapter were setup collaboratively by Alexandra L. Crampton, David Kukla, and Regeant Pandy in the Microfabricated Tissue Models Lab. David Kukla and Regeant Panday maintained experiments throughout the culture period, and Alexandra L. Crampton performed all ELISA, immunofluorescence staining, and data analysis for the work presented in this chapter.

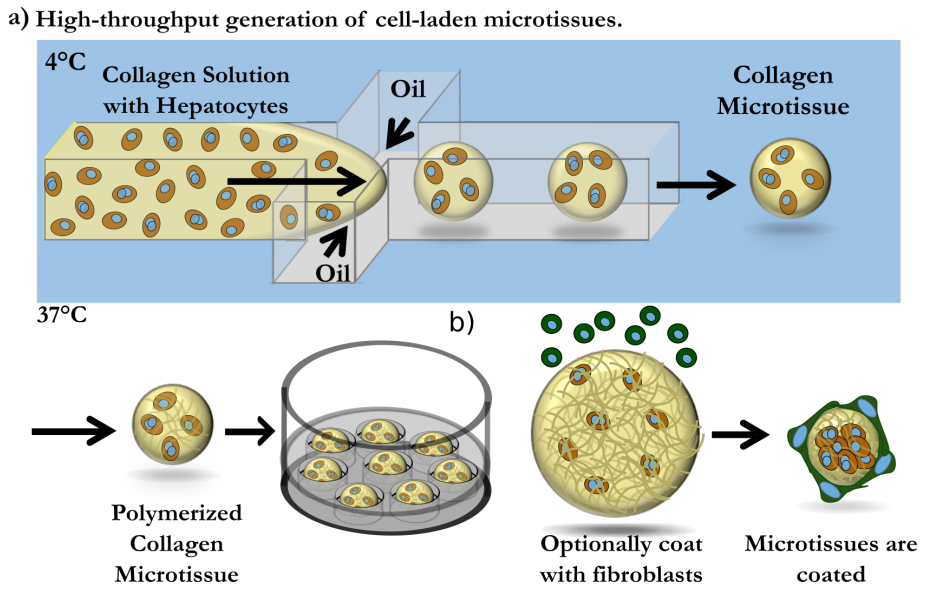


**Figure 7.1:** ***3D human liver tissue platform with tunable cell-cell and cell-ECM interactions for compound screening***

(a) Hepatocytes are suspended in pH-neutralized collagen solution and then perfused through a flow-focusing microfluidic device. Oil is perfused at a rate ~4 times faster than the aqueous phase to produce microtissues. Microtissues are formed using the microfluidic device at 4°C and collected at 37°C to promote the rapid polymerization of the collagen droplets and encapsulation of the cells within the droplets. Oil is removed, and polymerized microtissues are resuspended in culture medium and subsequently seeded into agarose (2% w/v) microwells cast within multi-well plates. (b) The hepatocytes are co-cultured with non-parenchymal cell types, such as 3T3-J2 murine embryonic fibroblasts via surface coating.

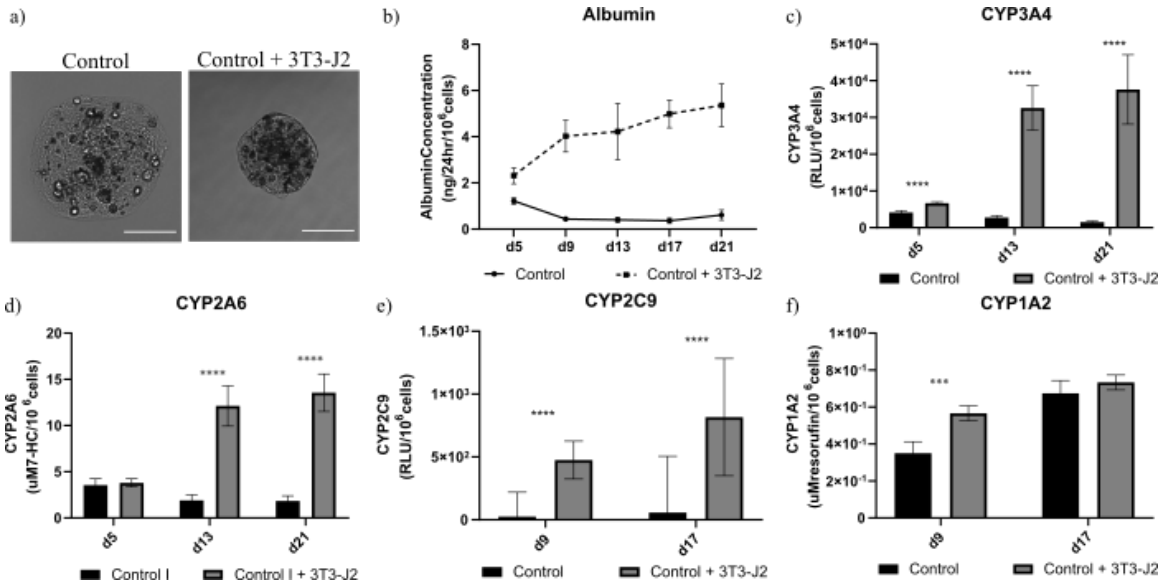


**Figure 7.2:** ***Co-culture of PHHs with 3T3-J2 mouse embryonic fibroblasts in microtissues enhances liver functions***

(a) Brightfield images for tested culture models (monoculture and co-culture coated with 3T3-J2 cells). (b) Albumin secretions throughout the 21 day experiment. Activities of different CYP450 isoenzymes, (c) CYP3A4, (d) CYP2A6, (e) CYP2C9, (f) CYP1A2 in PHH-only (control) and coated microtissues. Statistical significance is displayed for coated microtissues relative to co-encapsulated microtissues (***$p \leq 0.001$, and ****$p \leq 0.0001$).

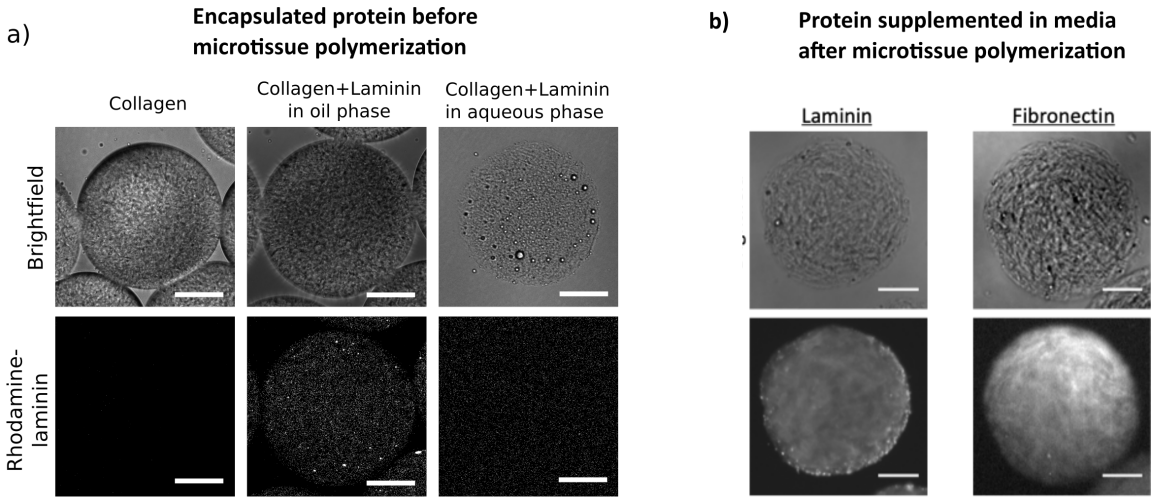


**Figure 7.3:** ***Validation of methods for incorporating ECM proteins into collagen I microtissues***
We initially tested incorporating ECM proteins into the chilled collagen solution before compartmentalization into individual microtissues (a). We observe that the protein is clearly within the droplets while still in the oil phase. However, shortly after breaking the emulsion with cell culture media, the supplemented protein is no longer contained within the droplet. We also examined soaking polymerized collagen I microtissues in a bath of supplemental protein (b). We observe that for our proteins of interest, detectable levels of protein are discernable within the microtissue constructs after 24 hours, with optimal saturation of protein achieved after several days. Representative images shown after 5 days of culture. Scale bars are 50 μm.

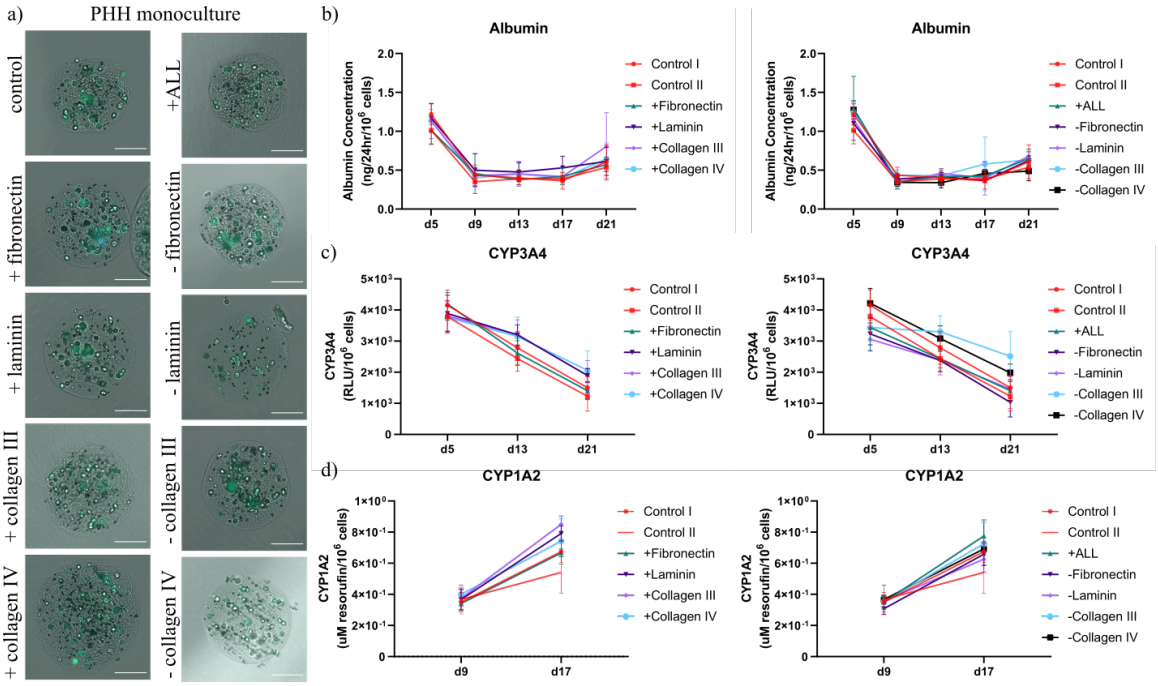


**Figure 7.4:** ***Targeted ECM screen for PHH monocultures in microtissues***

Immunofluoresence stining (a) for albumin (green) and nuclei (Hoechst, blue) show similar construct morphology and albumin production between all protein combinations tested. Examining the protein function with secreted albumin (b), we obsrve that the PHH monocoulture controls (collagen I, red) show a sharp decline from d5 to d9, and maintain low levels of activity throughought the remainder of the 21 day experiment. We observe similar performance for all supplemented ECM conditions tested for the PHH monoculture constructs. Examining CYP3A4 (c) and CYP1A2 (d) activity other indicators of PHH function, we observe no statistically significant differences in substrate metabolism between the controls (red) and any of the ECM conditions tested, with a steady decline in metabolism for all conditions. Error bars represent standard deviation. Scale bars are 100 μm.

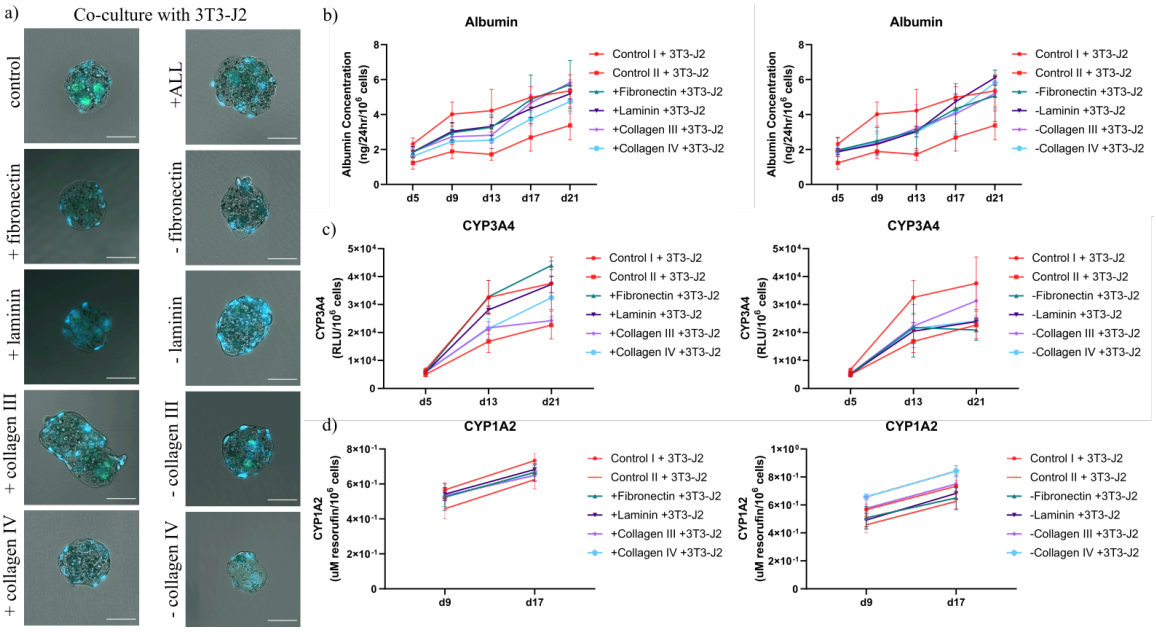


**Figure 7.5:** ***Targeted ECM screen for co-culture of PHH and 3T3-J2s in microtissues***

Immunofluoresence stining (a) for albumin (green) and nuclei (Hoechst, blue) show similar construct morphology and albumin production between all protein combinations tested. Examining the protein function with secreted albumin (b), we obsrve that the PHH co-ocoulture with 3T3-J2 controls (collagen I, red) show a gradual increase in albumin production from d5 to d21. There were, however, no ECM conditions that improved or diminished albumin production outside the range of the control replicates (red). Examining CYP3A4 (c) and CYP1A2 (d) activity as other indicators of PHH function, we observe a trend of increased activity over time with no statistically significant differences in substrate metabolism between the controls and any of the ECM conditions tested. Error bars represent standard deviation. Scale bars are 100 μm.

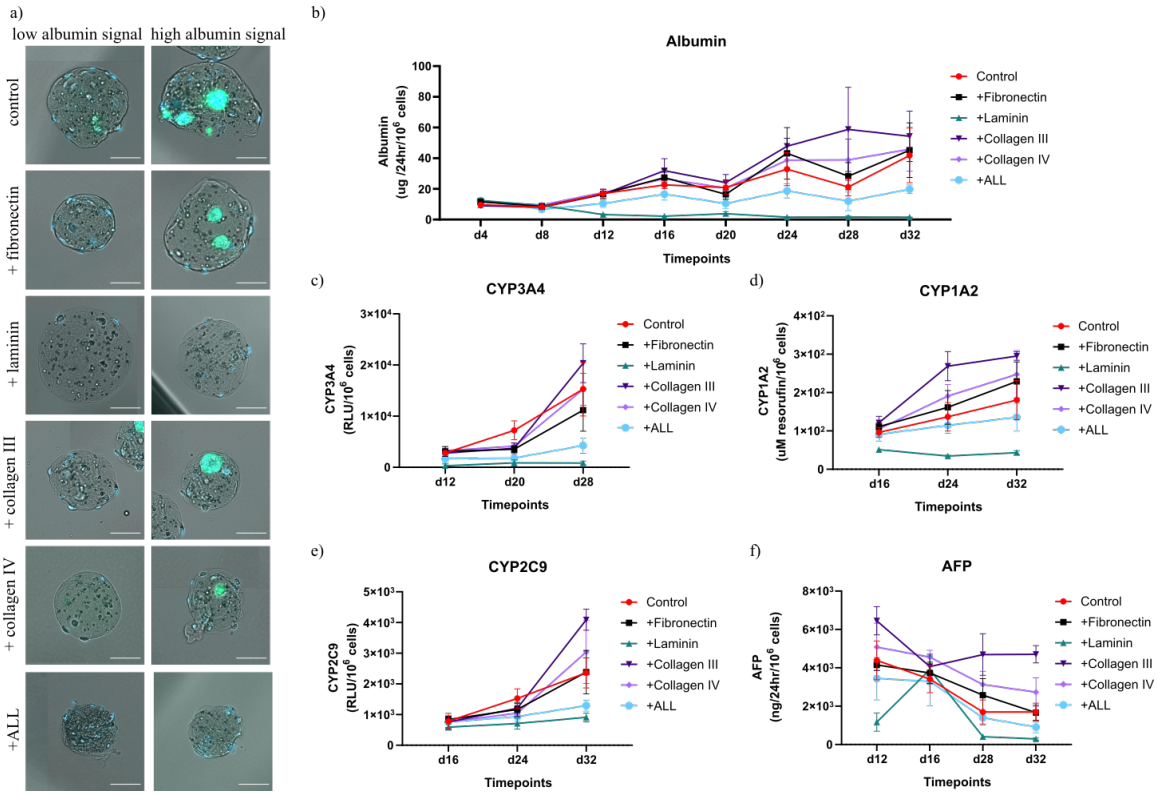


**Figure 7.6:** ***Targeted ECM screen for co-culture of iHeps and 3T3-J2s in microtissues***

Immunofluorescence staining (a) for albumin (green) and nuclei (Hoeschst, blue) show heterogeneity in cell morphology within most of the ECM conditions examined. Constructs began as single cell suspensions, and all conditions had some microtissues that retained this patterning of cells (low albumin signal). In all conditions tested except for +Laminin and +ALL, we qualitatively observe spheroid growth with high intensity of albumin staining (high albumin signal). Quantifying albumin production with ELISA over the timecourse of the experiment (b), we observe an extremely significant decrease in albumin production for the +Laminin condition and a significant decrease for the +ALL condition relative to the control condition replicates (collagen I only). This trend continued for the CYP450 enzyme activities tested, reflected in CYP3A4 (c), CYP1A2 (d), and CYP2C9 (e). We also examined AFP levels as an indicator of iHep maturity, and found no clear trends. All error bars report standard deviation. Scale bars are 100 μm.

## ***Chapter 8: Cryopreservation of Collagen Microtissues***

This chapter contains material from "A High-Throughput Workflow to Study Remodeling of ECM-Based Microtissues" by Alexandra L. Crampton*, Katherine A. Cummins*, and David K. Wood. *Tissue Engineering Part C: Methods*, volume 25, issue 1, pages 25-36, 2019; permission conveyed through Mary Ann Liebert, Inc., New Rochelle, NY. *These authors contributed equally.

### Introduction

One of the foundations of tissue engineering and *in vitro* model development is the ability to cryopreserve cells while minimally affecting viability and function upon thawing. For tissue engineering applications, cryopreservation is a prevelent method of providing a continuous source of cells[236–238]. Cryopreservation parameters are optimized for each cell type, but generally these methods begin with transferring cells to a chilled cryoprotective solution[239], slowing cell metabolism and minimizing toxicity of the cryoprotective agents[238]. The temperature of the cells is reduced further at a specific freezing rate[240,241] and cryopresrved cells are stored at subzero temperatures. Cells are then thawed and cryoprotective agent are removed before use[242].

A major challenge in any cryopreservation protocol is the delicate balance between cryoinjury and cytotoxic effects of cryoprotective agents[243]. The mechanism of action for cryoprotectants varies, but the overall effect is protection of the structures of the cells due to state change of water at low temperatures (<0 C). These protective qualities, though, are temperature-dependent, resulting in cytotoxicity if the thawing and/or removal of the cryoprotective agents is too slow[236–238]. Cryopreservation of larger constructs becomes more challenging[238,244,245]; however, we hypotheisze that the small-size scale and highly porous nature of our collagen microtissues may make these constructs amenable to standard cryopreservation protocols.

We aimed to assess efficacy of cryopreservation of microtissue constructs. We anticipate that our workflow would be improved if we could "pause" the experiment after fabriation of the tissues (Figure 8.1). This would facilitate use of microtissues from a single fabrication setup across several experiments over time, avoid waste, and improve

distribution of samples to off-site labs. To validate cryopreservation with our platform, we compare functional readouts such as viability, proliferation, compaction, and liver-specific functions of microtissues containing various cell types before and after freezing.

Materials and methods:

*Cryopreservation*

Microtissues were resuspended in freezing solution (90% FBS + 10% DMSO or Cryostore CS10 (BioLife Solutions)) and frozen in 500 µL aliquots. Tissues were cooled gently (-1°C/minute) using a Mr. Frosty (Thermo Scientific) overnight and then transferred to liquid nitrogen for 1 week. Control tissues from the same experiment were pipetted into plates containing microwells immediately after fabrication to compare the effects of freezing.

*Thawing of cryopreserved microtissues*

Microtissues were moved from liquid nitrogen storage and thawed for 2 minutes in a 37°C water bath. Microtissues in freezing media were diluted in warm media in a 50 mL conical tube and allowed to settle for 5 mintues. Supernatant was aspirated and additional warm media was added to the microtissues to further dilute the cryoprotectant. Microtissues again settled for 5 mintues before being distributed into plates for experiments. Constructs were optionally coated with 3T3-J2 fibroblasts for co-culture conditions, following the protocol detailed in Chapter 7.2 Methods. NIH 3T3 cells, MDA-MB 231 cells, and NHLF were cultured under conditions described in Chapter 5 for 1 week. HepG2 liver carcinoma cells were cultured in DMEM with 10% bovine serum (Gibco) and cultured for 2 weeks.

*Viability and proliferation staining*

Following the protocol outlined in Chapter 5, at various timepoints, tissues were gently pipetted and removed from microwells and collected in an Eppendorf tube. Constructs were washed thoroughly with DPBS and then incubated with a staining solution of 5 µM DRAQ5 (Invitrogen) and 5 µM Calcein AM at 37°C for 20 minutes. A

Zeiss Axio Observer was used to image each microtissue and images were analyzed to count the total number of cells (from the nuclear stain) and the number of live cells (from the Calcein) for each microtissue.

To visualize proliferation, microtissues were incubated for 4 hours with 10 μM 5-ethynyl-2'-deoxyuridine (EdU) before fixing with 3.7% formalin and a Click-iT EdU Alexa Fluor 647 kit (Invitrogen) was used following manufacturer's instructions. A Zeiss Axio Observer was used to image z-positions throughout each microtissue with a step size of 10 μm. At least 28 microtissues were examined for each condition.

*Immunofluorescence staining*

Tissues were stained following the potocol outlined in Chapter 5. Briefly, microtissues were collected in low-retention Eppendorf tubes and fixed with 3.7% formalin overnight at 4°C. Constructs were blocked and permeabilized with 10% FBS and 0.1% Triton X-100 for 1 hour at room temperature. The tissues were then incubated with primary antibody (rabbit anti-albumin (1:1000, Rockland) at 4°C overnight. The microtissues were washed thoroughly, and incubated with secondary antibody (1:500, Jackson) at 4°C overnight. A Zeiss Axio Observer was used to obtain widefield fluorescence images of constructs.

*ELISA for CYP2A6 activity*

Following the protocol described in Chapter 7, cytochrome P450 (CYP450) 2A6 activities were measured by incubating the cultures with 50 μM coumarin (Sigma-Aldrich). The concentration of metabolite, 7-HC, generated from coumarin was quantified via fluorescence detection (excitation/emission: 355/460 nm) on the Synergy H1 multi-mode plate reader[220]. Substrates were incubated in cultures for 2 days for trials before collecting media supernatant and storing at -80°C.

Results:

*Cell-laden microtissues retain high viability after cryopreservation*

Cryopreservation is important for preserving precious cell populations and, as an experimental tool, maximizes the number of experiments that can be completed out of a single cell source. Freezing large tissues is challenging because diffusion limitations prevent cryoprotectants from fully penetrating the tissue and results in damage during freezing. However, the small size scale of our microtissues allows for sufficient transport of cryoprotectant necessary for freezing while retaining the ability to study tissue-level functions.

To assess the compatibility of our microtissues with cryopreservation protocols, we first cultured NIH 3T3 cells, MDA-MB 231 cells, and NHLFs on tissue culture plastic following cell distributor instructions. We used these cells to fabricate cell-laden microtissues with 6 mg/mL collagen. Immediately after microtissue fabrication, we cultured half of our microtissues following standard protocols and cryopreserved the remainder using cell distributor recommended freezing solutions. Cryopreserved NIH 3T3, MDA-MB-231, and NHLF cells encapsulated in 6 mg/mL collagen microtissues demonstrated high viability 1 day after thawing (84, 87, and 83% respectively), which was similar to their controls (86, 94, and 90%). The percentage of live cells improved after a week of culture (92, 98, and 88%) (Figure 8.2a), which was also similar to the corresponding controls (90, 97, and 89%), with viability at the 2 week timepoint remaining similarly high (data not shown).

*Cells retain their ability to remodel ECM and to proliferate after encapsulation and cryopreservation in microtissues*

It is known that cryopreservation processes can alter cells dramatically, so maintaining cell functionality in addition to high viability is imperative for successful cryopreservation in this platform. Thus, we further assessed cell function after cryopreservation through a compaction and proliferation assay. To determine the difference in compaction between control and frozen tissues, we compared final microtissue diameters for each condition and found them to be insignificantly different ($p>0.05$) (Figure 8.2b). We also observed that at intermediate timepoints each cell type demonstrated similar compaction between cryopreserved and control microtissues.

Lastly, in addition to retaining contractile function, all three cell types retained proliferative ability after freezing, as all microtissues in every condition tested had cells that entered S phase (Figure 8.2c).

*Liver carcinoma cells continue to secrete albumin and demonstrate CYP3A4 activity after cryopreservation in microtissues*

Cryopreservation of cell-laden microtissues has distinct advantages for making the most out of precious cell sources that need 3D environments to maximize their efficacy *in vitro*. A specific example are liver cells since they thrive in the 3D microenvironment of the collagen microtissues, but we often will not fully utilize all of the tissues fabricated for a single experiment. To get the most out of these expensive and precious resources, we explored the compatibility of liver-derived cells with cryopresrvation in collagen microtissues.

Given our success with cancer cell lines, we opted first to explore cryoprervation of liver cells with a liver carcinoma line – HepG2. One of the challenges we anticipate facing with primary liver cells is that the cells will undergo two thawing steps in a relatively short period of time, as cells are thawed on the microtissue fabrication day, cryopreserved once encapsulated in microtissues, and thawed again for future use in experiments. To address this potential new workflow, we used HepG2 to test our cryopreservation protocol with cells that were thawed immediately before encapsulation and re-cryopreservation. We observed that HepG2 had similar viability regardless of the preparation of cells before encapsulation and cryopreservation (>95% for both cases). Based on these results, we proceeded with encapsulating cells immediately after thawing from cryo storage for all following experiments.

We then examined function of these constructs for liver-specific readouts. We visualized albumin in our constructs at the end of the culture period (d13) with immunofluoresence staining (Figure 8.3a). We confirmed that constructs that were not cryopreserved showed strong albumin staining after 13 days of culture with and without a supporting fibroblast (3T3-J2) layer (Figure 8.3a). We used these albumin production levels as a target for all other treatment conditions. We then tested two cryopreservation

solutions – FBS+10%DMSO and Cryostor CS10 – as the former was shown to work well in our system with other cell types, and the latter has been shown to improve viability and function of cryopreserved hepatocytes[246,247]. In all conditions tested (including the control), we observed three main phenotypes for microtissues after 13 days of culture: microtissues with 1) low cell number and single-cell distribution, 2) small clusters of cells, or infrequently 3) dense growth of cells that overgrows the original size of the microtissue. We did note that the addition of the supporting 3T3-J2 layer did increase the intensity of albumin staining, but the result was not as profound as for previously tested primary hepatocytes in microtissues (Figure 7.2, 7.4, 7.5 and Kukla *et al.*[217]). Additionally, the 3T3-J2 layer did not resolve the microtissue heterogeneity for any condition tested. Comparing the morphology and intensity of albumin staining to the controls after two weeks of culture we observed that the Cryostor CS10 had less impact on cell growth and organization in the co-culture condition than the mono-culture condition (Figure 8.3a). We also observed that the FBS/DMSO solution resulted in similar albumin staining for both the monoculture and co-culture conditions.

To quantify these observations, we assessed CYP2A6 function with ELISA. We observed that freezing these microtissues did not negatively impact CYP2A6 function since both cryoprotectants resulted in CYP2A6 activity that was equal or greater than the never-frozen control (Figure 8.3 b,c). We also again note that the improvement from co-culture with 3T3-J2s was not as pronounced with the HepG2 cell line as with previously tested PHHs[215,219] and iHeps[220], but was still statistically significant for the control (d13, p-val = 0.0028) and the CryostorCS10 condition (d9, p-val = .0076; d13, p-val < 0.0001). For the FBS/DMSO solution, there was no statistically significant change in CYP2A6 function with the addition of the 3T3-J2 cell layer.

Discussion:

Here, we present proof-of-concept that microtissues can be easily cryopreserved with methods typically used for single cell suspensions. The use of standard tissue culture cryopreservation protocols for a whole-construct application is unusual as diffusion limitations typically prevent the use of DMSO, as large tissues are difficult to saturate

efficiently. PEG is an extremely popular material for cell encapsulation, but transport limitations in these systems are severe, with pore sizes of the hydrogels ranging from ~40 to 200 Å[76]. This is a stark contrast to collagen gels that have pore sizes > 1 μm[77]. Because our tissue constructs are small and highly porous, we can use a range of cryoprotectants not usually available for whole tissue constructs, as we can quickly saturate the tissues with cryoprotectant agents and avoid deleterious effects[238]. Combined with the ability to cryopreserve the constructs, we can preserve precious cell populations to maximize the timescale and number of experiments that can be completed with a single cell source.

Succuessful cryopreservation protcols preserve both the viability as well as function of the cell upon thawing. We confirmed that after cryopreservation and subsequent thawing of microtissues, encapsulated cells are have high viablity immediately after thawing as well as after one week of culture, comparable to never-frozen controls. To assess cell function after cryopreservation, we examined gel contraction and proliferation. We observed that construct contraction and proliferation was similar to controls for all cell types tested. We validated this protocol with mouse fibroblasts (NIH-3T3), human cancer line (MDA-MB-231), and human lung fibroblast (NHLF), confirming that cryopreservation of microtissues is effictive with a range of cell sources.

We continued to explore the specific application of whole-construct cryopreservation with liver carcinoma cells (HepG2). As we previously found with other liver cell types[215,219,220], HepG2 have improved function (albumin and CYP2A6 activity) in co-culture with 3T3-J2 cells. Unlike PHHs, HepG2s do not show functional decline as a monoculture, which may make them a simplified, preliminary model despite the increaesd construct heterogenity with long-term culture. The positive staining for albumin in all conditions tested as well as detectable levels of CYP2A6 activity is encouraging, and motivates us to continue optimizing this protocol for use with primary cells (PHH).

With these HepG2 tissues, we also compared two cryopreservation media formulations – FBS/DMSO and Cryostor CS10. DMSO has been shown to have cytotoxic effects above tempratures of 10C[238,243], so we compared an alternative

cryopreservation medium that has precedent in the field for cryopreservation of hepatocytes[246,247]. For HepG2, we found that the functional improvement with the co-culture of 3T3-J2 was only observed with Cryostor CS10, making this our preferred choice for liver-specific assays.

We did observe heterogeneous phenotypes of HepG2 constructs after extended culture. Heterogeneity in microtissues is not necessarily a negative quality, and may infact better represent the heterogeniety in the cancer line itself. This parameter, however, does need to be accounted for to determine adequately large sample sizes for treatment conditions.

Cryopreservation is the best way to make the most of precious cell sources since microtissues are produced in such large quantities that--especially for biological discovery and protocol development – they cannot all be used effectively in a single experiment. This also promotes the dissemination of this technology since only standard cell culture plates and reagents are required to culture the microtissues after fabrication. In the case of receiving patient samples that cannot be duplicated, this cryopreservation protocol allows experiments to be spread across labs and timepoints. We are eager to continue optimizing this protocol and to epxand our experiments to include primary cells (including PHH) in the near future.

Acknowledgements

Portions of this work were conducted in the Minnesota Nano Center, which is supported by the National Science Foundation through the National Nano Coordinated Infrastructure Network (NNCI) under Award Number ECCS-1542202. We thank the National Science Foundation Division of Chemical, Bioengineering, Environmental, and Transport Systems (NSF CBET 1704332) and the National Institute of Environmental Health Sciences (NIH R21ES027622) for supporting this work. We also thank Dr. Salman R. Khetani for donating HepG2 cells. Experiments for Figure 8.2 were performed collaboratively with Katherine A. Cummins. For Figure 8.3, experiment setup and culture, immunofluorescence staining, and data analysis were performed by Alexandra L. Crampton; CYP2A6 ELISAs were performed by Regeant Panday.

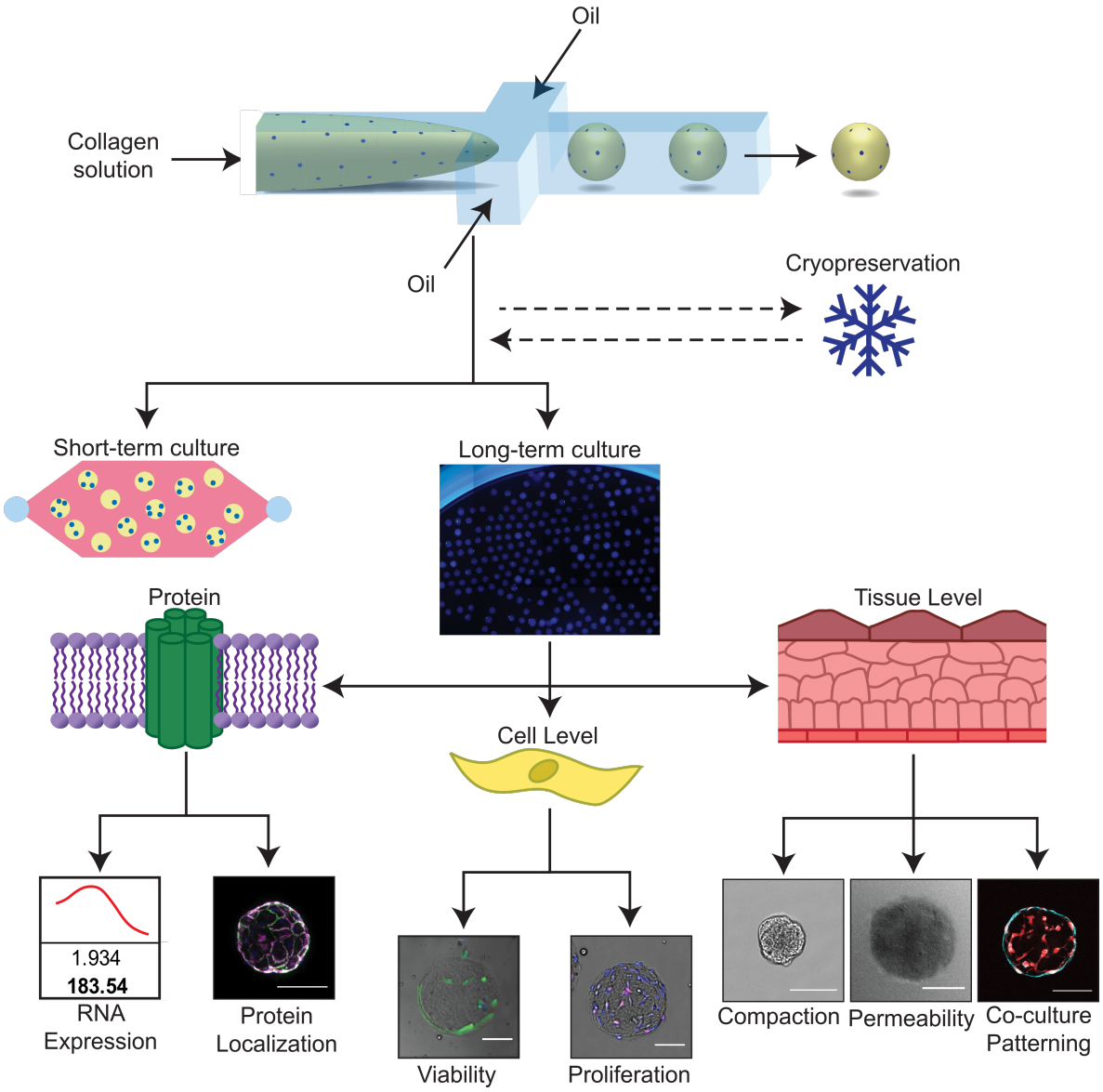


**Figure 8.1:** ***Cryopreservation adds flexibility to our microtissue-microwell workflow***

With the addition of cryopreservation to our previous workflow, we can fabricate large numbers of microtissues and distributue them across experiemnts in time. When needed, we can thaw microtissues and conduct high-throughput assessment of protein-, cell-, and tissue-level functions. Scale bars are 100 μm.

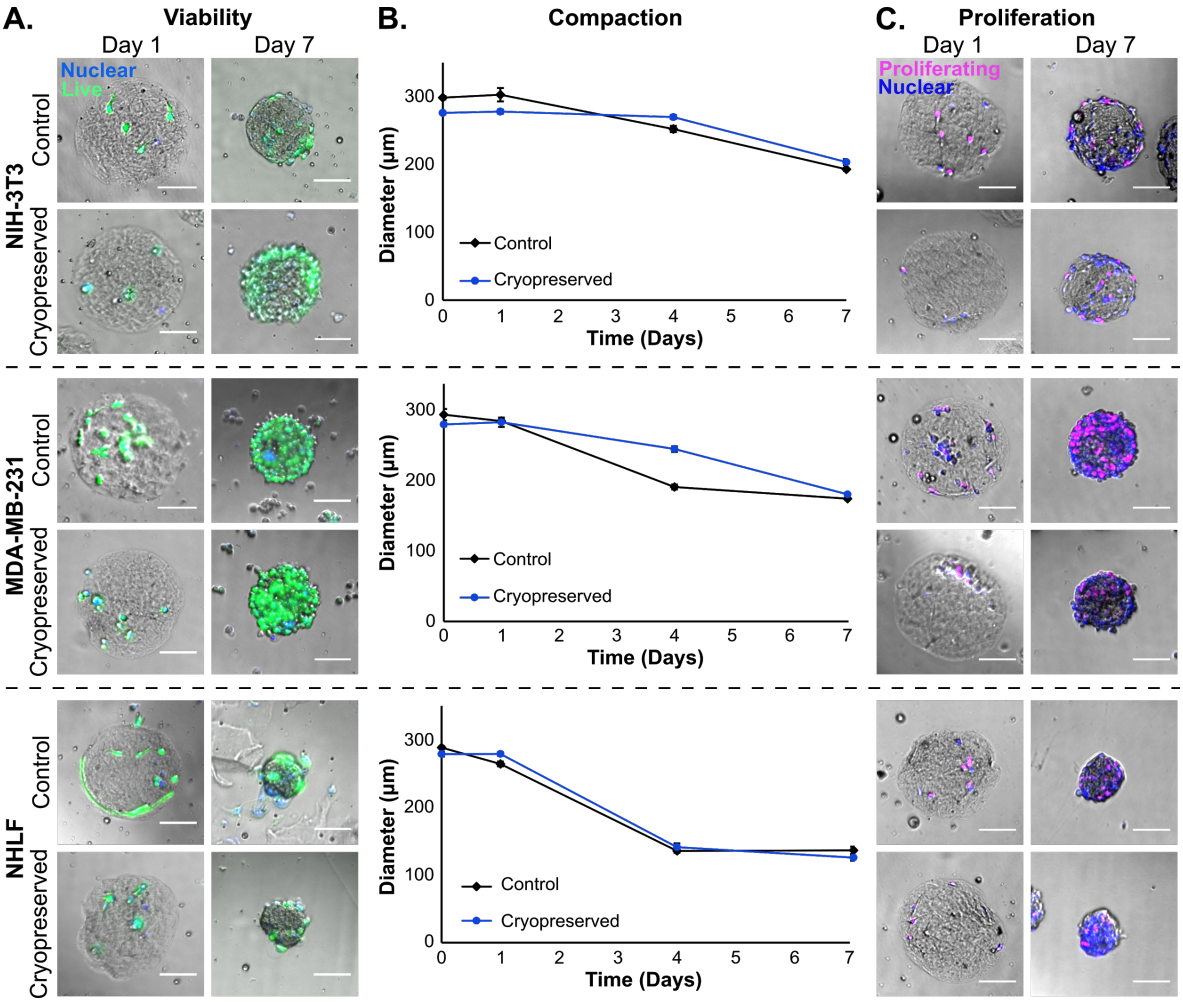


**Figure 8.2:** ***Encapsulated cells remain highly viable and functional after cryopreservation in microtissues***

(**A**) Brightfield and widefield fluorescence imaging of microtissues with encapsulated NIH 3T3, MDA-MB-231, and NHLF cells (nuclei shown in blue). Calcein AM (green) shows that all cell types had high viability (greater than 83%) after 1 week of freezing and were over 90% viable after 1 week of cultur in standard conditions, which was comparable to tissues that never underwent freezing. (**B**) Compaction of encapsulated cells indicated that before and after cryopreservation, cells were similarly contractile, compacting microtissues at similar rates and with the same trajectories. Shown with standard error and an average of 82 microtissues per condition. (**C**) Brightfield and widefield fluorescence imaging of cell proliferation after cryopreservation. Proliferative capacity, as determined with a Click-It EdU assay (nuclei shown in blue, proliferating cells in magenta). All microtissues in all conditions had cells that

proliferated, indicating that cells retained their proliferative capacity after cryopreservation in the microtissues. All scale bars 100 μm.

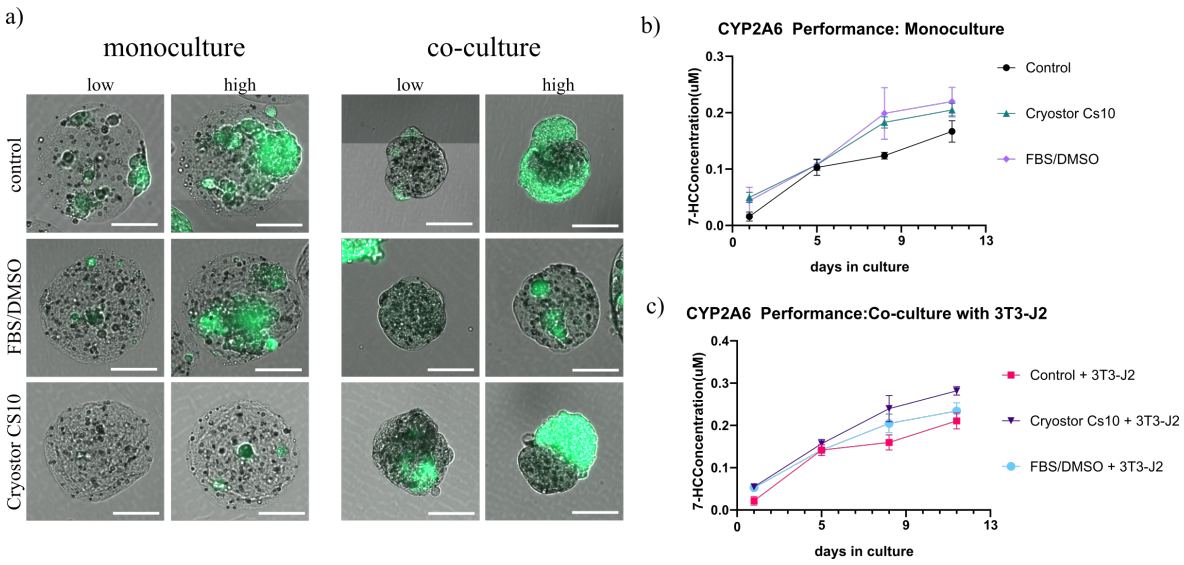


**Figure 8.3:** ***Cryopreservation with repetitive thawing of liver carcinoma, HepG2***

To assess cell morphology of HepG2 in our constructs, we used immunofluorescence staining (a) for albumin (green) (scale bar = 100 μm). Although cells were distributed homogenously within the microtissues immediately after fabrication, culture of this cell line for two weeks resulted in heterogeneity for all conditions (low denoting low cell number phenotype, and high denoting high cell number phenotype). We observed that CryostorCS10 does not perform as well for the HepG2 monoculture, but with the supporting 3T3-J2 cells this cryoprotectant results in tissues that are similar to the never-frozen controls. The FBS/DMSO cryopreservation solution results in similar cell morphology and growth regardless of the 3T3-J2 cell layer. We also assessed the impact these cryopreservatives have on CYP2A6 activity (b,c). We found that for both cryoprotectants tested resulted in CYP2A6 activity that was equal to or greater than the never-frozen control. Both trends noted previously from the immunofluorescence staining were echoed in the CYP2A6 assessment, with Cryostor CS10 performing best in the co-culture condition, and the FBS/DMSO solution performing equally for both monoculture and co-culture.

***Chapter 9: Overall conclusions***

High throughout systems for predictive drug screening and biological discovery are in critical need, as the current gold standard of 2D culture lacks physiological relevance in geometry and substrate interactions, leading to inaccurate drug screening results and slowing drug discovery. We present an alternative method that is accessible and affords physiologically relevant substrates for cell-ECM interactions. We showed that our method is biocompatible, with several cell types demonstrating high viability during and after the fabrication process.

Additionally, because our microtissues are composed entirely of natural ECM, cells can interact with and remodel their environment. We used this to our advantage and to create the first of its kind, small-scale contraction assay. We demonstrated that our assay is more sensitive than the current gold standard for contraction assays. We also showed that our system can be used with studies for contraction inhibitors, demonstrating potential for high-throughput drug screening.

Extracellular matrix remodeling can happen over short and long timescales. The first iteration of our platform supported short-term studies (<7 days), so we modified our platform to support long-term experiments using a low-adhesion microwell system to culture our collagen microtissues (detailed in Chapter 5). We used this improvement to the technology to further expand our breadth of readouts and methods for handling and storing microtissues.

We then focused on building model systems for specific applications. We first used our system to create the first demonstration of natural ECM carriers for measurements of endothelial permeability. We showed that endothelial cells adhere to the collagen constructs, and remodel via ECM contraction and deposition of basement membrane proteins - two key functions that are difficult to recapitulate *in vitro*. We also used our platform to quantify macro molecular permeability and found our measurements to be similar to *in vivo* results. We also showed that our platform could be used to assess changes in endothelial permeability, validated with known modulators of endothelial permeability. This study demonstrates the potential of this platform to enable high-throughput screening of functional readouts typically restricted to low-throughput

methods, and could be expanded further in the future to include precious cell sources like brain endothelial cells for mimics of the blood-brain barrier. We continued to explore specific applications next with a liver model.

Predictive systems for *in vitro* models of human liver toxicity are currently missing from the field of high-throughput screening and *in vitro* biology. We hypothesized that our system could be used to advance the goal of a predictive human hepatocyte model for toxicology studies. Working with the Khetani Lab at University of Illinois at Chicago (UIC), we translated our technology to their group conducted experiments collaboratively. We showed that the microtissues platform is compatible with PHHs and iHeps, and that in co-culture with 3T3-J2s these cells are viable and functional in our platform for long-term culture (21 days and 32 days respectively). We investigated the effect of combination of ECM components for PHHs and iHeps, demonstrating the potential for this platform to do combinatorial screens of ECM proteins in 3D microenvironments.

We also examined the possibility of cryopreserving complete microtissue constructs, and found that cells remain viable and functionally proficient after thawing. We are continuing to expand this work for cells sources that are non-platable and/or difficult to expand, making the most efficient use of delicate and precious resources. This methodology also affords exciting opportunities to disseminate our technology further, as after construct fabrication, all methods are completed using standard cell culture plates and equipment and could be seamlessly translated into the workflow of any lab already setup for cell culture.

The specific applications of this platform are broad, and we are continuing to develop new methods of patterning within the microtissues as well as the organ systems and biological phenomenon we are trying to mimic *in vitro*. We have collected preliminary data for explicitly patterning cells within microtissues, using two encapsulation steps to confine cells to a small portion of larger acellular constructs. Using this sequential encapsulation method, we will assess differences in cell distribution within our constructs over time, with cells responding to various growth conditions – the basis for our future 3D high-throughput 3D migration assay. We are eager to continue to

refine and expand the capabilities of our technology, as well as the *in vitro* biological systems we can generate with this platform.

We have shown that for several applications, our microtissue platform can be used for similar readouts as larger-scale *in vitro* assays. In addition, because of the small size scale, we can create at least 2,000 times more replicates with the same initial volume of reagents. This is particularly important as we progress to working with precious cells and ECM sources. In the future, this could mean that patient samples could be evaluated using the outlined microtissue platform. For example, to test the efficacy of a cancer treatment strategy, patient tumor cells could be encapsulated and cultured in microtissues under various treatment regimens, testing several treatment strategies simultaneously *in vitro*. Additionally, with advancements in induced pluripotent stem cell technology, cells from adults could be collected and differentiated toward different organs (e.g. brain, heart, liver, lungs), microtissues could be used to house these different cell types and examine patient-specific biology, as well as run studies for off-target effects (e.g. liver toxicity) of therapeutics on a patient-by-patient basis.

***Chapter 10: References***


1. Davies B, Morris T. Physiological Parameters in Laboratory Animals and Humans. Pharm Res. 1993;10(7):1093–5.
2. Vandamme TF. Use of rodents as models of human diseases. J Pharm Bioallied Sci. 2014 Jan;6(1):2–9.
3. Grüneberg H. Biology of the Laboratory Mouse. Nature. 1942 Jul;150(3795):101–2.
4. Van De Stolpe A, Den Toonder J. Workshop meeting report Organs-on-Chips: Human disease models. Lab Chip. 2013;13(18):3449–70.
5. Beebe DJ, Ingber DE, den Toonder J. Organs on Chips 2013. Lab Chip. 2013;13(18):3447.
6. Olson H, Betton G, Robinson D, Thomas K, Monro A, Kolaja G, et al. Concordance of the Toxicity of Pharmaceuticals in Humans and in Animals. Regul Toxicol Pharmacol. 2000 Aug 1;32(1):56–67.
7. Della-Morte D, Palmirotta R, Rehni AK, Pastore D, Capuani B, Pacifici F, et al. Pharmacogenomics and pharmacogenetics of thiazolidinediones: role in diabetes and cardiovascular risk factors. Pharmacogenomics. 2014 Dec 18;15(16):2063–82.
8. Wall RJ, Shani M. Are animal models as good as we think? Theriogenology. 2008 Jan 1;69(1):2–9.
9. Shanks N, Greek R, Greek J. Are animal models predictive for humans? Philos Ethics, Humanit Med. 2009 Jan 15;4(1):2.
10. Shanks N, Pyles RA. Evolution and medicine: the long reach of "Dr. Darwin" Philos Ethics, Humanit Med. 2007 Apr 3;2(1):4.
11. Hunter AJ. Have animal models of disease helped or hindered the drug discovery process? Ann N Y Acad Sci. 2011 Dec 1;1245(1):1–2.
12. Edmondson R, Broglie JJ, Adcock AF, Yang L. Three-Dimensional Cell Culture Systems and Their Applications in Drug Discovery and Cell-Based Biosensors. Assay Drug Dev Technol. 2014 May 15;12(4):207–18.
13. Duval K, Grover H, Han L-H, Mou Y, Pegoraro AF, Fredberg J, et al. Modeling Physiological Events in 2D vs. 3D Cell Culture. Physiology (Bethesda).

2017;32(4):266–77.

14. Hait WN. Anticancer drug development: the grand challenges. Nat Rev Drug Discov. 2010 Apr;9(4):253–4.
15. Dimasi JA, Grabowski HG. Economics of New Oncology Drug Development. J Clin Oncol. 2007;25:209–16.
16. Mazzoleni G, Di Lorenzo D, Steimberg N. Modelling tissues in 3D: the next future of pharmaco-toxicology and food research? Genes Nutr. 2009 Mar 18;4(1):13–22.
17. Engler AJ, Sen S, Sweeney HL, Discher DE. Matrix Elasticity Directs Stem Cell Lineage Specification. Cell. 2006 Aug 25;126(4):677–89.
18. Dupont S, Morsut L, Aragona M, Enzo E, Giulitti S, Cordenonsi M, et al. Role of YAP/TAZ in mechanotransduction. Nature. 2011 Jun 8;474(7350):179–83.
19. Xu X, Wang W, Kratz K, Fang L, Li Z, Kurtz A, et al. Controlling Major Cellular Processes of Human Mesenchymal Stem Cells using Microwell Structures. Adv Healthc Mater. 2014 Dec 1;3(12):1991–2003.
20. Fu J, Wang Y-K, Yang MT, Desai RA, Yu X, Liu Z, et al. Mechanical regulation of cell function with geometrically modulated elastomeric substrates. Nat Methods. 2010 Sep 1;7(9):733–6.
21. Ihalainen TO, Aires L, Herzog FA, Schwartlander R, Moeller J, Vogel V. Differential basal-to-apical accessibility of lamin A/C epitopes in the nuclear lamina regulated by changes in cytoskeletal tension. Nat Mater. 2015 Dec 24;14(12):1252–61.
22. Fennema E, Rivron N, Rouwkema J, van Blitterswijk C, de Boer J. Spheroid culture as a tool for creating 3D complex tissues. Trends Biotechnol. 2013 Feb 1;31(2):108–15.
23. Hsiao AY, Tung Y-C, Kuo C-H, Mosadegh B, Bedenis R, Pienta KJ, et al. Micro-ring structures stabilize microdroplets to enable long term spheroid culture in 384 hanging drop array plates. Biomed Microdevices. 2012 Apr 5;14(2):313–23.
24. Torisawa Y, Takagi A, Nashimoto Y, Yasukawa T, Shiku H, Matsue T. A multicellular spheroid array to realize spheroid formation, culture, and viability assay on a chip. Biomaterials. 2007 Jan 1;28(3):559–66.

25. Tung Y-C, Hsiao AY, Allen SG, Torisawa Y, Ho M, Takayama S. High-throughput 3D spheroid culture and drug testing using a 384 hanging drop array. Analyst. 2011 Jan 18;136(3):473–8.
26. Napolitano AP, Chai P, Dean DM, Morgan JR. Dynamics of the Self-Assembly of Complex Cellular Aggregates on Micromolded Nonadhesive Hydrogels. Tissue Eng. 2007 Aug 14;13(8):2087–94.
27. Nederman T, Norling B, Glimelius B, Brunk U. Demonstration of an Extracellular Matrix in Multicellular Tumor Spheroids1. Vol. 44, Cancer Research. 1984.
28. Cox TR, Erler JT. Remodeling and homeostasis of the extracellular matrix: implications for fibrotic diseases and cancer. Dis Model Mech. 2011 Mar 1;4(2):165–78.
29. Venning FA, Wullkopf L, Erler JT. Targeting ECM Disrupts Cancer Progression. Front Oncol. 2015 Oct 20;5:224.
30. Gialeli C, Theocharis AD, Karamanos NK. Roles of matrix metalloproteinases in cancer progression and their pharmacological targeting. FEBS J. 2011 Jan 1;278(1):16–27.
31. Desai O, Winkler J, Minasyan M, Herzog EL. The Role of Immune and Inflammatory Cells in Idiopathic Pulmonary Fibrosis. Front Med. 2018 Mar 20;5:43.
32. Klingberg F, Hinz B, White ES. The myofibroblast matrix: implications for tissue repair and fibrosis. J Pathol J Pathol. 2013;229:298–309.
33. Wei L. Immunological aspect of cardiac remodeling: T lymphocyte subsets in inflammation-mediated cardiac fibrosis. Exp Mol Pathol. 2011 Feb 1;90(1):74–8.
34. Sorokin L. The impact of the extracellular matrix on inflammation. Nat Rev Immunol. 2010 Oct 24;10(10):712–23.
35. Petrie RJ, Gavara N, Chadwick RS, Yamada KM. Nonpolarized signaling reveals two distinct modes of 3D cell migration. J Cell Biol. 2012;197(3):439–55.
36. Geiger B, Yamada KM. Molecular Architecture and Function of. Cold Spring Harb Perspect Biol. 2011;1–22.
37. Cukierman E, Pankov R, Stevens DR, Yamada KM. Taking Cell-Matrix

Adhesions to the Third Dimension Edna Cukierman,. Science. 2008; 294(2001):1708–13.

38. Sung KE, Su G, Pehlke C, Trier SM, Eliceiri KW, Keely PJ, et al. Control of 3-dimensional collagen matrix polymerization for reproducible human mammary fibroblast cell culture in microfluidic devices. Biomaterials. 2009 Sep 1;30(27):4833–41.
39. Materne EM, Tonevitsky AG, Marx U. Chip-based liver equivalents for toxicity testing-organotypicalness versus cost-efficient high throughput. Lab Chip. 2013;13(18):3481–95.
40. March S, Ng S, Velmurugan S, Galstian A, Shan J, Logan DJ, et al. A microscale human liver platform that supports the hepatic stages of plasmodium falciparum and vivax. Cell Host Microbe. 2013;14(1):104–15.
41. Bhatia SN, Ingber DE. Microfluidic organs-on-chips. Nat Biotechnol. 2014;32(8):760–72.
42. Sung KE, Beebe DJ. Microfluidic 3D models of cancer. Adv Drug Deliv Rev. 2014 Dec 15;79–80:68–78.
43. Wang C, Tang Z, Zhao Y, Yao R, Li L, Sun W. Three-dimensional *in vitro* cancer models: a short review. Biofabrication. 2014 Apr 14;6(2):022001.
44. Frantz C, Stewart KM, Weaver VM. The extracellular matrix at a glance. J Cell Sci. 2010;123(123):4195–200.
45. Provenzano PP, Inman DR, Eliceiri KW, Trier SM, Keely PJ. Contact Guidance Mediated Three-Dimensional Cell Migration is Regulated by Rho/ROCK-Dependent Matrix Reorganization. Biophys J. 2008 Dec 1;95(11):5374–84.
46. Hesse E, Hefferan TE, Tarara JE, Haasper C, Meller R, Krettek C, et al. Collagen type I hydrogel allows migration, proliferation and osteogenic differentiation of rat bone marrow stromal cells. J Biomed Mater Res. 2010;94A(2):442–9.
47. Zhu J, Marchant RE. Design properties of hydrogel tissue-engineering scaffolds. Expert Rev Med Devices. 2011 Sep;8(5):607–26.
48. Drury JL, Mooney DJ. Hydrogels for tissue engineering: scaffold design variables and applications. Biomaterials. 2003 Nov 1;24(24):4337–51.

49. Berry CC, Shelton JC, Lee DA. Cell-generated forces influence the viability, metabolism and mechanical properties of fibroblast-seeded collagen gel constructs. J Tissue Eng Regen Med. 2009 Jan 1;3(1):43–53.
50. Peshwa M, … FW-A. Viability, morphology and function of hepatocyte spheroids entrapped in collagen gel. Chem soc. 1993.
51. Wozniak MA, Keely PJ. Use of three-dimensional collagen gels to study mechanotransduction in T47D breast epithelial cells. Biol Proced Online. 2005;7(1):144–61.
52. Bell E, Ivarsson B, Merrill C. Production of a tissue-like structure by contraction of collagen lattices by human fibroblasts of different proliferative potential in vitro. Proc Natl Acad Sci. 1979 Mar 1;76(3):1274–8.
53. Vernon RB, Gooden MD. An Improved Method For The Collagen Gel Contraction Assay. Vitr Cell Dev Biol-Animal. 2002;38:97–101.
54. Ngo P, Ramalingam P, Phillips JA, Furuta GT. Collagen Gel Contraction Assay. In: Cell-Cell Interactions in Health and Disease. New Jersey: Humana Press; 2006. p. 103–10.
55. Freyman TM, Yannas I V, Yokoo R, Gibson LJ. Fibroblast Contractile Force Is Independent of the Stiffness Which Resists the Contraction. 2001;
56. Moraes C, Simon AB, Putnam AJ, Takayama S. Aqueous two-phase printing of cell-containing contractile collagen microgels. Biomaterials. 2013 Dec;34(37):9623–31.
57. Corstorphine L, Sefton M V. Effectiveness factor and diffusion limitations in collagen gel modules containing HepG2 cells. J Tissue Eng Regen Med. 2011 Feb 1;5(2):119–29.
58. Appel AA, Anastasio MA, Larson JC, Brey EM. Imaging challenges in biomaterials and tissue engineering. Biomaterials. 2013 Sep 1;34(28):6615–30.
59. Langhans SA. Three-Dimensional in Vitro Cell Culture Models in Drug Discovery and Drug Repositioning. Front Pharmacol. 2018 Jan 23;9:6.
60. Smith LE, Smallwood R, Macneil S. A comparison of imaging methodologies for 3D tissue engineering. Microsc Res Tech. 2010 Dec 1;73(12):1123–33.

61. Chan BP, Hui TY, Yeung CW, Li J, Mo I, Chan GCF. Self-assembled collagen–human mesenchymal stem cell microspheres for regenerative medicine. Biomaterials. 2007 Nov 1;28(31):4652–66.
62. Wong H-L, Wang M-X, Cheung P-T, Yao K-M, Chan BP. A 3D collagen microsphere culture system for GDNF-secreting HEK293 cells with enhanced protein productivity. Biomaterials. 2007 Dec 1;28(35):5369–80.
63. Lee M, Lo AC, Cheung PT, Wong D, Chan BP. Drug carrier systems based on collagen–alginate composite structures for improving the performance of GDNF-secreting HEK293 cells. Biomaterials. 2009 Feb 1;30(6):1214–21.
64. Cheng H, Luk KDK, Cheung KMC, Chan BP. In vitro generation of an osteochondral interface from mesenchymal stem cell–collagen microspheres. Biomaterials. 2011 Feb 1;32(6):1526–35.
65. McGuigan AP, Sefton M V. Vascularized organoid engineered by modular assembly enables blood perfusion. Proc Natl Acad Sci U S A. 2006 Aug 1;103(31):11461–6.
66. Berg RA. Collagen matrix beads for soft tissue repair. 1989. p. 6.
67. Nguyen KT, West JL. Photopolymerizable hydrogels for tissue engineering applications. Biomaterials. 2002 Nov 1;23(22):4307–14.
68. Wan J. Microfluidic-Based Synthesis of Hydrogel Particles for Cell Microencapsulation and Cell-Based Drug Delivery. Polymers (Basel). 2012 Apr 23;4(2):1084–108.
69. Jamalabadi MYA, DaqiqShirazi M, Kosar A, Shadloo MS. Effect of injection angle, density ratio, and viscosity on droplet formation in a microfluidic T-junction. Theor Appl Mech Lett. 2017 Jul 1;7(4):243–51.
70. Li CY, Wood DK, Hsu CM, Bhatia SN. DNA-templated assembly of droplet-derived PEG microtissues. Lab Chip. 2011 Aug 8;11(17):2967.
71. Li CY, Wood DK, Huang JH, Bhatia SN. Flow-based pipeline for systematic modulation and analysis of 3D tumor microenvironments. Lab Chip. 2013 Apr 23;13(10):1969.
72. Burdick JA, Anseth KS. Photoencapsulation of osteoblasts in injectable RGD-

modified PEG hydrogels for bone tissue engineering. Biomaterials. 2002 Nov 1;23(22):4315–23.

73. Bryant SJ, Anseth KS, Lee ' DA, Bader DL. Crosslinking density influences the morphology of chondrocytes photoencapsulated in PEG hydrogels during the application of compressive strain. Vol. 22, Journal of Orthopaedic Research. 2004.
74. Hern DL, Hubbell JA. Incorporation of adhesion peptides into nonadhesive hydrogels useful for tissue resurfacing. J Biomed Mater Res. 1998 Feb 1;39(2):266–76.
75. Lutolf MP, Lauer-Fields JL, Schmoekel HG, Metters AT, Weber FE, Fields GB, et al. Synthetic matrix metalloproteinase-sensitive hydrogels for the conduction of tissue regeneration: Engineering cell-invasion characteristics. Proc Natl Acad Sci. 2003 Apr 29;100(9):5413–8.
76. Nicodemus GD, Bryant SJ. Cell Encapsulation in Biodegradable Hydrogels for Tissue Engineering Applications. Tissue Eng Part B Rev. 2008 Jun 10;14(2):149–65.
77. Harjanto D, Maffei JS, Zaman MH. Quantitative Analysis of the Effect of Cancer Invasiveness and Collagen Concentration on 3D Matrix Remodeling. Barbosa MA, editor. PLoS One. 2011 Sep 27;6(9):e24891.
78. Che X, Nuhn J, Schneider I, Que L, Che X, Nuhn J, et al. High Throughput Studies of Cell Migration in 3D Microtissues Fabricated by a Droplet Microfluidic Chip. Micromachines. 2016 May 5;7(5):84.
79. Hong S, Hsu H-J, Kaunas R, Kameoka J. Collagen microsphere production on a chip. Lab Chip. 2012 Aug 14;12(18):3277.
80. Matsunaga YT, Morimoto Y, Takeuchi S, Matsunaga YT, Morimoto ] Y, Takeuchi † S, et al. Molding Cell Beads for Rapid Construction of Macroscopic 3D Tissue Architecture. Adv Mater. 2011;23:90–4.
81. Brett M-E, DeFlorio R, Stone DE, Eddington DT. A microfluidic device that forms and redirects pheromone gradients to study chemotropism in yeast. Lab Chip. 2012 Jul 31;12(17):3127.
82. J. Christopher Love, Daniel B. Wolfe, Heiko O. Jacobs and, Whitesides* GM.

Microscope Projection Photolithography for Rapid Prototyping of Masters with Micron-Scale Features for Use in Soft Lithography. 2001;

83. Xia Y, Whitesides GM. Soft Lithography. Annu Rev Mater Sci. 1998 Aug 28;28(1):153–84.
84. Collins TJ. ImageJ for microscopy. Biotechniques. 2007 Jul 16;43(1S):S25–30.
85. Forster B, Van De Ville D, Berent J, Sage D, Unser M. Extended depth-of-focus for multi-channel microscopy images: A complex wavelet approach. In: 2004 2nd IEEE International Symposium on Biomedical Imaging: Macro to Nano (IEEE Cat No 04EX821). IEEE; p. 660–3.
86. Baharvand H, Hashemi SM, Kazemi Ashtiani S, Farrokhi A. Differentiation of human embryonic stem cells into hepatocytes in 2D and 3D culture systems in vitro. Int J Dev Biol. 2006 Sep 1;50(7):645–52.
87. Fischbach C, Chen R, Matsumoto T, Schmelzle T, Brugge JS, Polverini PJ, et al. Engineering tumors with 3D scaffolds. Nat Methods. 2007 Oct 2;4(10):855–60.
88. Yeung T, Georges PC, Flanagan LA, Marg B, Ortiz M, Funaki M, et al. Effects of substrate stiffness on cell morphology, cytoskeletal structure, and adhesion. Cell Motil Cytoskeleton. 2005 Jan 1;60(1):24–34.
89. Discher DE. Tissue Cells Feel and Respond to the Stiffness of Their Substrate. Science (80- ). 2005 Nov 18;310(5751):1139–43.
90. Wells RG. The role of matrix stiffness in regulating cell behavior. Hepatology. 2008 Jan 7;47(4):1394–400.
91. Lo C-M, Wang H-B, Dembo M, Wang Y. Cell Movement Is Guided by the Rigidity of the Substrate. Biophys J. 2000 Jul 1;79(1):144–52.
92. Loessner D, Stok KS, Lutolf MP, Hutmacher DW, Clements JA, Rizzi SC. Bioengineered 3D platform to explore cell–ECM interactions and drug resistance of epithelial ovarian cancer cells. Biomaterials. 2010 Nov 1;31(32):8494–506.
93. Lukashev ME, Werb Z. ECM signalling: orchestrating cell behaviour and misbehaviour. Trends Cell Biol. 1998 Nov 1;8(11):437–41.
94. Rosso F, Giordano A, Barbarisi M, Barbarisi A. From Cell-ECM interactions to tissue engineering. J Cell Physiol. 2004 May 1;199(2):174–80.

95. Bell E, Ivarsson B, Merrill C. Production of a tissue-like structure by contraction of collagen lattices by human fibroblasts of different proliferative potential in vitro (tissue structure/hydrated collagen lattice/fibroblast function/cell aging/contractility). Vol. 76, Cell Biology. 1979.
96. Gillery P, Maquart F-X, Borel J-P. Fibronectin dependence of the contraction of collagen lattices by human skin fibroblasts. Exp Cell Res. 1986 Nov 1;167(1):29–37.
97. Levi-Schaffer F, Garbuzenko E, Rubin A, Reich R, Pickholz D, Gillery P, et al. Human eosinophils regulate human lung- and skin-derived fibroblast properties in vitro: a role for transforming growth factor beta (TGF-beta). Proc Natl Acad Sci U S A. 1999 Aug 17;96(17):9660–5.
98. Zagai U, Skold CM, Trulson A, Venge P, Lundahl J. The effect of eosinophils on collagen gel contraction and implications for tissue remodelling. Clin Exp Immunol. 2004 Mar 1;135(3):427–33.
99. Grinnell F, Lamke CR. Reorganization Of Hydrated Collagen Lattices By Human Skin Fibroblasts. Vol. 66, J. Cell Sci. 1984.
100. Guidry C, Grinnell F. Studies on the mechanism of hydrated collagen gel reorganization by human skin fibroblasts. J Cell Sci. 1985;79(1).
101. Steinberg BM, Smith K, Colozzo M, Pollack R. Establishment and transformation diminish the ability of fibroblasts to contract a native collagen gel. J Cell Biol. 1980 Oct 1;87(1):304–8.
102. Anderson SN, Ruben Z, Fuller GC. Cell-Mediated Contraction of Collagen Lattices in Serum-free Medium: Effect of Serum and Nonserum Factors. Vol. 26, In Vitro Cell. Dev. Biol. 1990.
103. Gehler S, Baldassarre M, Lad Y, Leight JL, Wozniak MA, Riching KM, et al. Filamin A–β1 Integrin Complex Tunes Epithelial Cell Response to Matrix Tension. Wang Y-L, editor. Mol Biol Cell. 2009 Jul 15;20(14):3224–38.
104. Bangasser BL, Rosenfeld SS, Odde DJ. Determinants of Maximal Force Transmission in a Motor-Clutch Model of Cell Traction in a Compliant Microenvironment. Biophys J. 2013 Aug 6;105(3):581–92.

105. Bangasser BL, Odde DJ. Master Equation-Based Analysis of a Motor-Clutch Model for Cell Traction Force. Cell Mol Bioeng. 2013 Dec 29;6(4):449–59.
106. Stevenson MD, Sieminski AL, McLeod CM, Byfield FJ, Barocas VH, Gooch KJ. Pericellular Conditions Regulate Extent of Cell-Mediated Compaction of Collagen Gels. Biophys J. 2010 Jul 7;99(1):19–28.
107. Zhu YK, Umino T, Liu XD, Wang HJ, Romberger DJ, Spurzem JR, et al. Contraction Of Fibroblast-Containing Collagen Gels: Initial Collagen Concentration Regulates The Degree Of Contraction And Cell Survival. Vitr Cell Dev Biol - Anim. 2001;37(1):10.
108. Moon AG, Tranquillo RT. Fibroblast-populated collagen microsphere assay of cell traction force: Part 1. Continuum model. AIChE J. 1993 Jan 1;39(1):163–77.
109. Parizi M, Howard EW, Tomasek JJ. Regulation of LPA-Promoted Myofibroblast Contraction: Role of Rho, Myosin Light Chain Kinase, and Myosin Light Chain Phosphatase. Exp Cell Res. 2000 Feb 1;254(2):210–20.
110. Washida N, Wakino S, Tonozuka Y, Homma K, Tokuyama H, Hara Y, et al. Rho-kinase inhibition ameliorates peritoneal fibrosis and angiogenesis in a rat model of peritoneal sclerosis. Nephrol Dial Transplant. 2011 Sep 1;26(9):2770–9.
111. Moon S, Hasan SK, Song YS, Xu F, Keles HO, Manzur F, et al. Layer by Layer Three-dimensional Tissue Epitaxy by Cell-Laden Hydrogel Droplets. Tissue Eng Part C Methods. 2010 Feb 17;16(1):157–66.
112. Kanematsu A, Marui A, Yamamoto S, Ozeki M, Hirano Y, Yamamoto M, et al. Type I collagen can function as a reservoir of basic fibroblast growth factor. J Control Release. 2004 Sep 30;99(2):281–92.
113. Bashkin P, Doctrow S, Klagsbrun M, Svahn CM, Folkman J, Vlodavsky I. Basic fibroblast growth factor binds to subendothelial extracellular matrix and is released by heparitinase and heparin-like molecules. Biochemistry. 1989 Feb;28(4):1737–43.
114. Gospodarowicz D, Neufeld G, Schweigerer L. Fibroblast growth factor: Structural and biological properties. J Cell Physiol. 1987 Jan 1;133(S5):15–26.
115. Jones JI, Gockerman A, Busby WH, Camacho-Hubner C, Clemmons DR.

Extracellular matrix contains insulin-like growth factor binding protein-5: potentiation of the effects of IGF-I. J Cell Biol. 1993 May 1;121(3):679–87.

116. Keane TJ, Dziki J, Sobieski E, Smoulder A, Castleton A, Turner N, et al. Restoring Mucosal Barrier Function and Modifying Macrophage Phenotype with an Extracellular Matrix Hydrogel: Potential Therapy for Ulcerative Colitis. J Crohn's Colitis. 2016 Aug 20;11(3):jjw149.
117. Tannock IF, Lee CM, Tunggal JK, Cowan DSM, Egorin MJ. Limited penetration of anticancer drugs through tumor tissue: a potential cause of resistance of solid tumors to chemotherapy. Clin Cancer Res. 2002 Mar 1;8(3):878–84.
118. Choi I-K, Lee Y-S, Yoo JY, Yoon A-R, Kim H, Kim D-S, et al. Effect of decorin on overcoming the extracellular matrix barrier for oncolytic virotherapy. Gene Ther. 2010 Feb 12;17(2):190–201.
119. Demidova-Rice TN, Geevarghese A, Herman IM. Bioactive peptides derived from vascular endothelial cell extracellular matrices promote microvascular morphogenesis and wound healing in vitro. Wound Repair Regen. 2011 Jan 1;19(1):59–70.
120. Martino MM, Tortelli F, Mochizuki M, Traub S, Ben-David D, Kuhn GA, et al. Engineering the Growth Factor Microenvironment with Fibronectin Domains to Promote Wound and Bone Tissue Healing. Sci Translaational Med. 2011;3(100).
121. Pampaloni F, Stelzer E, Masotti A. Three-Dimensional Tissue Models for Drug Discovery and Toxicology. Recent Pat Biotechnol. 2009 Jun 1;3(2):103–17.
122. Weigelt B, Ghajar CM, Bissell MJ. The need for complex 3D culture models to unravel novel pathways and identify accurate biomarkers in breast cancer. Adv Drug Deliv Rev. 2014 Apr 20;69–70:42–51.
123. Sant S, Johnston PA. The production of 3D tumor spheroids for cancer drug discovery. Drug Discov Today Technol. 2017 Mar 1;23:27–36.
124. Klingelhutz AJ, Gourronc FA, Chaly A, Wadkins DA, Burand AJ, Markan KR, et al. Scaffold-free generation of uniform adipose spheroids for metabolism research and drug discovery. Sci Rep. 2018 Dec 11;8(1):523.
125. Hagemann J, Jacobi C, Hahn M, Schmid V, Welz C, Schwenk-Zieger S, et al.

Spheroid-based 3D Cell Cultures Enable Personalized Therapy Testing and Drug Discovery in Head and Neck Cancer. Anticancer Res. 2017 May 1;37(5):2201–10.

126. Breslin S, O'Driscoll L. Three-dimensional cell culture: the missing link in drug discovery. Drug Discov Today. 2013 Mar 1;18(5–6):240–9.
127. Mehta G, Hsiao AY, Ingram M, Luker GD, Takayama S. Opportunities and challenges for use of tumor spheroids as models to test drug delivery and efficacy. J Control Release. 2012 Dec 10;164(2):192–204.
128. McMurtrey RJ. Analytic Models of Oxygen and Nutrient Diffusion, Metabolism Dynamics, and Architecture Optimization in Three-Dimensional Tissue Constructs with Applications and Insights in Cerebral Organoids. Tissue Eng Part C Methods. 2016 Mar 20;22(3):221–49.
129. Halldorsson S, Lucumi E, Gómez-Sjöberg R, Fleming RMT. Advantages and challenges of microfluidic cell culture in polydimethylsiloxane devices. Biosens Bioelectron. 2015 Jan 15;63:218–31.
130. Chiu DT, deMello AJ, Di Carlo D, Doyle PS, Hansen C, Maceiczyk RM, et al. Small but Perfectly Formed? Successes, Challenges, and Opportunities for Microfluidics in the Chemical and Biological Sciences. Chem. 2017 Feb 9;2(2):201–23.
131. Li X (James), Valadez A V, Zuo P, Nie Z. Microfluidic 3D cell culture: potential application for tissue-based bioassays. Bioanalysis. 2012 Jun 13;4(12):1509–25.
132. Brett M-E, Crampton AL, Wood DK. Rapid generation of collagen-based microtissues to study cell–matrix interactions. TECHNOLOGY. 2016 Jun 26;04(02):80–7.
133. Crampton AL, Cummins KA, Wood DK. A high-throughput microtissue platform to probe endothelial function *in vitro*. Integr Biol. 2018 Sep 1;10(9):555–65.
134. Kinney MA, Sargent CY, McDevitt TC. The Multiparametric Effects of Hydrodynamic Environments on Stem Cell Culture. Tissue Eng Part B Rev. 2011 Aug 18;17(4):249–62.
135. Lock LT, Farance I, Baraniak P, Tsai A-C, Ma T, Rowley JA. Rapid and economic generation of consistent hmsc spheroids for macroscopic tissue biofabrication and

therapeutic applications. Cytotherapy. 2015 Jun 1;17(6):S77.

136. Wood DK, Weingeist DM, Bhatia SN, Engelward BP. Single cell trapping and DNA damage analysis using microwell arrays. Proc Natl Acad Sci U S A. 2010 Jun 1;107(22):10008–13.

137. Gong X, Lin C, Cheng J, Su J, Zhao H, Liu T, et al. Generation of Multicellular Tumor Spheroids with Microwell-Based Agarose Scaffolds for Drug Testing. Kerkis I, editor. PLoS One. 2015 Jun 19;10(6):e0130348.

138. Dahlmann J, Kensah G, Kempf H, Skvorc D, Gawol A, Elliott DA, et al. The use of agarose microwells for scalable embryoid body formation and cardiac differentiation of human and murine pluripotent stem cells. Biomaterials. 2013 Mar 1;34(10):2463–71.

139. Choi YY, Chung BG, Lee DH, Khademhosseini A, Kim J-H, Lee S-H. Controlled-size embryoid body formation in concave microwell arrays. Biomaterials. 2010 May 1;31(15):4296–303.

140. Pluen A, Netti PA, Jain RK, Berk DA. Diffusion of Macromolecules in Agarose Gels: Comparison of Linear and Globular Configurations. Biophys J. 1999 Jul 1;77(1):542–52.

141. Fatin-Rouge N, Starchev K, Buffle J. Size Effects on Diffusion Processes within Agarose Gels. Biophys J. 2004 May 1;86(5):2710–9.

142. Blomlof J, Blomlof L, Lindskog S. Effect of different concentrations of EDTA on smear removal and collagen exposure in periodontitis-affected root surfaces. J Clin Periodontol. 1997 Aug 1;24(8):534–7.

143. Simpson JP, Penkman KEH, Demarchi B, Koon H, Collins MJ, Thomas-Oates J, et al. The effects of demineralisation and sampling point variability on the measurement of glutamine deamidation in type I collagen extracted from bone. J Archaeol Sci. 2016 May 1;69:29–38.

144. Mohammadi H, Arora PD, Simmons CA, Janmey PA, McCulloch CA. Inelastic behaviour of collagen networks in cell-matrix interactions and mechanosensation. J R Soc Interface. 2014 Nov 12;12(102):20141074–20141074.

145. Barcus CE, Keely PJ, Eliceiri KW, Schuler LA. Stiff collagen matrices increase

tumorigenic prolactin signaling in breast cancer cells. J Biol Chem. 2013 May 3;288(18):12722–32.

146. Riegler J, Labyed Y, Rosenzweig S, Javinal V, Castiglioni A, Dominguez CX, et al. Tumor Elastography and Its Association with Collagen and the Tumor Microenvironment. Clin Cancer Res. 2018 Sep 15;24(18):4455–67.
147. Carey SP, Martin KE, Reinhart-King CA. Three-dimensional collagen matrix induces a mechanosensitive invasive epithelial phenotype. Sci Rep. 2017 Feb 10;7(1):42088.
148. Lakshman N, Petroll WM. Growth Factor Regulation of Corneal Keratocyte Mechanical Phenotypes in 3-D Collagen Matrices. Investig Opthalmology Vis Sci. 2012 Mar 1;53(3):1077.
149. Kobayashi T, Liu X, Kim HJ, Kohyama T, Wen F-Q, Abe S, et al. TGF-β1 and serum both stimulate contraction but differentially affect apoptosis in 3D collagen gels. Respir Res. 2005 Dec 2;6(1):141.
150. Goulet S, Bihl MP, Gambazzi F, Tamm M, Roth M. Opposite effect of corticosteroids and long-acting β2-agonists on serum- and TGF-β1-induced extracellular matrix deposition by primary human lung fibroblasts. J Cell Physiol. 2007 Jan 1;210(1):167–76.
151. Collins DJ, Neild A, deMello A, Liu A-Q, Ai Y. The Poisson distribution and beyond: methods for microfluidic droplet production and single cell encapsulation. Lab Chip. 2015 Aug 11;15(17):3439–59.
152. Janson LW, Kolega J, Taylor DL. Modulation of contraction by gelation/solation in a reconstituted motile model. J Cell Biol. 1991 Sep 1;114(5):1005–15.
153. Sohail MA, Hashmi AZ, Hakim W, Watanabe A, Zipprich A, Groszmann RJ, et al. Adenosine induces loss of actin stress fibers and inhibits contraction in hepatic stellate cells via Rho inhibition. Hepatology. 2009 Jan 1;49(1):185–94.
154. Sukriti S, Tauseef M, Yazbeck P, Mehta D. Mechanisms Regulating Endothelial Permeability. Pulm Circ. 2014 Dec 1;4(4):535–51.
155. Mantovani A, Bussolino F, Dejana E. Cytokine regulation of endothelial cell function. FASEB J. 1992 May 1;6(8):2591–9.

156. Friedman M, Byers SO. Endothelial permeability in atherosclerosis. Arch Pathol. 1963;76:99–105.
157. Veress B, Bálint A, Kóczé A, Nagy Z, Jellinek H. Increasing aortic permeability by atherogenic diet. Atherosclerosis. 1970 May 1;11(3):369–71.
158. Chatzizisis YS, Umit Coskun A, Jonas M, Edelman ER, Feldman CL, Stone PH. Role of Endothelial Shear Stress in the Natural History of Coronary Atherosclerosis and Vascular Remodeling Molecular, Cellular, and Vascular Behavior. J Am Coll Cardiol. 2007;49(25).
159. Koch AE, Harlow LA, Haines GK, Amento EP, Unemori EN, Wong WL, et al. Vascular endothelial growth factor. A cytokine modulating endothelial function in rheumatoid arthritis. J Immunol. 1994 Apr 15;152(8):4149–56.
160. Koch AE. The role of angiogenesis in rheumatoid arthritis: recent developments. Ann Rheum Dis. 2000 Nov 1;59 Suppl 1(suppl 1):i65-71.
161. Middleton J, Americh L, Gayon R, Julien D, Aguilar L, Amalric F, et al. Endothelial cell phenotypes in the rheumatoid synovium: activated, angiogenic, apoptotic and leaky. Arthritis Res Ther. 2004 Mar 8;6(2):60.
162. Cecchelli R, Dehouck B, Descamps L, Fenart L, Buée-Scherrer V, Duhem C, et al. In vitro model for evaluating drug transport across the blood–brain barrier. Adv Drug Deliv Rev. 1999 Apr 5;36(2–3):165–78.
163. Cecchelli R, Berezowski V, Lundquist S, Culot M, Renftel M, Dehouck M-P, et al. Modelling of the blood–brain barrier in drug discovery and development. Nat Rev Drug Discov. 2007 Aug 1;6(8):650–61.
164. Lockman PR, Koziara JM, Mumper RJ, Allen DD. Nanoparticle Surface Charges Alter Blood–Brain Barrier Integrity and Permeability. J Drug Target. 2004 Dec 3;12(9–10):635–41.
165. Di L, Kerns EH, Fan K, McConnell OJ, Carter GT. High throughput artificial membrane permeability assay for blood–brain barrier. Eur J Med Chem. 2003 Mar 1;38(3):223–32.
166. Hatherell K, Couraud P-O, Romero IA, Weksler B, Pilkington GJ. Development of a three-dimensional, all-human in vitro model of the blood–brain barrier using

mono-, co-, and tri-cultivation Transwell models. J Neurosci Methods. 2011 Aug 15;199(2):223–9.

167. Dreher MR, Liu W, Michelich CR, Dewhirst MW, Yuan F, Chilkoti A. Tumor Vascular Permeability, Accumulation, and Penetration of Macromolecular Drug Carriers. JNCI J Natl Cancer Inst. 2006 Mar 1;98(5):335–44.
168. Greish K. Enhanced permeability and retention of macromolecular drugs in solid tumors: A royal gate for targeted anticancer nanomedicines. J Drug Target. 2007 Jan 8;15(7–8):457–64.
169. Yuan F, Leunig M, Huang SK, Berk DA, Papahadjopoulos D, Jain RK. Microvascular permeability and interstitial penetration of sterically stabilized (stealth) liposomes in a human tumor xenograft. Cancer Res. 1994 Jul 1;54(13):3352–6.
170. Iyer AK, Khaled G, Fang J, Maeda H. Exploiting the enhanced permeability and retention effect for tumor targeting. Drug Discov Today. 2006 Sep 1;11(17–18):812–8.
171. Danhier F, Feron O, Préat V. To exploit the tumor microenvironment: Passive and active tumor targeting of nanocarriers for anti-cancer drug delivery. J Control Release. 2010 Dec 1;148(2):135–46.
172. Tozer GM, Kanthou C, Baguley BC. Disrupting tumour blood vessels. Nat Rev Cancer. 2005 Jun 1;5(6):423–35.
173. Siflinger-Birnboim A, del Vecchio PJ, Cooper JA, Blumenstock FA, Shepard JM, Malik AB. Molecular sieving characteristics of the cultured endothelial monolayer. J Cell Physiol. 1987 Jul 1;132(1):111–7.
174. Maruo N, Morita I, Shirao M, Murota S. IL-6 increases endothelial permeability in vitro. Endocrinology. 1992 Aug 1;131(2):710–4.
175. Casnocha SA, Eskin SG, Hall ER, McIntire L V. Permeability of human endothelial monolayers: effect of vasoactive agonists and cAMP. J Appl Physiol. 1989 Nov;67(5):1997–2005.
176. Bratzler RL, Chisolm GM, Colton CK, Smith KA, Lees RS. The distribution of labeled low-density lipoproteins across the rabbit thoracic aorta in vivo.

Atherosclerosis. 1977 Nov 1;28(3):289–307.

177. Ma X, Zhang H, Pan Q, Zhao Y, Chen J, Zhao B, et al. Hypoxia/Aglycemia-Induced Endothelial Barrier Dysfunction and Tight Junction Protein Downregulation Can Be Ameliorated by Citicoline. Tang YL, editor. PLoS One. 2013 Dec 16;8(12):e82604.
178. Kevil CG, Payne DK, Mire E, Alexander JS. Vascular permeability factor/vascular endothelial cell growth factor-mediated permeability occurs through disorganization of endothelial junctional proteins. J Biol Chem. 1998 Jun 12;273(24):15099–103.
179. Nooteboom A, Hendriks T, Ottehöller I, van der Linden CJ. Permeability characteristics of human endothelial monolayers seeded on different extracellular matrix proteins. Mediators Inflamm. 2000;9(5):235–41.
180. Nooteboom A, Van Der Linden CJ, Hendriks T. Tumor necrosis factor-alpha and interleukin-1beta mediate endothelial permeability induced by lipopolysaccharide-stimulated whole blood. Crit Care Med. 2002;30(9):2063–8.
181. Zervantonakis IK, Hughes-Alford SK, Charest JL, Condeelis JS, Gertler FB, Kamm RD. Three-dimensional microfluidic model for tumor cell intravasation and endothelial barrier function. Proc Natl Acad Sci. 2012;109(34):13515–20.
182. Jeon JS, Bersini S, Whisler JA, Chen MB, Dubini G, Charest JL, et al. Generation of 3D functional microvascular networks with human mesenchymal stem cells in microfluidic systems. Integr Biol. 2014 Apr 22;6(5):555–63.
183. Moya ML, Hsu Y-H, Lee AP, Hughes CCW, George SC. *In Vitro* Perfused Human Capillary Networks. Tissue Eng Part C Methods. 2013;19(9):730–7.
184. Mannino RG, Santiago-Miranda AN, Pradhan P, Qiu Y, Mejias JC, Neelapu SS, et al. 3D microvascular model recapitulates the diffuse large B-cell lymphoma tumor microenvironment in vitro. Lab Chip. 2017 Jan 31;17(3):407–14.
185. Gryglewski RJ, Moncada S, Palmer RMJ. Bioassay of prostacyclin and endothelium-derived relaxing factor (EDRF) from porcine aortic endothelial cells. Br J Pharmacol. 1986 May 1;87(4):685–94.
186. Feng X, Tonnesen MG, Mousa SA, Clark RAF. Fibrin and Collagen Differentially

but Synergistically Regulate Sprout Angiogenesis of Human Dermal Microvascular Endothelial Cells in 3-Dimensional Matrix. Int J Cell Biol. 2013;2013:1–11.

187. Schindelin J, Arganda-Carreras I, Frise E, Kaynig V, Longair M, Pietzsch T, et al. Fiji: an open-source platform for biological-image analysis. Nat Methods. 2012 Jul 1;9(7):676–82.
188. Kramer CY. Extension of Multiple Range Tests to Group Means with Unequal Numbers of Replications. Biometrics. 1956 Sep;12(3):307.
189. Liu XD, Skold M, Umino T, Zhu YK, Romberger DJ, Spurzem JR, et al. Endothelial cell–mediated type I collagen gel contraction is regulated by hemin. J Lab Clin Med. 2000 Aug 1;136(2):100–9.
190. Han S, Shin Y, Jeong HE, Jeon JS, Kamm RD, Huh D, et al. Constructive remodeling of a synthetic endothelial extracellular matrix. Sci Rep. 2016 Nov 21;5(1):18290.
191. Jaffe EA, Minick CR, Adelman B, Becker CG, Nachman R. Synthesis of basement membrane collagen by cultured human endothelial cells. J Exp Med. 1976 Jul 1;144(1):209–25.
192. Kramer RH, Fuh GM, Karasek M a. Type IV collagen synthesis by cultured human microvascular endothelial cells and its deposition into the subendothelial basement membrane. Biochemistry. 1985;24(25):7423–30.
193. Kramer RH, Bensch KG, Davison PM, Karasek MA. Basal lamina formation by cultured microvascular endothelial cells. J Cell Biol. 1984 Aug 1;99(2):692–8.
194. Jaffe EA, Mosher DF. Synthesis of fibronectin by cultured human endothelial cells. J Exp Med. 1978 Jun 1;147(6):1779–91.
195. Nguyen M, Arkell J, Jackson CJ. Human endothelial gelatinases and angiogenesis. Int J Biochem Cell Biol. 2001 Oct 1;33(10):960–70.
196. Chang C, Werb Z. The many faces of metalloproteases: cell growth, invasion, angiogenesis and metastasis. Trends Cell Biol. 2001 Nov 1;11:S37–43.
197. Egawa G, Nakamizo S, Natsuaki Y, Doi H, Miyachi Y, Kabashima K. Intravital analysis of vascular permeability in mice using two-photon microscopy. Sci Rep.

2013;3:1932.

198. Van Duinen V, Van Den Heuvel A, Trietsch SJ, Lanz HL, Van Gils JM, Van Zonneveld AJ, et al. 96 perfusable blood vessels to study vascular permeability in vitro. Sci Rep. 2017;7:18071.
199. Faraci FM, Choi J, Baumbach GL, Mayhan WG, Heistad DD. Microcirculation of the Area Postrema Permeability and Vascular Responses.
200. Burns A, Ow H, Wiesner U. Fluorescent core–shell silica nanoparticles: towards "Lab on a Particle" architectures for nanobiotechnology. Chem Soc Rev. 2006 Oct 23;35(11):1028–42.
201. Real-Hohn A, Zancan P, Da Silva D, Martins ER, Salgado LT, Mermelstein CS, et al. Filamentous actin and its associated binding proteins are the stimulatory site for 6-phosphofructo-1-kinase association within the membrane of human erythrocytes. Biochimie. 2010 May 1;92(5):538–44.
202. Yuan F, Dellian M, Fukumura D, Leunig M, Berk DA, Torchilin VP, et al. Vascular Permeability in a Human Tumor Xenograft: Molecular Size Dependence and Cutoff Size1. Vol. 55, CANCER RESEARCH. 1995.
203. Rizzo V, Kim D, Durán WN, DeFouw DO. Ontogeny of Microvascular Permeability to Macromolecules in the Chick Chorioallantoic Membrane during Normal Angiogenesis. Microvasc Res. 1995 Jan 1;49(1):49–63.
204. Marcos-Ramiro B, García-Weber D, Millán J. TNF-induced endothelial barrier disruption: beyond actin and Rho. Thromb Haemost. 2014 Nov 20;112(12):1088–102.
205. Connolly DT, Heuvelman DM, Nelson R, Olander J V, Eppley BL, Delfino JJ, et al. Tumor vascular permeability factor stimulates endothelial cell growth and angiogenesis. J Clin Invest. 1989 Nov 1;84(5):1470–8.
206. Naomasa N, Norio N, Shoso Y. The effect of histamine on cultured endothelial cells A study of the mechanism of increased vascular permeability. Eur J Pharmacol. 1992 Oct 20;221(2–3):325–31.
207. van Nieuw Amerongen GP, Draijer R, Vermeer MA, Van Hinsbergh VWM. Transient and Prolonged Increase in Endothelial Permeability Induced by

Histamine and Thrombin Role of Protein Kinases, Calcium, and RhoA. 1998.

208. Harlan JM, Harker LA, Reidy MA, Gajdusek CM, Schwartz SM, Striker GE. Lipopolysaccharide-mediated bovine endothelial cell injury in vitro. Lab Invest. 1983 Mar;48(3):269–74.

209. Atienzar FA, Blomme EA, Chen M, Hewitt P, Kenna JG, Labbe G, et al. Key Challenges and Opportunities Associated with the Use of In Vitro Models to Detect Human DILI: Integrated Risk Assessment and Mitigation Plans. Biomed Res Int. 2016 Sep 5;2016:1–20.

210. Underhill GH, Khetani SR. Bioengineered Liver Models for Drug Testing and Cell Differentiation Studies. Cell Mol Gastroenterol Hepatol. 2018 Jan 1;5(3):426-439.e1.

211. Bell CC, Hendriks DFG, Moro SML, Ellis E, Walsh J, Renblom A, et al. Characterization of primary human hepatocyte spheroids as a model system for drug-induced liver injury, liver function and disease. Sci Rep. 2016 Jul 4;6(1):25187.

212. Soldatow VY, Lecluyse EL, Griffith LG, Rusyn I. In vitro models for liver toxicity testing. Toxicol Res (Camb). 2013 Jan 1;2(1):23–39.

213. Bale SS, Vernetti L, Senutovitch N, Jindal R, Hegde M, Gough A, et al. *In vitro* platforms for evaluating liver toxicity. Exp Biol Med. 2014 Sep 24;239(9):1180–91.

214. Norona LM, Nguyen DG, Gerber DA, Presnell SC, LeCluyse EL. Editor's Highlight: Modeling Compound-Induced Fibrogenesis *In Vitro* Using Three-Dimensional Bioprinted Human Liver Tissues. Toxicol Sci. 2016 Dec 1;154(2):354–67.

215. Khetani SR, Berger DR, Ballinger KR, Davidson MD, Lin C, Ware BR. Microengineered Liver Tissues for Drug Testing. J Lab Autom. 2015 Jun 23;20(3):216–50.

216. Foster AJ, Chouhan B, Regan SL, Rollison H, Amberntsson S, Andersson LC, et al. Integrated in vitro models for hepatic safety and metabolism: evaluation of a human Liver-Chip and liver spheroid. Arch Toxicol. 2019 Apr 26;93(4):1021–37.

217. Kukla DA, Crampton AL, Wood DK, Khetani SR. Engineering Long-term 3D Human Liver Microtissues for Drug Development Using Droplet Microfluidics. *In Preparation* 2019.
218. Khetani SR, Kanchagar C, Ukairo O, Krzyzewski S, Moore A, Shi J, et al. Use of Micropatterned Cocultures to Detect Compounds That Cause Drug-Induced Liver Injury in Humans. Toxicol Sci. 2013 Mar 1;132(1):107–17.
219. Ware BR, Durham MJ, Monckton CP, Khetani SR. A Cell Culture Platform to Maintain Long-term Phenotype of Primary Human Hepatocytes and Endothelial Cells. Cell Mol Gastroenterol Hepatol. 2018 Jan 1;5(3):187–207.
220. Berger DR, Ware BR, Davidson MD, Allsup SR, Khetani SR. Enhancing the functional maturity of induced pluripotent stem cell-derived human hepatocytes by controlled presentation of cell-cell interactions *in vitro*. Hepatology. 2015 Apr 1;61(4):1370–81.
221. Khetani SR, Bhatia SN. Microscale culture of human liver cells for drug development. Nat Biotechnol. 2008 Jan 18;26(1):120–6.
222. Schepers A, Li C, Chhabra A, Seney BT, Bhatia S. Engineering a perfusable 3D human liver platform from iPS cells. Lab Chip. 2016 Jul 5;16(14):2644–53.
223. Godoy P, Hewitt NJ, Albrecht U, Andersen ME, Ansari N, Bhattacharya S, et al. Recent advances in 2D and 3D in vitro systems using primary hepatocytes, alternative hepatocyte sources and non-parenchymal liver cells and their use in investigating mechanisms of hepatotoxicity, cell signaling and ADME. Arch Toxicol. 2013 Aug 23;87(8):1315–530.
224. Rojkind M, Giambrone M-A, Biempica L. Collagen Types in Normal and Cirrhotic Liver. Gastroenterology. 1979 Apr 1;76(4):710–9.
225. Schuppan D, Cramer T, Bauer M, Strefeld T, Hahn EG, Herbst H. Hepatocytes as a source of collagen type XVIII endostatin. Lancet (London, England). 1998 Sep 12;352(9131):879–80.
226. Schuppan D. Structure of the Extracellular Matrix in Normal and Fibrotic Liver: Collagens and Glycoproteins. Semin Liver Dis. 1990;10(1):1–10.
227. Gressner, M. A. Hepatic proteoglycans-A brief survey of their pathobiochemical

implications. Hepatogastroenterology. 1983;30:225–9.

228. Gerbal-Chaloin S, Funakoshi N, Caillaud A, Gondeau C, Champon B, Si-Tayeb K. Human Induced Pluripotent Stem Cells in Hepatology: Beyond the Proof of Concept. Am J Pathol. 2014 Feb 1;184(2):332–47.

229. Scott CW, Peters MF, Dragan YP. Human induced pluripotent stem cells and their use in drug discovery for toxicity testing. Toxicol Lett. 2013 May 10;219(1):49–58.

230. Greenhough S, Medine CN, Hay DC. Pluripotent stem cell derived hepatocyte like cells and their potential in toxicity screening. Toxicology. 2010 Dec 30;278(3):250–5.

231. Schwartz RE, Fleming HE, Khetani SR, Bhatia SN. Pluripotent stem cell-derived hepatocyte-like cells. Biotechnol Adv. 2014 Mar 1;32(2):504–13.

232. Engle SJ, Puppala D. Integrating Human Pluripotent Stem Cells into Drug Development. Cell Stem Cell. 2013 Jun 6;12(6):669–77.

233. Bhatia SN, Balis UJ, Yarmush ML, Toner M. Effect of cell–cell interactions in preservation of cellular phenotype: cocultivation of hepatocytes and nonparenchymal cells. FASEB J. 1999 Nov 1;13(14):1883–900.

234. Davidson MD, Kukla DA, Khetani SR. Microengineered cultures containing human hepatic stellate cells and hepatocytes for drug development. Integr Biol. 2017 Aug 1;9(8):662–77.

235. Nguyen T V, Ukairo O, Khetani SR, Mcvay M, Kanchagar C, Seghezzi W, et al. Establishment of a Hepatocyte-Kupffer Cell Coculture Model for Assessment of Proinflammatory Cytokine Effects on Metabolizing Enzymes and Drug Transporters s. DRUG Metab Dispos Drug Metab Dispos. 2015;43:774–85.

236. Litvan GG. Mechanism of cryoinjury in biological systems. Cryobiology. 1972 Jun 1;9(3):182–91.

237. Hubálek Z. Protectants used in the cryopreservation of microorganisms. Cryobiology. 2003 Jun 1;46(3):205–29.

238. Best BP. Cryoprotectant Toxicity: Facts, Issues, and Questions. Rejuvenation Res. 2015 Oct 19;18(5):422–36.

239. Bank HL, Brockbank KG. Basic principles of cryobiology. J Card Surg. 1987 Mar;2(1 Suppl):137–43.
240. Mandawala AA, Harvey SC, Roy TK, Fowler KE. Cryopreservation of animal oocytes and embryos: Current progress and future prospects. Theriogenology. 2016 Oct 15;86(7):1637–44.
241. Yong KW, Wan Safwani WKZ, Xu F, Wan Abas WAB, Choi JR, Pingguan-Murphy B. Cryopreservation of Human Mesenchymal Stem Cells for Clinical Applications: Current Methods and Challenges. Biopreserv Biobank. 2015 Aug 17;13(4):231–9.
242. Gao H-H, Li Z-P, Wang H-P, Zhang L-F, Zhang J-M. Cryopreservation of whole bovine ovaries: comparisons of different thawing protocols. Eur J Obstet Gynecol Reprod Biol. 2016 Sep;204:104–7.
243. Karlsson JOM, Toner M. Long-term storage of tissues by cryopreservation: Critical issues. Biomaterials. 1996;
244. Sarangi SK, Pramanik K. Cryopreservation in Tissue Engineering: Challenges & Prospects. In: 2010 Advanced Technologies for Enhancing Quality of Life. IEEE; 2010. p. 114–20.
245. Wu Y, Wen F, Gouk SS, Lee EH, Kuleshova L. Cryopreservation Strategy For Tissue Engineering Constructs Consisting Of Human Mesenhymal Stem Cells And Hydrogel Biomaterials. Cryo Letters. 36(5):325–35.
246. Sosef MN, Baust JM, Sugimachi K, Fowler A, Tompkins RG, Toner M. Cryopreservation of isolated primary rat hepatocytes: enhanced survival and long-term hepatospecific function. Ann Surg. 2005 Jan;241(1):125–33.
247. Jitraruch S, Dhawan A, Hughes RD, Filippi C, Lehec SC, Glover L, et al. Cryopreservation of Hepatocyte Microbeads for Clinical Transplantation. Cell Transplant. 2017 Aug 13;26(8):1341–54.